Title
Toolbox for hybrid variable-bandwidth innate immunity peptides

Author
Kordbacheh, Shadi

Publication Date
2022

Peer reviewed|Thesis/dissertation

UNIVERSITY OF CALIFORNIA

Los Angeles

Toolbox for hybrid variable-bandwidth innate immunity peptides

A dissertation submitted in partial satisfaction of the

requirements for the degree of Doctor of Philosophy

in Bioengineering

by

Shadi Kordbacheh

2022

ABSTRACT OF THE DISSERTATION

Toolbox for hybrid variable-bandwidth innate immunity peptides

by

Shadi Kordbacheh

Doctor of Philosophy in Bioengineering

University of California, Los Angeles, 2022

Professor Andrea M. Kasko, Chair

Rising to dangerously high levels all over the world, antibiotic resistance is now a critical global problem. To inhibit or kill bacteria, most antibiotics target the growth process of bacterial cells. Therefore, most antibiotics are ineffective for slowly growing bacteria with lower cellular influx. Current therapeutic approaches most commonly utilize broad-spectrum antibiotics and/or drug cocktails to target a wide range of bacteria. Unfortunately, broad-spectrum antibiotics can target both beneficial and pathogenic bacteria. This nonspecificity imparts significant pressure on bacterial species to evolve into resistant strains. In addition, beneficial bacteria do not always fully recover, increasing susceptibility to infections and diseases. It is not practical to develop antibiotics for all species of interest. To mitigate these issues, we must engineer new antibiotics in a drastically different way to prevent running out of effective therapies.

Bacteria are capable of producing defensive molecules. These secreted multi-functional molecules inhibit other closely related strains competing for the same environmental niches. We were inspired by the defensive behavior of bacteria to engineer novel antibiotics featuring tunable functionalityThis tunability allows for an adjustable bandwidth of antimicrobial activity against multiple species within a specific set of environmental conditions. Moreover, we produced antibiotics able to inhibit pathogenic bacteria without harming host cells or beneficial commensal bacteria. We were interested in antimicrobial peptides (AMPs) as antibiotics, since they target generic features common to the outer membrane of many pathogenic species. These antibiotics allow us to regulate complex microbial communities by inhibiting or killing detrimental bacteria without harming host-associated microbial communities, that have beneficial impacts on human health. Additionally, these new antibiotics help beneficial bacteria win the competition over environmental niches. Therefore, the development of resistance is significantly inhibited compared to that of conventional antibiotics. To engineer new antimicrobials, we leveraged recently developed sequence design rules, using both positive charge and hydrophobicity as necessary conditions for antimicrobial activity. These hybrid antimicrobial molecules can be used for treating resistant infections and regulating species distribution in microbial communities.

We engineered tunable antimicrobial peptides with a 'threshold' activity profile using pH-switchable charge. To tune the antimicrobial activity of α−helical AMPs, we modified functional groups on the side chain of specific basic amino acids (lysine and arginine). By incorporating electron withdrawing and/or hydrophobic compounds on the side chains of arginine and lysine residues, the pK_a at which these residues become positively charged can be lowered. Therefore,

by incorporating different masking groups in different locations, we adjust the activity of the antimicrobial peptides by turning them on at specific and tunable pH values.

The dissertation of Shadi Kordbacheh is approved.

Gerard Chee Lai Wong

Jacob J. Schmidt

William M. Gelbart

Andrea M. Kasko, Committee Chair

University of California, Los Angeles

2022

Acknowledgment

I would like to express my deepest appreciation to my thesis chair, supervisor, and mentor, Professor Andre M Kasko. Under your supervision, I learned how to be a better scientist. Your dedication, hard-work, and keen interest to guide your students has always been a great example for me to look up to. I would like to thank my Ph.D. committee members, Professor Wong, Professor Schmidt, and Professor Gelbart. I am so lucky that I could benefit from your knowledge and experience in different aspects of my thesis. I appreciate all your scientific advice along my Ph.D. journey.

To my parents: Fati and Javad. Words cannot describe how grateful I am to be your child. Dad, thank you for supporting me in all stages in my life even if my decisions did not make sense at the time. Mom, thanks for teaching and helping me stay focused on my goals. Thank you both for being so open minded and supportive my whole life. That helped me grow into the independent, eager woman I am today.

To my sister- Thank you for being born ten years before me so I learnt how to live better ten years ahead of my age. Thanks for all the motivation since I was a kid till now.

To my niece Tara- Thanks for coming to this world in my darkest days and brighten up our lives.

Dr. Khatibzadeh- My most helpful and motivating professor at Amir Kabir University of Technology. Thanks for all the conferences you encouraged me to participate in. Also, thank you for always being the coolest person in all trips we had together around the world.

To Dr. Amirani- My chemistry Olympiad teacher as the first person introduced chemistry to me in best way possible. From those days on, my love for chemistry never faded. Also, thank you for

pushing me to choose polymer engineering as my undergraduate major. Polymer world is wonderful.

To Fafa- Our postdoctoral research fellow in Kasko lab who knew the answers to all questions. Thank you for teaching me all the techniques, especially, how to use HPLC very precisely. You are the absolute best.

To Brianna- My twine from different moms and the best hood mate I could ever ask for. Thank you for letting me occupy half of your fume hood so I had the chance to have a lovely friend like you. Thanks for all prospectus edits and being next to me when life wasn't so kind to me.

To Walter- Thanks for all the emotional support and backing me up when I really needed someone to help me.

To Brooke- The nicest person in the world. Thanks for always being kind and positive. Thank you for all the ordering you did for us. You have no idea how much easier my lab life was after you joint Kasko lab.

To Elizabeth- My American version. You have no idea how joyful it was when you totally knew what I mean to tell you without even a world and just by a look. Thanks for sharing the hood with me and being the tidiest hood mate ever. Thanks for always having similar taste as mine which made decision making so easy. And last but not least, thanks for loving beer as much as I do.

To Amaka- Who brought happiness and laughter to the lab. Thanks for all your understanding when I was being tired and annoying and all your prayers when I had a problem in my life.

To Reza and Ana- Best friends I made in the US. Thanks for all your moral support during these years.

To Arezoo and Shadi- My cool neighbors! Thanks for always being the coolest people I could be surrounded with. Thanks for always saying yes to all my plans and all the WURTKUCHE runs.

To Alireza- Who I don’t know where to start from when I want to acknowledge him. Thanks for millions of things you did for me. Thank you for all the moral support, research motivation and endless kindness for the past eleven years of my life.

To Ali- Thanks for bringing peace and trust to my life so I can focus better on my research again.

To Babak- Who I am going to call family since he is much more valuable than a friend to me. Thanks for listening to me when I just needed someone to hear me. Thanks for all the support and motivation.

To Nima- Thanks for teaching me all transport phenomena courses and making me study hard. My time studying with you in college was so fun, motivating me to study more! Thanks for listening to all my nags for years and never complaining. Thanks for encouraging me apply for Ph.D. in the US and changed my path to a better one.

اسرار ازل را نه تو دانی و نه من

وین حل معما نه تو خوانی و نه من

هست از پس پرده گفتگوی من و تو

چون پرده در افتد نه تو مانی و نه من

خیام

Nor you nor I can read the etern decree

To that enigma we can find no key

They talk of you and me behind the veil

But, if that veil be lifted, where are we?

-Khayyam

Table of Contents

List of Figures

List of Schemes

List of Tables

BIOGRAPHICAL SKETCH

NAME: Kordbacheh, Shadi

eRA COMMONS USERNAME (credential, e.g., agency login): SKORDBACHEH

POSITION TITLE: Graduate Student Researcher

EDUCATION/TRAINING *(Begin with baccalaureate or other initial professional education, such as nursing, include postdoctoral training and residency training if applicable. Add/delete rows as necessary.)*

INSTITUTION AND LOCATION	DEGREE *(If applicable)*	Start Date MM/YYYY	Completion Date MM/YYYY	FIELD OF STUDY
AmirKabir University, Tehran, Iran	B.S.	09/2008	09/2012	Polymer Sciences and Engineering
University of California, Los Angeles (UCLA), USA	M.Sc.	09/2014	03/2017	Bioengineering
University of California, Los Angeles (UCLA), USA	Ph.D. candidate	09/2014	present	Bioengineering

A. Positions and Honors

Positions and Employment

2014-Present Graduate Student Researcher, Department of Bioengineering,

University of California, Los Angeles, Advisor: Dr. Andrea M Kasko

2014-Present Member, American Chemical Society (ACS)

2016-Present Member, Biomedical Engineering Society (BMES)

Awards and Honors

2014 Department of Bioengineering fellowship award

2015 Nonresident Graduate Academic Doctoral Award (NRT)

2020 DAAD RISE Professional scholarship award

2020 POLY 2020 Spring Excellence in Graduate Polymer Research award

B. Synergistic activities

2015	Teaching assistant (UCLA)
2017	Teaching associate (UCLA)
2019	Teaching fellow (UCLA)

C. Publication

1. Murphy R, Kordbacheh S, Skoulas D, *et al.*: Three-dimensionally printable shear-thinning triblock copolypeptide hydrogels with antimicrobial potency. *Biomater Sci.* 2021; **9**(15): 5144–9.
2. Deshayes, S., Xian, W., Schmidt, N. W., Kordbacheh, S., Lieng, J., Wang, J., Zarmer, S., Germain, S. S., Voyen, L., Thulin, J., Wong, G. C. L., & Kasko, A. M. (2017). Designing hybrid antibiotic peptide conjugates to cross bacterial membranes. Bioconjugate Chemistry, **28**(3), 793–804.
3. Kordbacheh, S., and Kasko, A. M. (2021). Peptide and protein engineering by modification of backbone and sidechain functional groups. *Polym. Int.* **70**, 889–896.

Chapter 1: Introduction and background

The development of bacterial resistance to conventional antibiotics is a critical public health problem. Antibiotic resistance results in at least 2 million illnesses and 23,000 deaths in the United States every year. Antibiotic misuse and overuse can lead to antibiotic resistance. Approximately 70% of hospital acquired infections in the United States are resistant to at least one antibiotic[1]. For example, methicillin-resistant *Staphylococcus aureus* (MRSA)[2], vancomycin-resistant enterococci (VRE)[3], and vancomycin-resistant Staphylococcus aureus (VRSA)[4] have emerged as common nosocomial infections. Despite the need for new antimicrobial agents, progress in antibiotic development has been very slow. The growing gap between the slow progress in antibiotic development and the fast increase of drug resistance has become one of the most urgent challenges for global health. Concerns about antibiotics commonly focus on bacterial resistance; however, permanent changes to our protective flora could have more serious consequences. Treatment with broad-spectrum antibiotics often disrupts the natural symbiotic relationship between these species in human microbiome. New diseases and more infections are often the consequence of this disruption[5]. For instance, in healthy adults, the colon contains as many as 10^{12} bacteria per gram of contents[6]. The indigenous microflora of the colon provides important host defense by inhibiting colonization and overgrowth of C. difficile and other potential pathogens[7]. Antimicrobial therapy can disrupt this host defense by playing a major role in the pathogenesis of Clostridium difficile infections (CDI). By disrupting of the indigenous microflora of the colon, antimicrobials allow *C. difficile* to grow to high concentrations, producing toxin and leading to CDI. Although nearly all classes of antimicrobials have been associated with CDI, clindamycin, third-generation cephalosporins, penicillin, and

penicillin-derivatives have traditionally been considered to pose the greatest risk[8]. All over the world, C.diff. leads to approximately 250,000 hospitalizations per year[9]. Therefore, we need antibiotics with an optimal spectrum of antimicrobial activity to target pathogenic species while leaving the beneficial bacteria intact. Here, we engineered optimal intermediate-spectrum anti-microbial peptides (AMPs) using environment-responsive charge created by basic amino acid side-chain functionalization. Successful implementation of this engineered AMPs will result in a synthetic 'toolbox' for targeting specific pathogenic strains and controlling species composition in microbial communities.

1.1. Why antimicrobial peptides

AMPs exist widely in nearly all organisms and take part in innate immunity[10,11]. They act as natural antibiotics to protect the host from bacterial infections and are one of the most promising choices for next-generation antibiotics. AMPs display broad-spectrum antimicrobial activity against organisms ranging from viruses to parasites[11-17] and use non-specific interactions to target generic features common to the outer membrane of pathogenic species[18]. Currently, over 1,000 diverse AMPs have been discovered in both prokaryote and eukaryote cells. While traditional antibiotics such as, β−lactams, quinolones, macrolides, and tetracyclines, feature a core structure responsible for antimicrobial activity, AMPs do not. Additionally, most AMPs tend to be relatively short (less than 50 amino acids) and share two fundamental features: net cationic charge (+2 to +9) and amphiphilicity[11,12,19,15,16,20,21]. Their cationic charge forms a strong electrostatic interaction with the negatively-charged bacterial membrane. In addition to this charged interaction, the hydrophobic patches of the amphiphilic AMPs insert to the non-polar interior of

the lipid bilayer[12,15,16,22,23,24,25]. These combined interactions can destabilize the bacterial membranes via pore formation, blebbing, budding, or vascularization (Figure .1)[13,23,26,27,28,29,30]. With this in mind, we designed new synthetic AMPs that mimic the cationic charge and amphiphilicity AMPs use to inhibit and kill bacteria, while controlling antimicrobial activity.

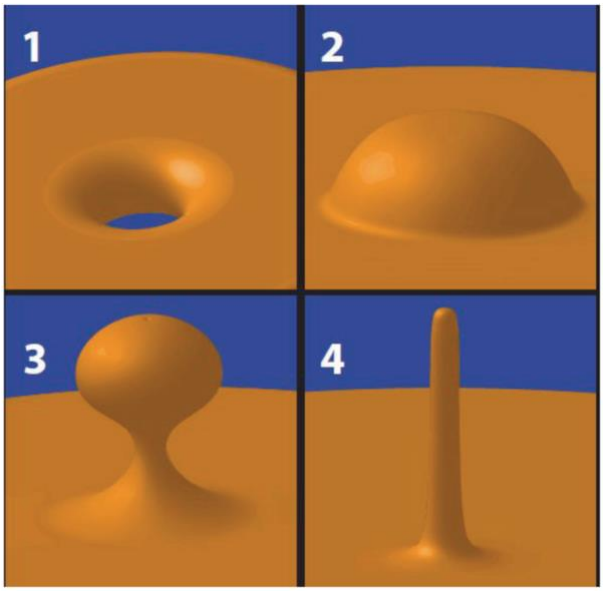

Figure 1.1: Diagram of different membrane destabilization mechanism such as poration (1), blebbing (2), budding (3), vascularization (4)[31].

1.2. Negative Gaussian curvature, essential geometry for membrane destabilization

Small angle X-ray scattering (SAXS) data indicates that the antibacterial activity of a broad range of natural AMPs is correlated with the ability of the peptides to induce negative Gaussian curvature on model bacterial membranes. The same effect was not seen on mammalian membranes. Synthetic AMPs show similar behavior for the model bacterial membranes, suggesting a common mechanism to selectively permeate bacterial membranes[32,33,34].

Prokaryotic membranes differ from eukaryotic membranes, as they are rich in phosphatidylethanolamines (PE) with negative intrinsic curvature (C_0<0)[35]. The necessity of negative Gaussian (or saddle-splay) curvature generation provides a template for the amino acid composition of AMPs. For example, the α- defensin Cryptdin-4 (Crp-4)[36,37,38] generates saddle-splay curvature in model bacterial membranes with high PE but not in model eukaryotic membranes with high phosphatidylcholines (PC). The amount of phosphatidylserine (PS) is equal in both model membrane vesicles[31]. Defensins constitute one of two major AMP families and were among the first AMPs to be described. Defensins consist of three subfamilies of cationic, Cysteine-rich AMPs, α−, β−, and θ− defensins. All these AMPs have broad-spectrum antimicrobial activities[26]. Incubation of Crp-4 with small unilamellar vesicles (SUVs) with high PE lipid composition (DOPS/DOPE = 20/80) produced a Pn3m bicontinuous cubic phase where two non-intersecting water channels are separated by a lipid bilayer (Figure .2)[39,40], while SAXS data shows no Pn3m cubic phase with the model mammalian membrane rich in phosphatidylcholines (PC) (DOPS/DOPE/DOPC = 20/40/40)[31]. Usually, negative Gaussian curvature modulus is negative and therefore acts as a free energy barrier for pore formation. However, lipids with negative intrinsic curvatures, such as PE, can modify the negative Gaussian modulus toward positive. Therefore, the decreased energy barrier gives the AMP selectivity to only destabilize membranes rich in PE. Both eukaryotic and prokaryotic cells have quasi-2D membranes on which the saddle-splay curvature deformations can manifest as pores, blebs, or buds (Figure 1.3)[41]. Confocal microscopy data shows that Crp-4 can cause dye leakage from bacterial membrane models, but negligible dye leakage from mammalian membrane models. Both SAXS studies and confocal microscopy showed selective membrane destabilization induced by AMPs in model membranes rich in PE

(with negative intrinsic curvature) and negligible destabilization in membranes rich in PC (zero intrinsic curvature) (Figure 1.4)[31].

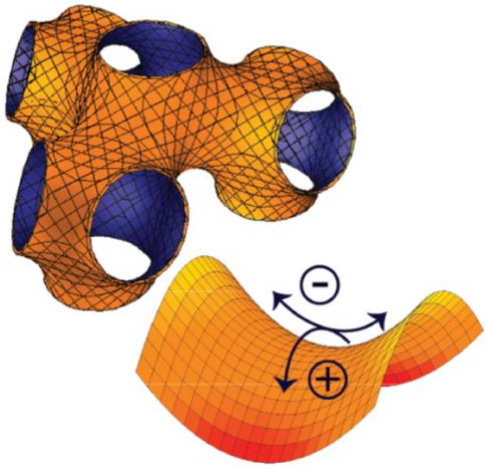

Figure 1.2: (upper left) illustration of the Pn3m cubic phase, (lower right) negative Gaussian curvature requires positive curvature in one direction and negative curvature in the perpendicular direction to locally produce a saddle shape[31].

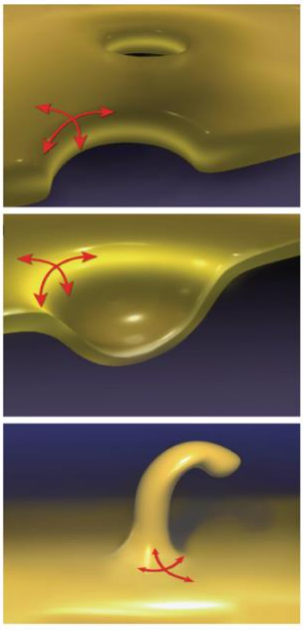

Figure 1.3: negative Gaussian curvature in quasi-2D membranes[41].

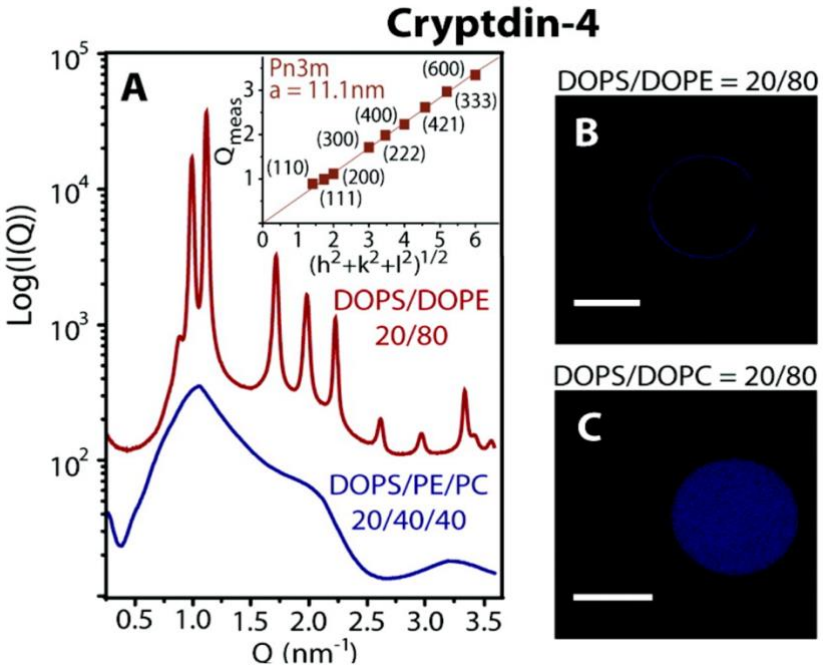

Figure 1.4: Generation of negative Gaussian curvature in model membrane rich in PE, but not in PC by Crp-4, P/L =1/45 (A), Dye leakage happened in vesicle rich in PE (B), but not PC (C). Scale bars are 10 µm.

1.3. Rule of amino acid composition

To retain the ability to induce negative Gaussian curvature on bacterial membranes, significant constraints are placed on the amino acid composition of antimicrobial peptides. AMPs are cationic and coated by counteranions from dissociated salts at the physiological conditions (Manning layer)[42]. The negatively charged bacterial membrane is covered on both sides by a layer of condensed counteractions (Gouy–Chapman layer)[43]. The attraction between the cationic antimicrobial peptides and the anionic bacterial membrane is driven by the entropic gain from the release of condensed counterions. To maximize the strong electrostatic attraction between

the antimicrobial peptide and bacterial cell membrane, the membrane wraps around the AMP, generating negative curvature on the membrane[41]. Moreover, AMPs are amphiphilic allowing the non-polar contents of the AMP to be inserted into the non-polar interior of the lipid bilayer. This increases the hydrophobic volume of the perturbed lipid monolayer and thereby creates positive curvature[23]. The negative curvature, induced by electrostatic interactions, and the positive curvature, created by hydrophobic areas of the AMP, occur perpendicular to each other resulting in the induction of negative Gaussian curvature, which is necessary for membrane destabilization. Three basic amino acids (lysine, histidine and arginine) are responsible for the cationic charge in AMP sequences, but they all work differently[44]. Studies showed that poly-arginine can generate negative Gaussian curvature on the bacterial membrane without hydrophobic compounds in its sequence, but in contrast poly-lysine can only generate negative curvature rather than negative Gaussian curvature. This observed difference in activity can be clearly explained by their structural differences. The guanidinium side group in arginine can form multidentate hydrogen bonds with phosphates in lipid head groups, allowing them to associate with multiple lipid molecules. This multidentate hydrogen bonding creates positive curvature buckling strain, which when combined with negative curvature strain from electrostatic interactions (along an orthogonal direction) generates saddle-splay curvature[45]. In contrast, the amine in lysine can only form monodentate hydrogen bonds, eliminating the possibility to generate positive curvature from buckling. Therefore, poly-lysine only generates negative curvature from electrostatic interactions (Figure 1.5)[46]. Based upon this marked difference, we can deduce a general rule for amino acid composition of antimicrobial peptides. Decreasing arginine content in the AMP sequence will result in less induced negative Gaussian curvature.

This decrease can be compensated for by an increase in the number of lysine residues and ratio of hydrophobic content. A comparison between the amino acid content of β−sheet bonded defensins and α−helical AMPs indicates that the average arginine composition of α−helical AMPs is approximately 50% that of defensins, but the content of hydrophobic amino acids in α−helical AMPs is almost double. Although, the proportion of most hydrophilic amino acids for α−helical AMPs and defensins are similar, the proportion of lysine in α−helical AMPs is almost triple than of defensins. Hence, β−sheet AMPs rely on arginine to generate negative Gaussian curvature, while α−helical AMPs utilize lysine and hydrophobic content (Figure 1.6). This saddle-splay curvature selection rule is observed in 1,080 cationic peptides with known antimicrobial activity[31]. A plot of NK/NR, the ratio of the number of lysine residues to the number of arginine residues, versus % hydrophobic content shows a trend consistent with the saddle-splay curvature selection rule. More sophisticated measurements to quantify peptide hydrophobicity (using three established scales: Kyte-Doolittle[47], Eisenberg Consensus[48], and Wimley-White Biological[49]), show a strong positive correlation between hydrophobicity and log (NK/NR)[50]. The data shows a strong, exponential-like dependence between hydrophobicity and NK/NR, consistent with the saddle-splay curvature selection rule (Figure 1.7)[31].

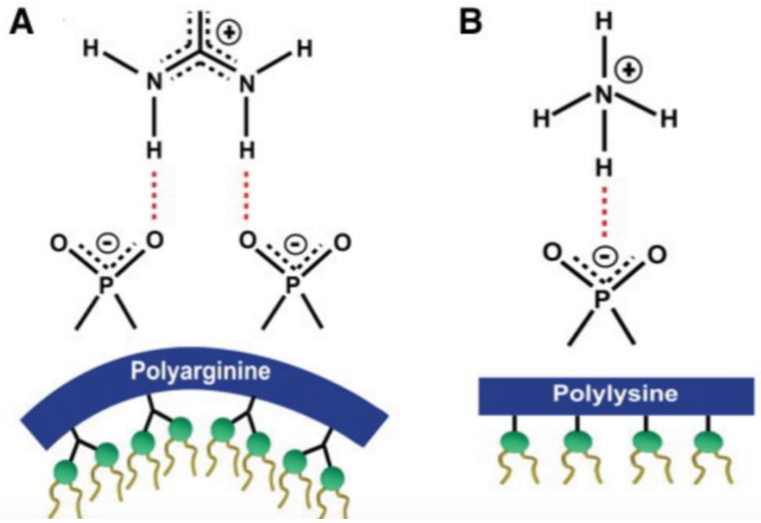

Figure 1.5: Multidentate coordination of arginine's guanidinium side chain (A), monodentate coordination of lysin's amine side chain (B).

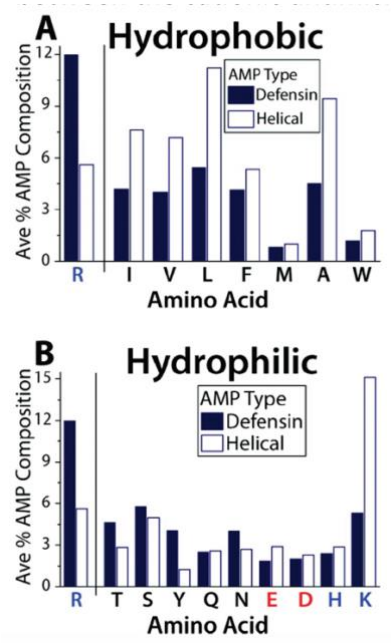

Figure 1.6: On average defensins contain greater amounts of R and less hydrophobic amino acids (A), the proportion of hydrophobic amino acids is comparable in defensins and α− helical AMPs. In contrast K is used 300% more in α−helical AMPs

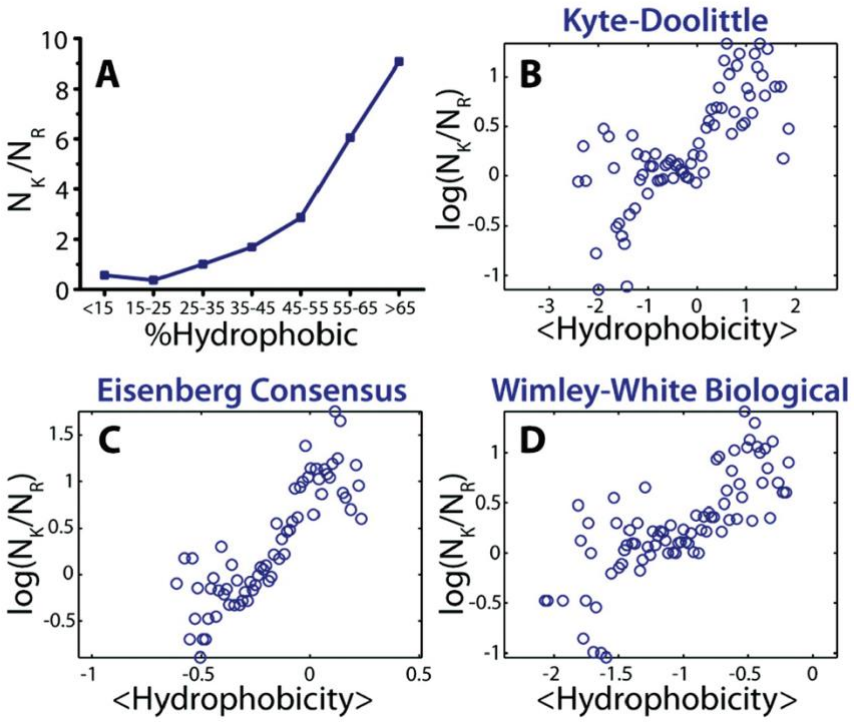

Figure 1.7: Demonstration of the exchange between R with K and hydrophobicity based upon 1080 cationic AMPs in the antimicrobial database. Strong positive dependence between the peptide lysine to arginine ratio and peptide hydrophobicity percentage can be observed (A), More robust calculations of hydrophobicity based upon the Kyte-Doolittle (B), Eisenberg Consensus (C), Wimley-White (D).

1.4. Innovation of our work

We to combined new chemistry and the geometric rules concluded from synchrotron small angle X-ray scattering (SAXS) studies to develop antimicrobials capable of targeting environmental niches for the first time[32,33,34,45,51,52]. The novel modification of specific amino acid side chains in

the AMPs, alters the pK_a and hydrophobicity. Utilizing this new chemistry, we tuned AMPs to target a specific environmental niche depending on the pH of the environment. We used synchrotron small angle x-ray scattering (SAXS) studies to study the interaction of AMPs with model bacterial membranes. SAXS shows the fundamental deformation modes induced in model cell membranes by peptides.

Chapter 2: Modification of individual basic amino acids

2.1. Introduction

If we only utilize naturally-occurring basic amino acids for AMP synthesis, our toolbox would be extremely limited. Except for histidine, all the naturally-occurring basic amino acids are protonated in a wide pH range and even histidine becomes protonated under mildly acidic conditions. Therefore, we altered naturally-occurring amino acids to allow for protonation at lower pH, similar to those observed in pathogenic conditions[53]. We have chosen to modify basic amino acids by adding electron withdrawing and/or hydrophobic groups, as both should decrease the pK_a[54,55,56]. We utilized Michael addition reactions to form α−aminoesters on the side chain of the basic amino acids (Scheme 2.1).

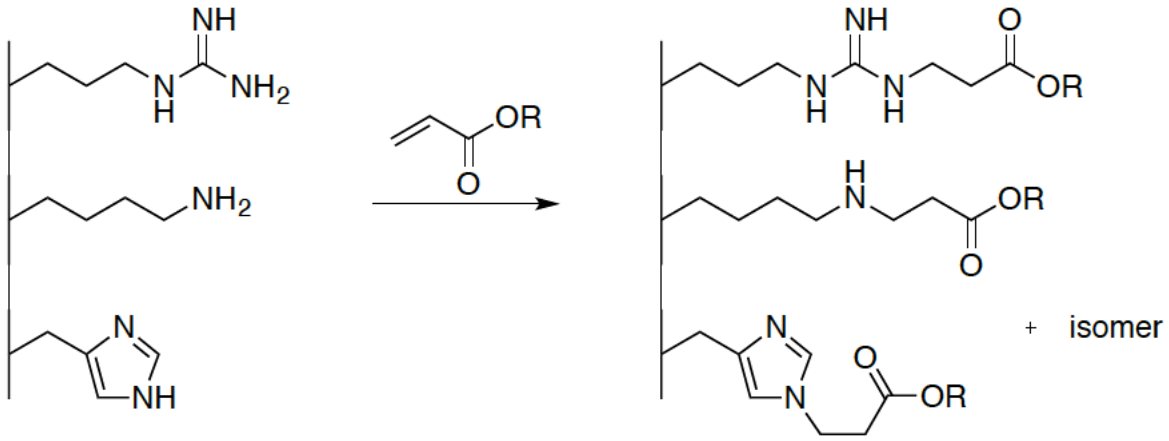

Scheme 2.1: Modification of arginine, lysine and histidine via Michael addition.

2.2. Result and discussion

2.2.1. BOC-Lys-OH modification

First, we attempted to modify lysine via Michael addition using 2-hydroxyethyl acrylate (Scheme 2.2a). ESI-MS confirmed double addition of 2-hydroxyethyl acrylate (Figure 2.1). While conversion of the primary amine of BOC-Lys-OH to a tertiary amine after double addition of 2-hydroxyethyl acrylate can lower the pK_a more than the single addition, the isolated double addition product readily underwent hydrolysis (Figure 2.1). The basic reaction conditions favored ester bond hydrolysis,[60] leaving two carboxylic acid groups on the isolated product (Scheme 2.2a). The pK_a of carboxylic acids is typically about 2.5, depending on the identity of the side chain the carboxylic acid group is attached to. Therefore, this functional group will be deprotonated under almost all physiological conditions, yielding basic amino acids with negative charges rather than the desired positive charge. In an attempt to minimize hydrolysis, carbonate buffers with pH 9 to 10 were used. To lower the reaction pH even more, borate buffers with pH 8,8.5, and 9 were also utilized. However, in all cases hydrolysis occurred after 2-hydroxyethyl acrylate was reacted with BOC-Lys-OH.

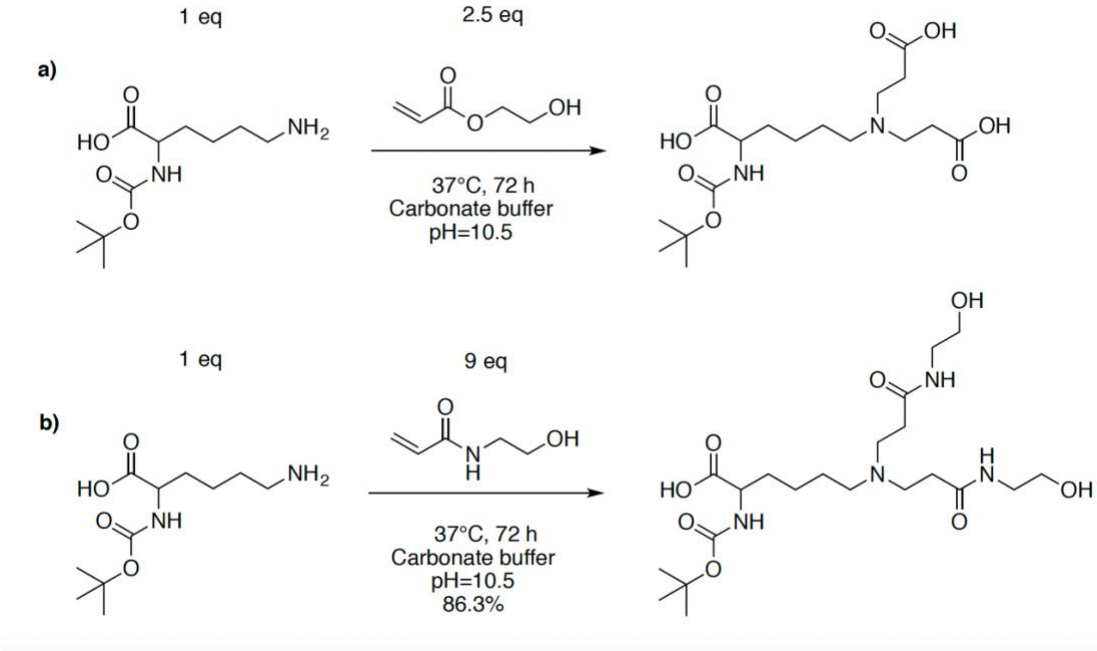

Scheme 2.2: Modification of BOC-Lys-OH with 2-hydroxyethyl acrylate (a) and modification of BOC-Lys-OH with N-hydroxyethyl acrylamide (b).

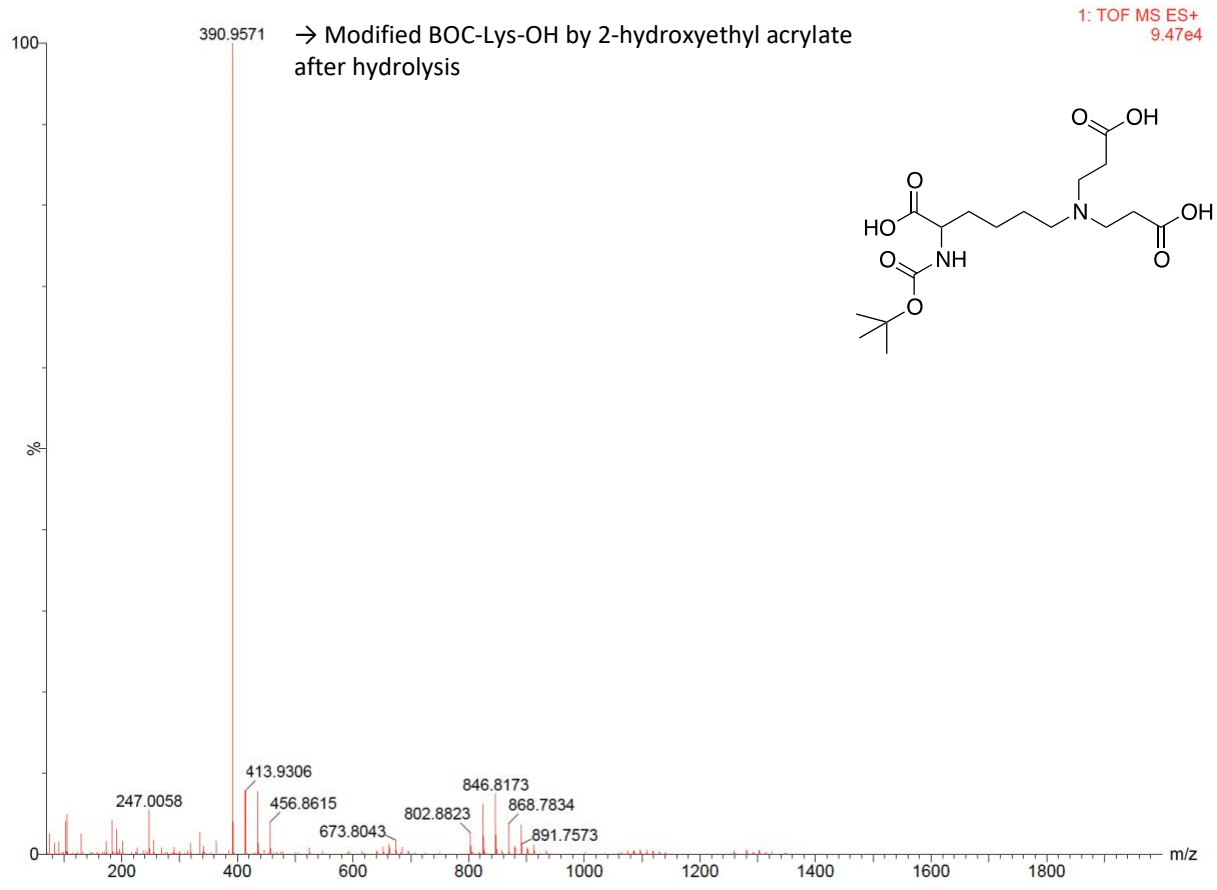

Figure 2.1: ESI-MS result of BOC-Lys-OH modification with 2-hydroxyethyl acrylate

In another attempt to eliminate the degradation side reaction, 2-hydroxyethyl acrylate was replaced with *N*-hydroxyethyl acrylamide (Scheme 2.2b). *N*-hydroxyethyl acrylamide features an amide bond instead of an ester bond, making it more stable against hydrolysis.[61]As expected, ESI-EM data, demonstrated that hydrolysis did not occur in the modification of BOC-Lys-OH with *N*-hydroxyethyl acrylamide (Figure 2.2). The final compound was purified using reverse-phase HPLC to give the final product in 86.3% yield.

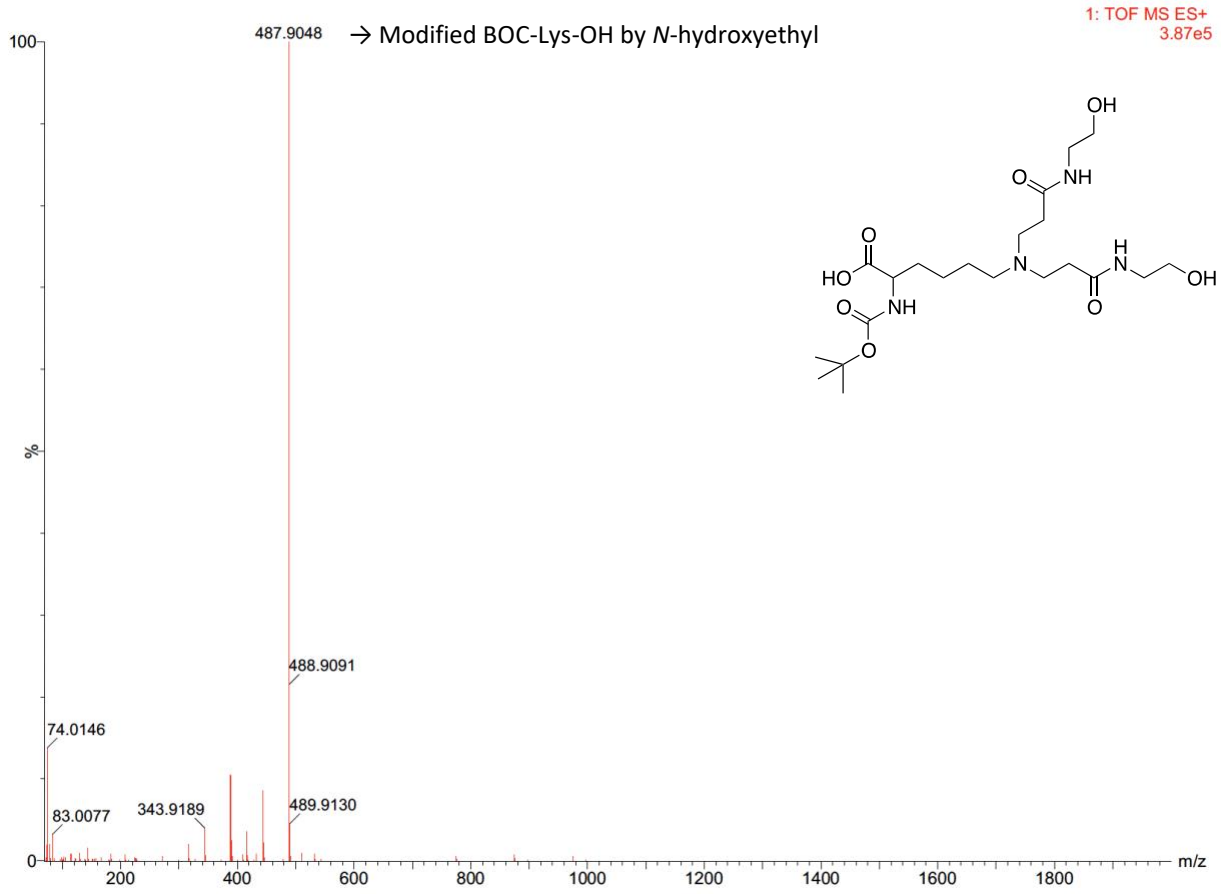

Figure 2.2: ESI-MS result of BOC-Lys-OH modification with and N-hydroxyethyl acrylamide.

2.2.2. BOC-His-OH modification

To modify BOC-His-OH, we first attempted the Michael addition via 2-hydroxyethyl acrylate (Scheme 2.3a). While only a single addition was expected for BOC-His-OH modification with 2-hydroxyethyl acrylate, a second Michael addition was possible due to resonance. The second Michael addition renders the imidazole positively charged regardless of the environmental pH. As the goal was to lower the pK_a through conjugation, making basic amino acids selectively positively charged at lower pH, the isolated modified BOC-His-OH did not suit the purpose of our

project. In an attempt to reduce the reactivity of the imidazole amine, pH 6.7 PBS buffer was used as the reaction solvent, but the result was the same. Based on previous success with lysine, reactions with *N*-hydroxyethyl acrylamide were also attempted as the Michael acceptor (Scheme 2.3b). However, despite using identical conditions, no reaction had occurred even after 72 hours at 37°C. To avoid the possibility of getting double addition of 2-hydroxyethy acrylate on the imidazole ring, BOC-His-OH was substituted by BOC-His (BOC)-OH (Scheme 2.4). The reaction was performed in DCM due to insolubility of BOC-His (BOC)-OH in water . ESI-MS showed no reaction between BOC-His (BOC)-OH and 2-hydroxyethy acrylate. Since the pK_a of imidazole in histidine (pK_a 6.45) is close to the physiological pH (pH 7.4), modification of histidine would not have as significant impact as lysine and arginine with higher pK_as, 10.2 and 12.5, respectively. Therefore, we decided to focus on lysine and arginine modifications.

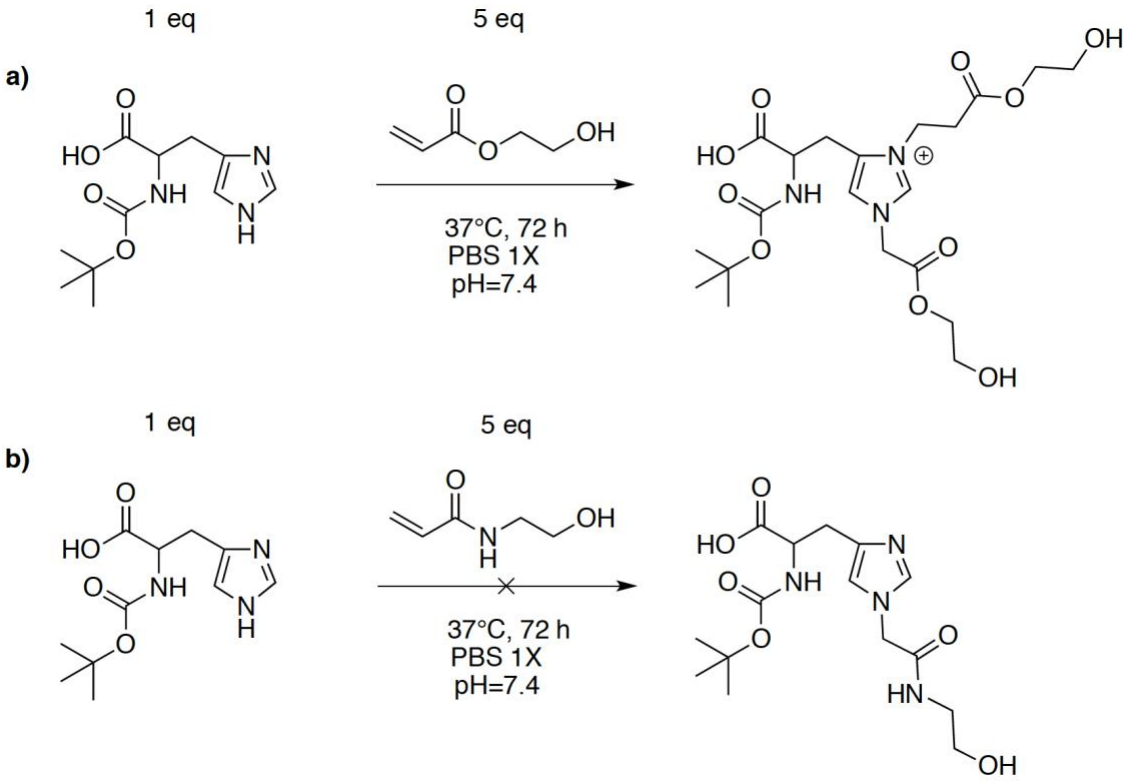

Scheme 2.3: Modification of BOC-His-OH with 2-hydroxyethyl acrylate (a) and modification of BOC-His-OH with N-hydroxyethyl acrylamide (b).

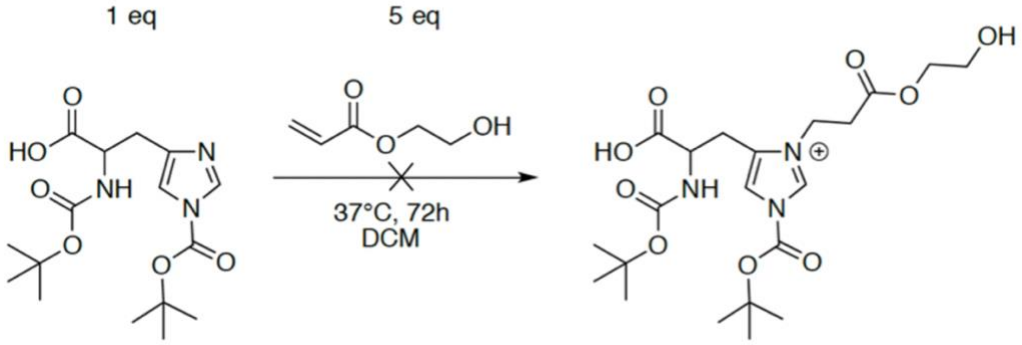

Scheme 2.4: Modification of BOC-His (BOC)-OH with 2-hydroxyethyl acrylate.

2.2.3. BOC-Arg-OH modification

We attempted to modify BOC-Arg-OH via Michael addition (Scheme 2.5). However, the Michael additions by 2-hydroxyethyl acrylate (Scheme 2.5a) and N-hydroxyethyl acrylamide (Scheme 2.5b) did not worked for modification of guanidinium group in BOC-Arg-OH. Another method to generate a highly basic reaction solution for Michael addition, is to use highly basic catalysts such a Barton's base. This method was attempted to modify BOC-Arg-OH (Scheme 2.5c). However, Michael addition did not happen even in this highly basic condition. Since Michael addition did not work in different reaction conditions for BOC-Arg-OH, the addition reaction with glyoxal has been performed (Scheme 2.6). The two hydroxyl groups in the modified guanidinium are electron withdrawing (due to the lack of resonance in the ring) and therefor can lower the pK_a of guanidinium in BOC-Arg-OH. ESI-MS confirmed the addition of glyoxal to BOC-Arg-OH (Figure 2.3). The final product was purified by reverse-phase HPLC, giving the product in 71.6% yield.

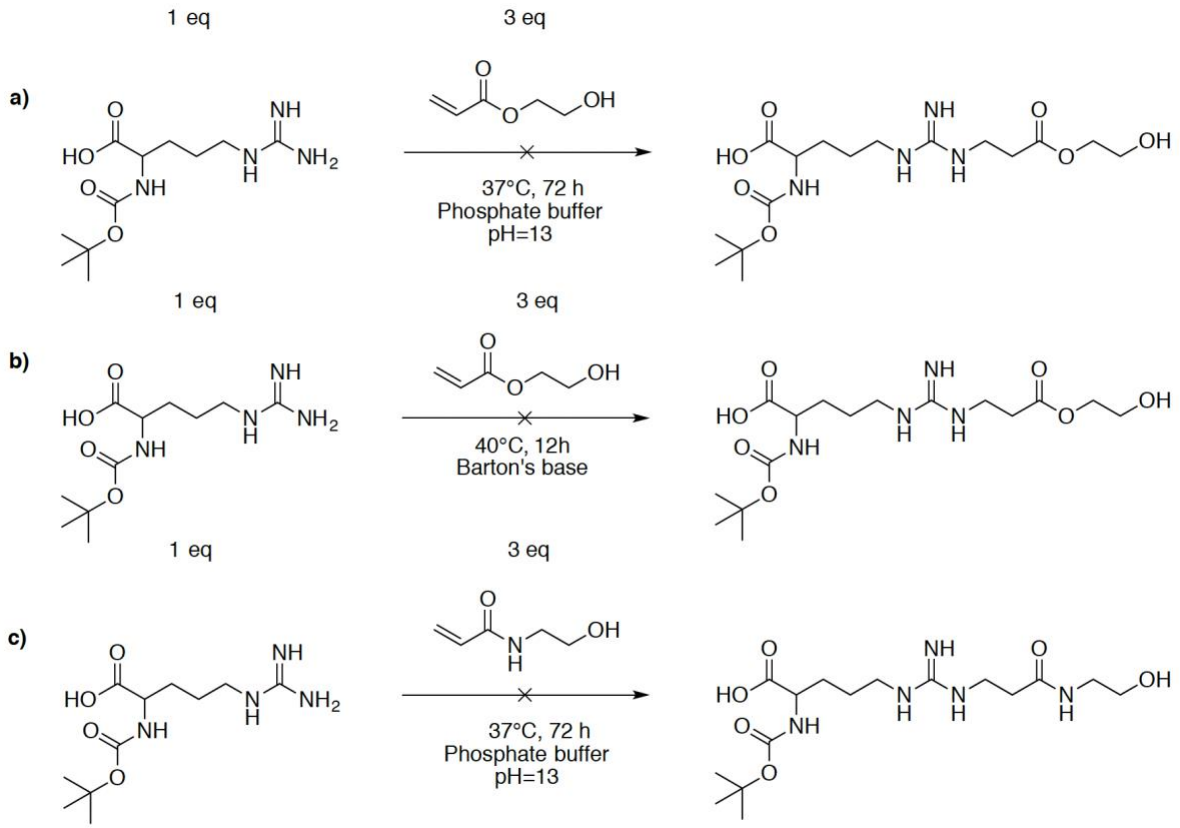

Scheme 2.5: Modification of BOC-Arg-OH with 2-hydroxyethyl acrylate (a), modification of BOC-Arg-OH with 2-hydroxyethyl acrylate by using Barton's base via Michael addition (b) and Modification of BOC-Arg-OH with N-hydroxyethyl acrylamide (c).

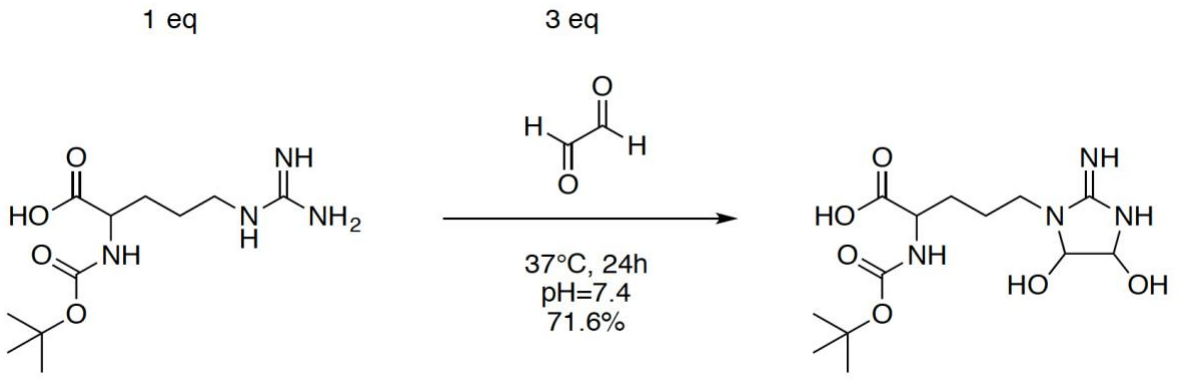

Scheme 2.6: Modification of BOC-Arg-OH with glyoxal.

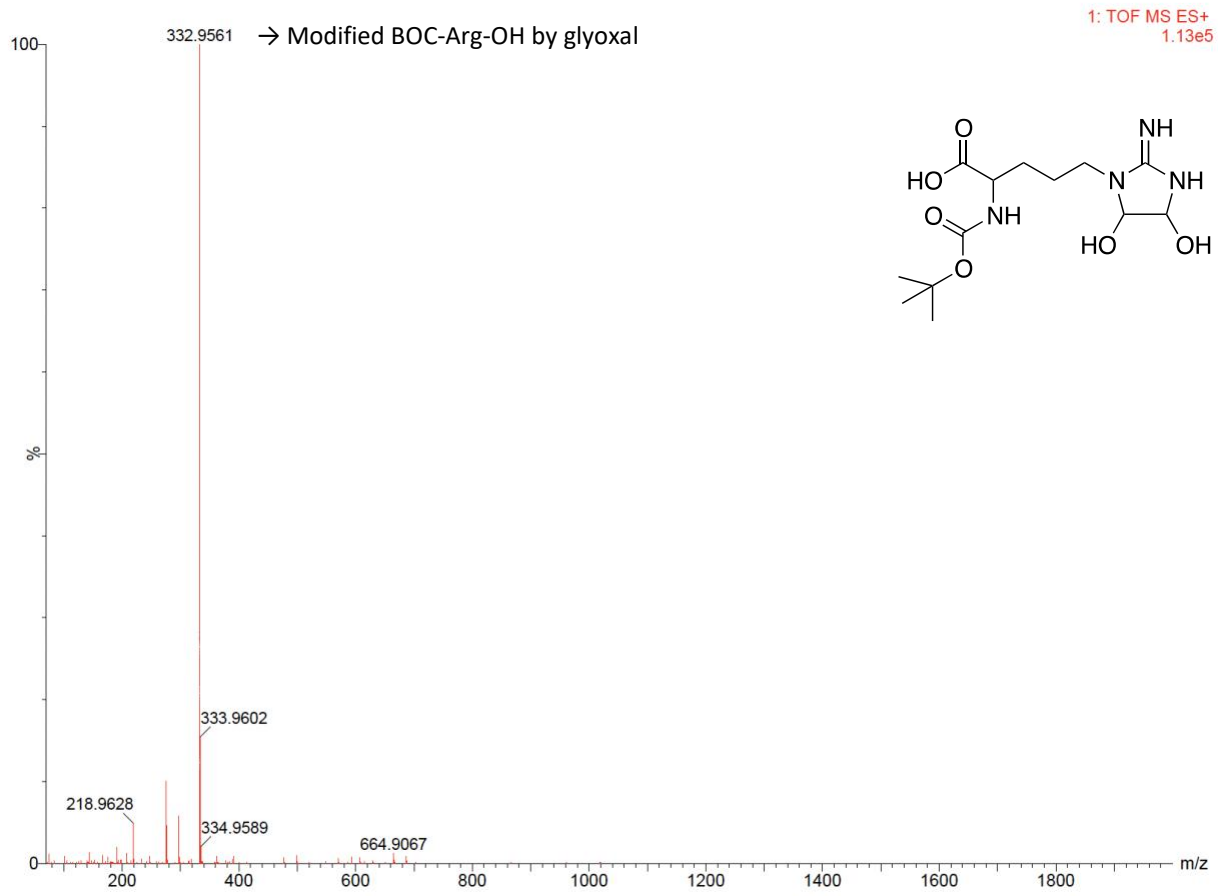

Figure 2.3: ESI-MS result of BOC-Arg-OH modification with glyoxal.

The modification of BOC-Arg-OH with glyoxal had a significant impact on our project. As mentioned before, we were not able to modify BOC-Arg-OH by *N*-hydroxyethyl acrylamide. However, the modification of BOC-Lys-OH with *N*-hydroxyethyl acrylamide was successful (yield 86.3%). On the other hand, while the addition of glyoxal to BOC-Arg-OH was successful, this compound did not go through reaction with BOC-Lys-OH (Scheme 2.7 and Figure 2.4). This result confirms the orthogonal modification of BOC-Lys-OH and BOC-Arg-OH (Table 2.1).

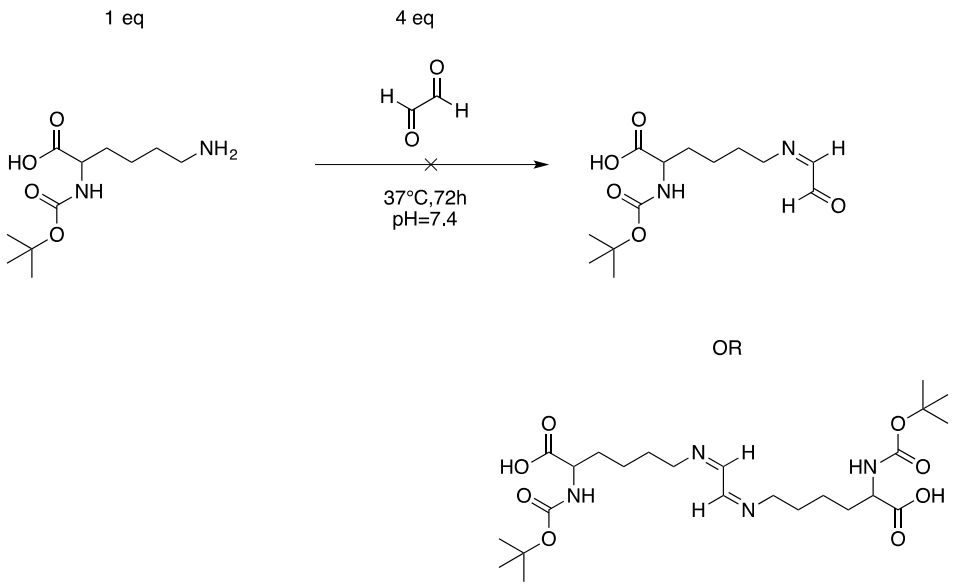

Scheme 2.7: Modification of BOC-Lys-OH by glyoxal.

Table 2.1 Orthogonality in the modification of lysine and arginine (reaction yields in %).

	***N*-Hydroxyethyl acrylamide**	**Glyoxal**
BOC-Lys-OH	86.3%	-
BOC-Arg-OH	-	71.6%

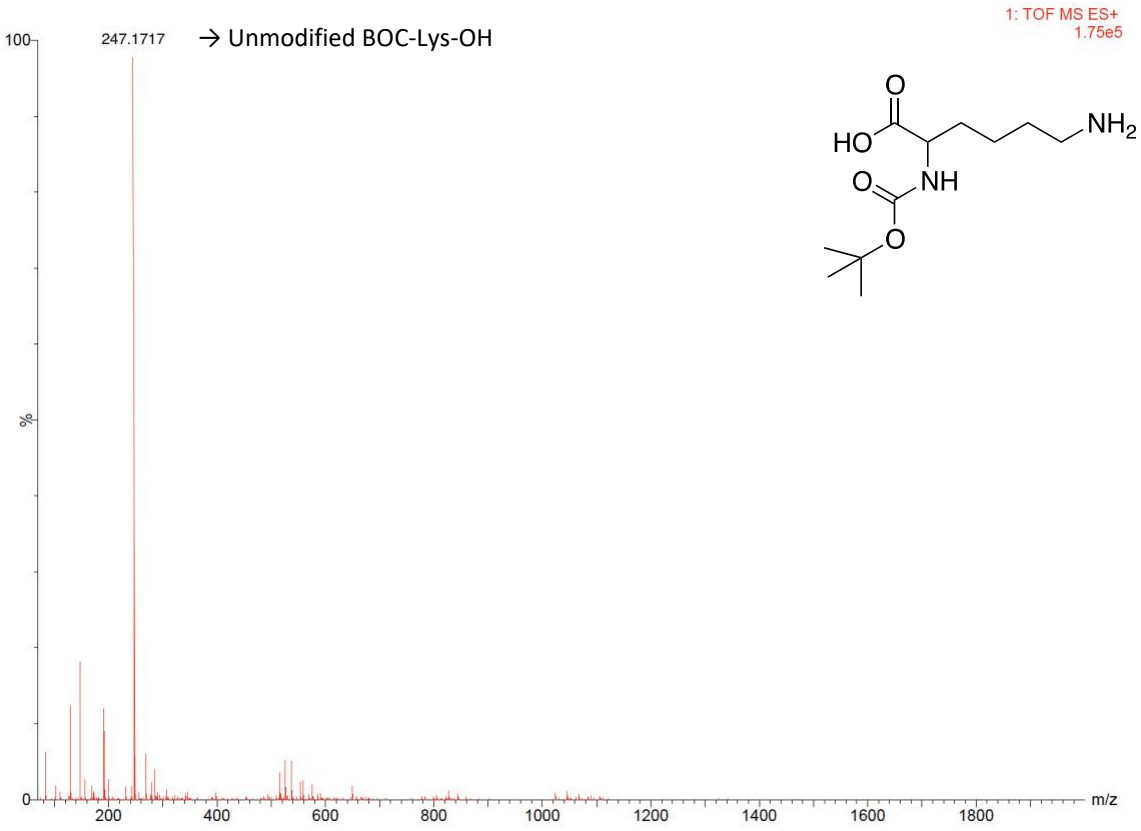

Figure 2.4: ESI-MS result of BOC-Lys-OH modification with glyoxal.

2.2.4. Modified BOC-Lys-OH modification and BOC-Arg-OH modification pK_a measurement

The goal was to lower the pK_a of amine and guanidinium in the lysine and arginine side chains, respectively. Hence, the pK_as of unmodified lysine and arginine were measured and compared with modified versions. In case of lysine, the pk_a of the primary amine in the side chain of unmodified compound was compared to the tertiary amine in modified lysine (Scheme 2.8). According to the titration curve of BOC-Lys-OH (unmodified lysine), the primary amine has pK_a=10.4 and the carboxyl group has pK_a=3.2. However, after modification with *N*-hydroxyethyl acrylamide the pK_a of the amine (tertiary amine in the modified version) dropped to 8.7 (Figure

2.5). After modification of BOC-Lys-OH other pK_as appeared on the curve that are related to the amide bond of *N*-hydroxyethyl acrylamide in modified lysine (pK_a=12.2) and the carboxy group (pK_a=4.5) (Figure 2.5). About arginine, the pk_a of the guanidinium in the side chain of unmodified version was compared to the modified one (Scheme 2.9). As shown in the titration curve of BOC-Arg-OH (unmodified arginine), guanidinium has pK_a=12 and the carboxyl group has pK_a=3.2 but after modification with glyoxal the pK_a of the modified guanidinium dropped to 9.3 (Figure 2.6). In addition, pKa of carboxyl group in the modified version changed to 5.4 (Figure 2.6)

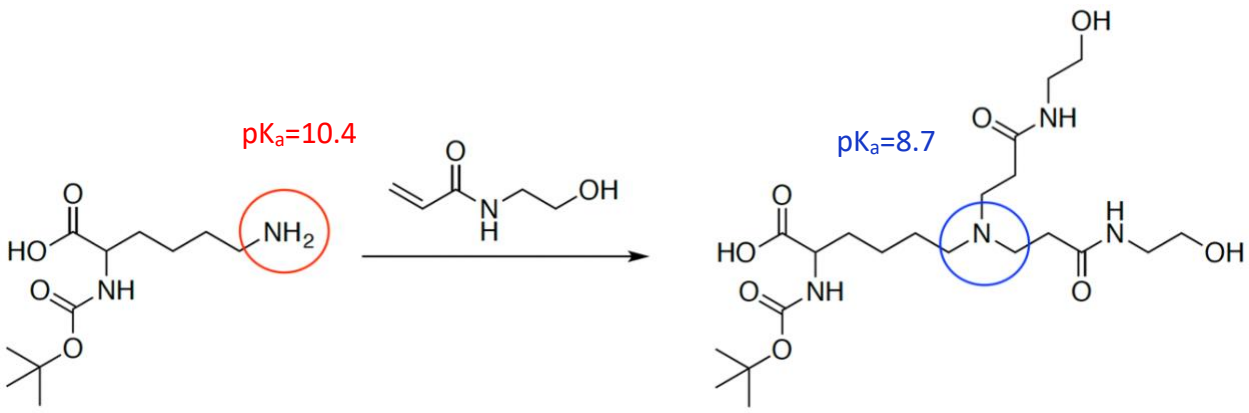

Scheme 2.8: Demonstration of the primary amin pK_a change in modification to tertiary amine.

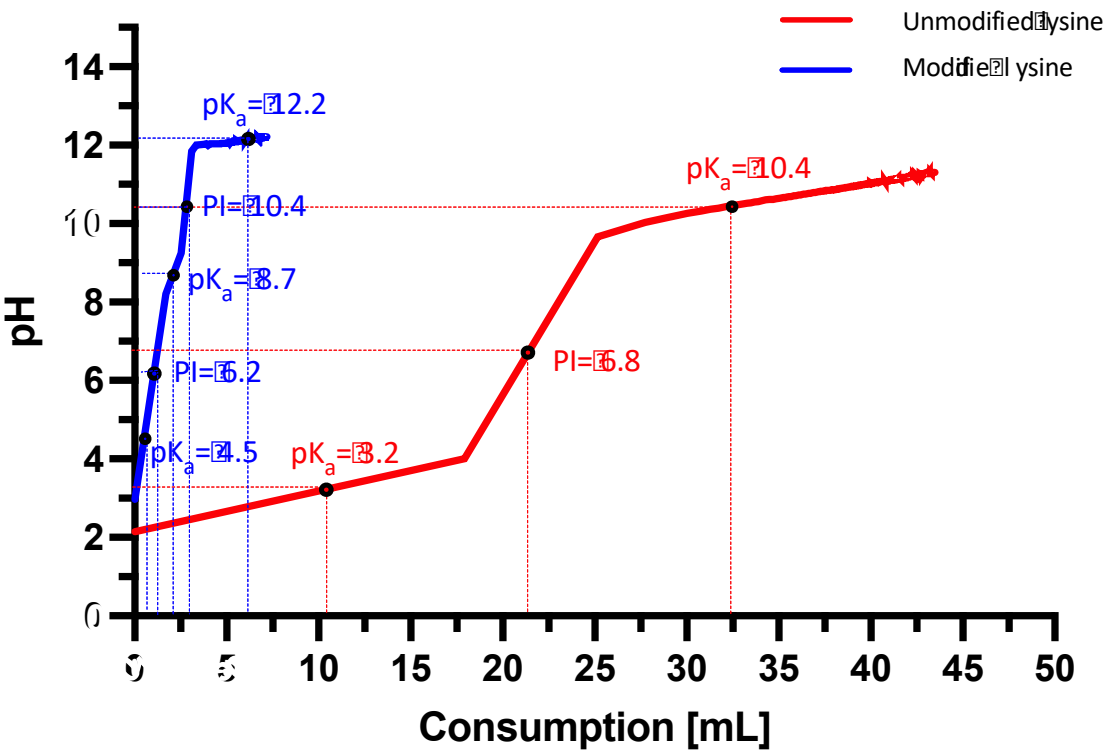

Figure 2.5: Unmodified lysine vs modified lysine titration curve.

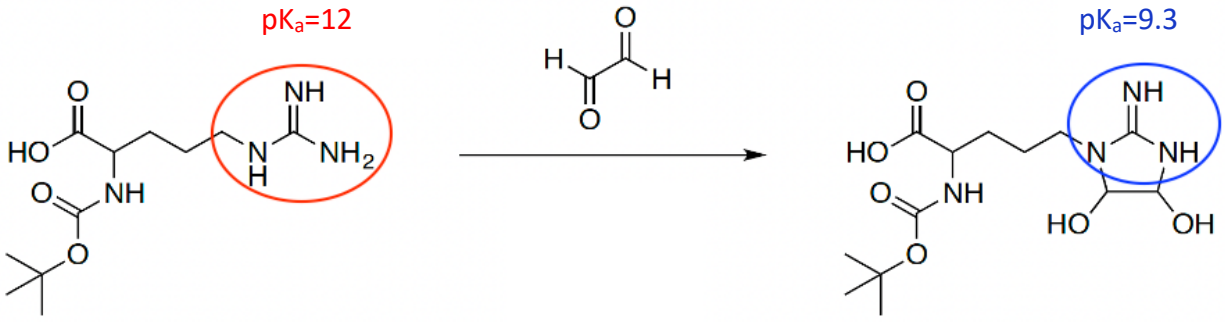

Scheme 2.9: Demonstration of the guanidinium pK_a change in modification by glyoxal.

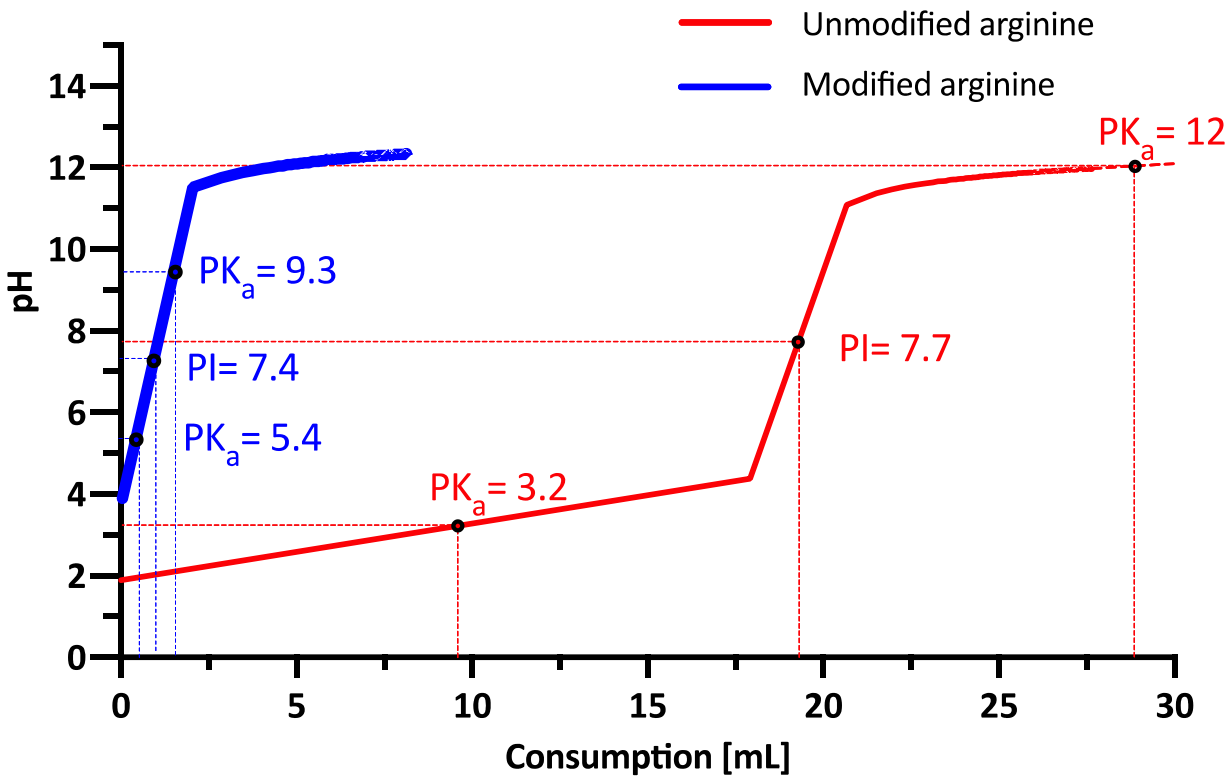

Figure 2.6: Unmodified arginine vs modified arginine titration curve.

2.3. Material and method

2.3.1. Material

BOC-Lys-OH, BOC-His-OH, BOC-His (BOC)-OH, BOC-Arg-OH (AAPPTec). 2-hydroxyethyl acrylate, *N*-hydroxyethyl acrylamide (Aldrich). Dichloromethane (DCM) (Fisher Scientific). Triethylamine (TEA) (Alfa Aesar). Carbonate buffer, Phosphate buffer, Phosphate-buffered saline (PBS), glyoxal (Sigma-Aldrich). 2-tert-Butyl-1,1,3,3-tetramethylguanidine (Barton's base) (Sigma).

2.3.2. Modification of lysine

2.3.2.1. BOC-Lys-OH modification by 2-hydroxyethyl acrylate

pH 10.5 carbonate buffer was chosen as the reaction solvent. Michael addition was Performed with 2-hydroxyethyl acrylate (1 equiv) as the Michael acceptor. After 72 hours at 37°C, an aliquot was taken to check conversion to the desired product. Based on electrospray mass spectrometry data (ES-MS) (Waters LCT Premier with ACQUITY LC and autosampler), the reaction was not complete and a significant amount of unreacted BOC-Lys-OH remained in the reaction solution. To increase conversion, additional 1.5 equivalents of 2-hydroxyethyl acrylate was added to the reaction mixture. After another 24 hours at 37°C, ES-MS confirmed reaction completion.

2.3.2.2. BOC-Lys-OH modification by *N*-hydroxyethyl acrylamide

pH 10.5 carbonate buffer was used as the reaction solvent. *N*-hydroxyethyl acrylamide was added (9 equiv). After 72 hours at 37°C, the reaction was complete based on ESI-MS data.

2.3.3. Modification of histidine

2.3.3.1. BOC-His-OH modification by 2-hydroxyethyl acrylate

pH 7.4 PBS was selected as the buffer for the reaction. 2-hydroxyethyl acrylate was selected as the Michael acceptor (5 equiv). After 72 hours at 37°C, completion of the reaction was confirmed by ESI-MS.

2.3.3.2. BOC-His-OH modification by 2-hydroxyethyl acrylate

pH 7.4 PBS was used as the reaction solvent. 2-hydroxyethyl acrylate was added (5 equiv). After 72 hours at 37°C, no reaction happened based on ESI-MS data.

2.3.3.3. BOC-His (BOC)-OH modification by *N*-hydroxyethyl acrylamide

As BOC-His (BOC)-OH was not soluble in water, DCM was used as the solvent and TEA was added dropwise to yield basic reaction conditions (pH 8-9). *N*-hydroxyethyl acrylamide was added (9 equiv). ESI-MS confirmed no reaction had occurred for BOC-His (BOC)-OH modification by *N*-hydroxyethyl acrylamide after 72 hours at 37°C.

2.3.4. Modification of arginine

2.3.4.1. BOC-Arg-OH modification by 2-hydroxyethyl acrylate

Sodium phosphate buffer (pH 13) was used as the solvent. 2-hydroxyethyl acrylate as the Michael acceptor was used (3 equiv). After 72 hours at 37°C, no reaction was observed between BOC-Arg-OH and 2-hydroxyethyl acrylate.

2.3.4.2. BOC-Arg-OH modification by 2-hydroxyethyl acrylate

The addition reaction with *N*-hydroxyethyl acrylamide was also attempted but showed no reaction with BOC-Arg-OH in the previously described reaction condition.

2.3.4.3. BOC-Arg-OH modification, using Barton's base

Barton's base as a highly basic catalysts was used in water. After 12 hours at 40°C, BOC-Arg-OH remained unreacted. The addition reaction with *N*-hydroxyethyl acrylamide was also attempted but showed no reaction with BOC-Arg-OH in the previously described reaction condition

2.3.4.4. BOC-Arg-OH modification by glyoxal

At neutral condition, glyoxal (3 equiv) was added to BOC-Arg-OH. After 24 hours at 37°C, ESI-MS confirmed the addition of glyoxal to BOC-Arg-OH (71.6% yield)

2.3.5. Reverse-Phase high performance liquid chromatography (RP-HPLC)

Modified BOC-Lys-OH and BOC-Arg-OH were purified by preparative RP-HPLC (JASCO system) at 17 mL/ min on a Waters C18 column (250 Å~ 22 mm, 5 mm) using a gradient of A [H_2O + 0.1% TFA] and B [CH_3CN + 0.1% TFA]: 0% of B for 5 min, 0% → 100% for 36 min and then 100% for 5 min; detection at 214nm. Acetonitrile was evaporated under reduced pressure and the aqueous solution was freeze-dried (LABCONCO FreeZone 4.5) to give a white solid (86.3% for BOC-Lys-OH and 71.6% for BOC-Arg-OH).

2.3.6. pK_a Measurement of modified basic amino acids

Titration was performed on the pure modified BOC-Lys-OH and BOC-Arg-OH to confirm the change in the pK_a values of the side chain functional groups, amine and guanidinium, respectively. Titration was performed by METLER TOLLEDO EasyPlus^{TM} (setting: end point (EP) and extra cautious) with 0.1M NaOH as the titrant.

2.4. Conclusion

Through various modification reactions, we were able to lower the pK_as of the side chain functional groups of BOC-Lys-OH (10.4 → 87) and BOC-Arg-OH (12 → 9.3). In addition, we found conditions yielding orthogonality in the modification of lysine and arginine. Unlike histidine, lysine and arginine both feature side chains with high pK_a, 10.2 and 12.5, respectively. Lowering the pK_a of the functional groups on their side chains could significantly alter the selectivity of the AMP. As the initial pK_a of lysine and arginine side groups are relatively close to one another, identifying conditions to achieve orthogonality in their modifications was less probable. However, the nonreactivity of the guanidinium, found in arginine with Michael acceptors, such as *N*-hydroxyethyl acrylamide, resulted in the orthogonal modification of arginine and lysine.

Chapter 3: Modification of basic amino acids in peptide sequence

3.1. Introduction

we have demonstrated the ability to modify individual amino basic acids (lysine and arginine), in chapter 2, under orthogonal reaction conditions. In this chapter, we demonstrate the orthogonal modification of lysine and arginine on peptides instead of individual amino acids. Modification of amino acids while they are in peptide sequences is more efficient and cheaper than modification of each individual amino acids. In fact, if we perform the modifications while the amino acids are already a part of a peptide sequence, we can perform one step purification of the final compound; however, if we modify each amino acid first and then include the modified amino acids into a peptide sequence, then we would need at least two step purification, one for purifying the individual amino acid and second for purification of the final product. Moreover, as a result of our orthogonal modification conditions, we would be possible to perform a one-pot modification of lysine and arginine which is less complicated and expensive than trying each modification separately. Magainin 2 and ZY13 as broad-spectrum natural and synthetic AMPs, respectively, were chosen to show our ability to modify lysine and arginine, orthogonally, in AMP sequences. Magainin 2[62] has four basic lysines in its sequence, making the peptide positively charged. ZY13[63] has six lysines and two arginines in its residues (Figure 3.1). By lowering the pK_a of the amine side group on lysines and guanidinium on arginines through chemical modification, antimicrobial activity could be limited to a lower and more specific pHs. These proof of concept experiments can then be applied to other AMPs for tuning their antimicrobial activities.

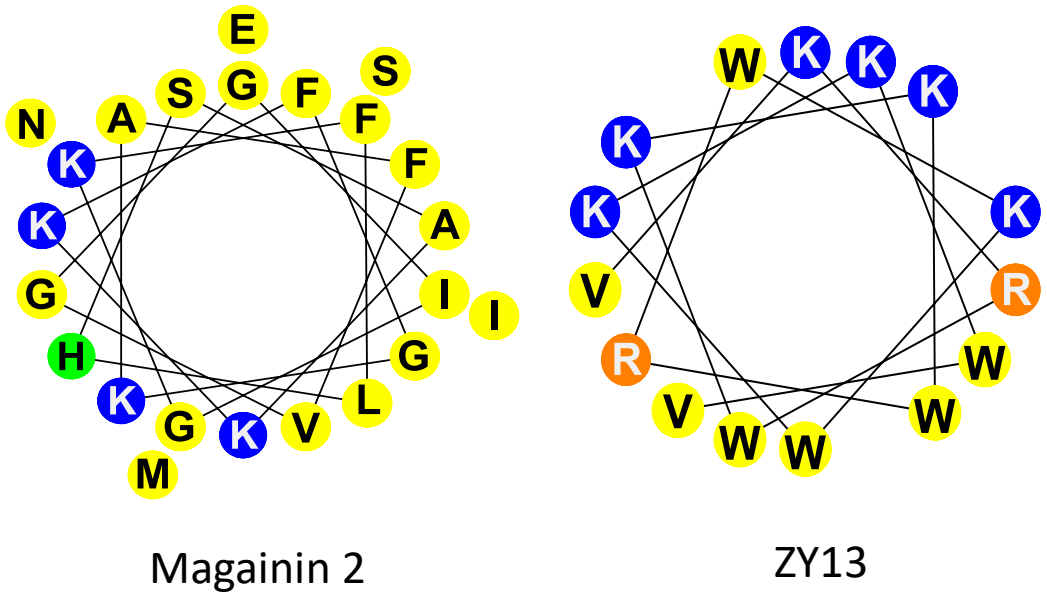

Figure 3.1: Helical wheel projection of Magainin 2 and ZY13.

3.2. Results and discussion

3.2.1. Modification of lysine in GKGRG

GKGRG is a short synthetic peptide containing only one lysine and one arginine. We designed GKGRG in order to assess the orthogonal modification of lysine and arginine while they are part of a peptide sequence. The glycines worked as spacers for the short peptide since there was no functional group on glycine side chain which can interfere with orthogonal modification of lysine and arginine. After modification of lysine residues of GKGRG (Scheme 3.1), purification by preparative mode of RF-HPLC was performed. The peptide composition's retention time was between 10 min and 11 min (Figure 3.2). At 10.28 min and 10.45 min, two peaks, fraction 1 and fraction 2, were collected. Both fractions were characterized by ESI-MS. ESI-MS confirmed the conjugation of lysine with *N*-hydroxyethyl acrylamide (Figure 3.3). However, for both fractions

we obtained a peptide complex instead of only one molecular weight. In fact, there were different molecular weight possibilities for the final compound in modification of lysines in GKGRG (Scheme 3.1). The primary amine of lysine in GKGRG could go through single or double addition of *N*-hydroxyethyl acrylamide. Moreover, there was a primary amine at the *N*-terminal of GKGRG which as well could go through single or double addition of *N*-hydroxyethyl acrylamide. After purification of the final compounds, ESI-MS showed single, double and triple addition of *N*-hydroxyethyl acrylamide to the primary amines in GKGRG sequence in both fraction 1 and 2 (F1 and F2) (the same molecular weights were observed in both fractions). We used different RF-HPLC methods to be able to have one molecular weight for each fraction; however, even with more separate peaks still the same compounds appeared in both fractions.

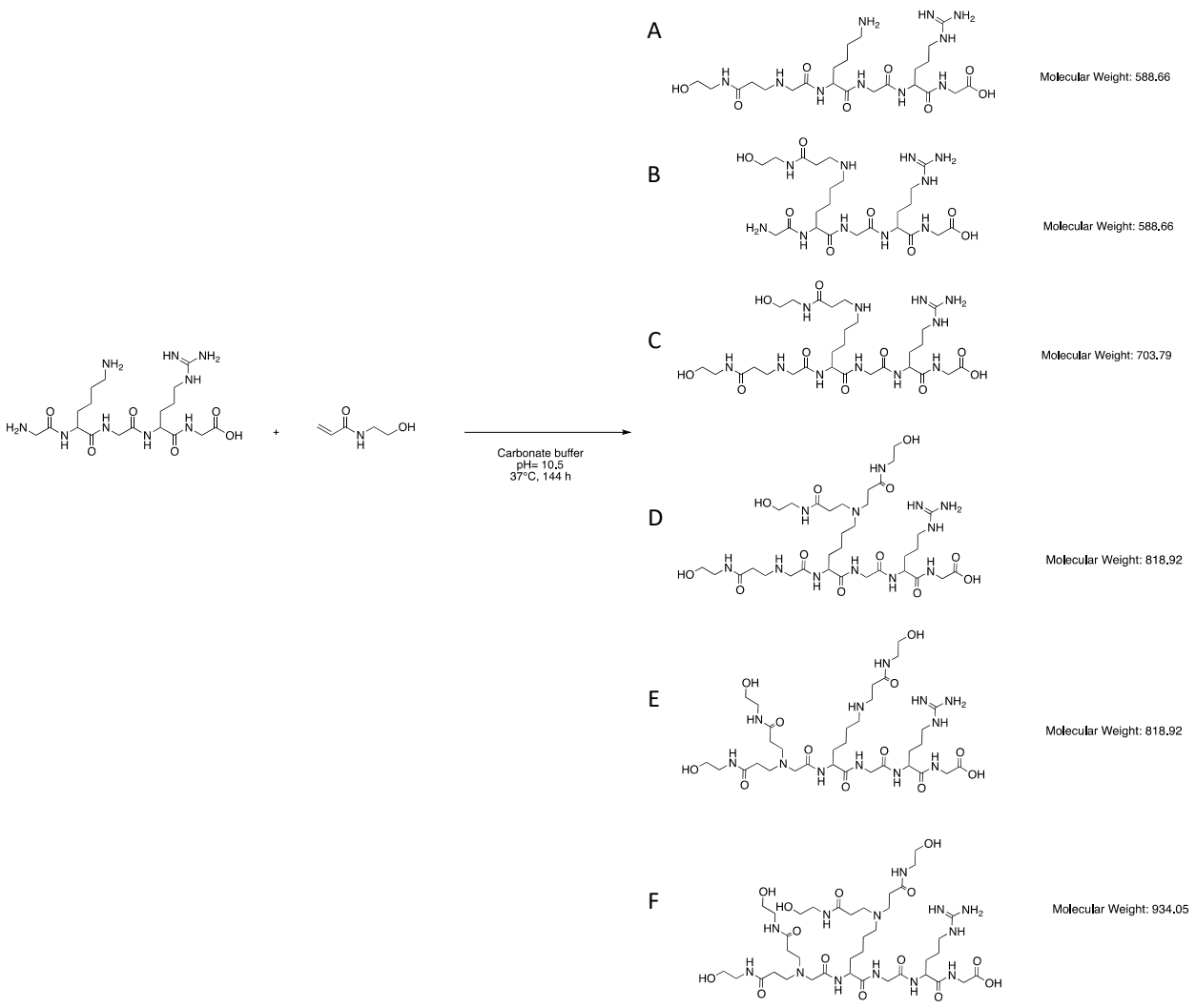

Scheme 3.1: Modification of lysine in GKGRG and different possibilities.

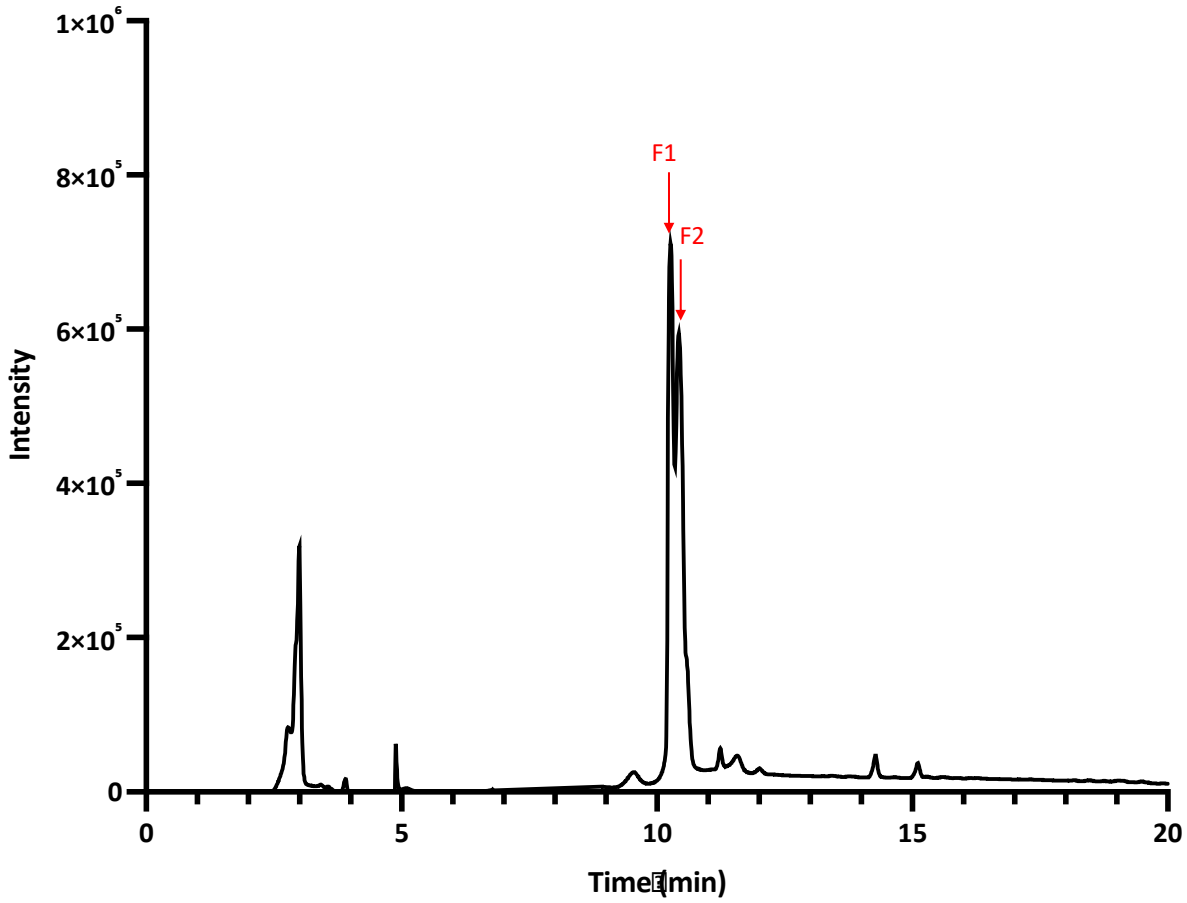

Figure 3.2: Preparative RF-HPLC spectrum for modification of lysine in GKGRG.

Figure 3.1D,E

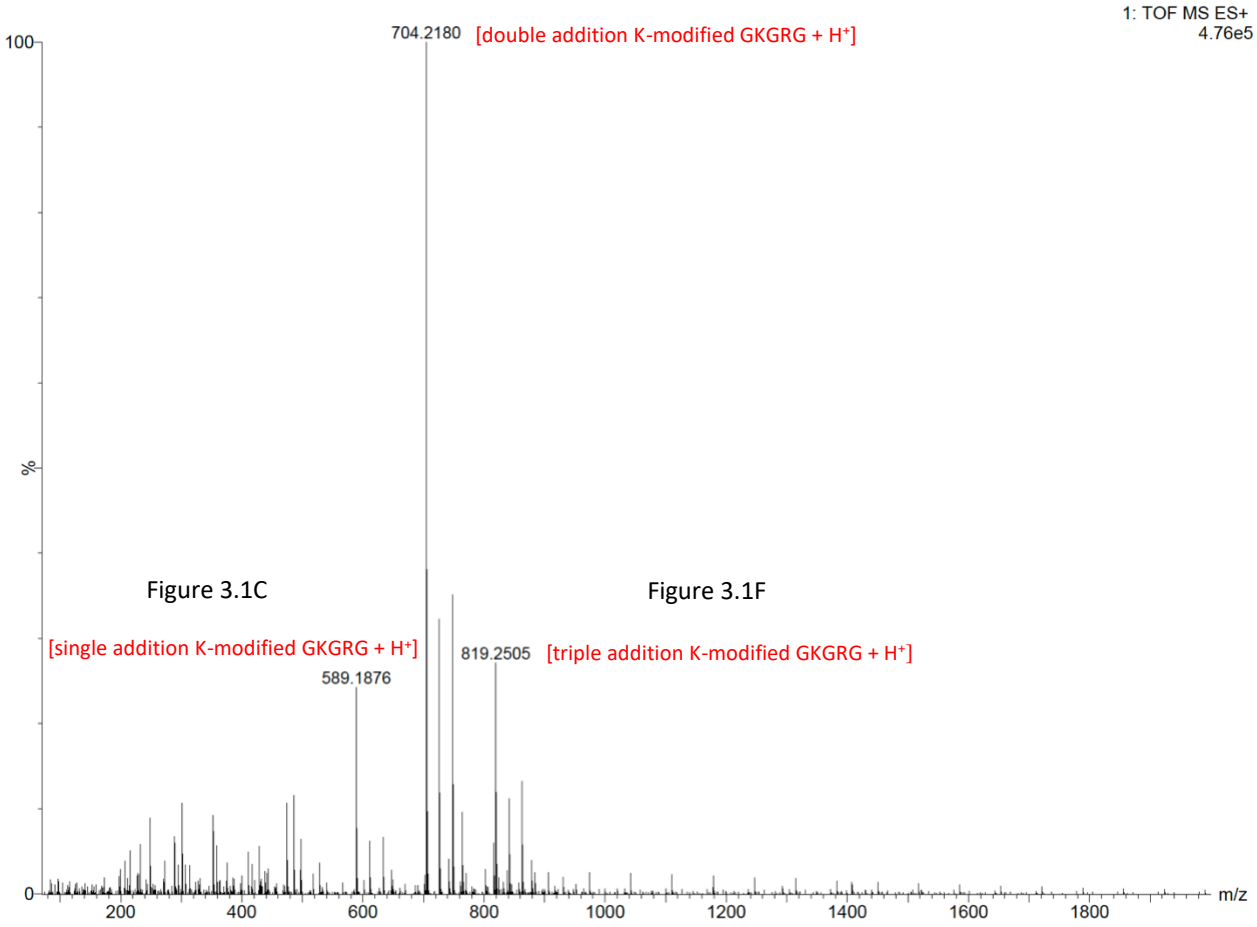

Figure 3.3: ESI-MS spectrum of modification of lysine in GKGRG

3.2.2. Modification of arginine in GKGRG

GKGRG had only one arginine in its sequence which could be modified by glyoxal. After modification of arginine in GKGRG (Scheme 3.2), purification was performed by preparative mode of RF-HPLC (Figure 3.4). Even though, there was just one expected product for this reaction, RP-HPLC showed five different peaks between 9.9-12.4 min. All five fractions were collected and mass spectroscopy was performed to characterize the fractions. ESI-MS confirmed the conjugation of arginine and glyoxal (Figure 3.5). In addition, there is just one molecular weight

was observed in all five fractions (F1:10.35, F2:10.36, F3:10.71, F4:11.2 and F5:11.31) by ESI_MS which belonged to R- modified GKGRG accepting a positive charge in the form of H^+ and Na^+.

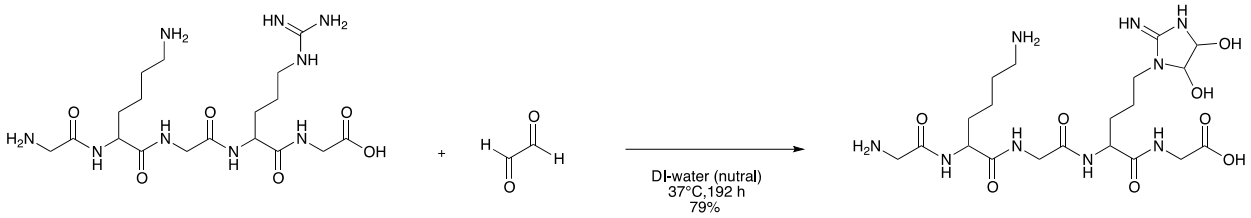

Scheme 3.2: Modification of arginine in GKGRG.

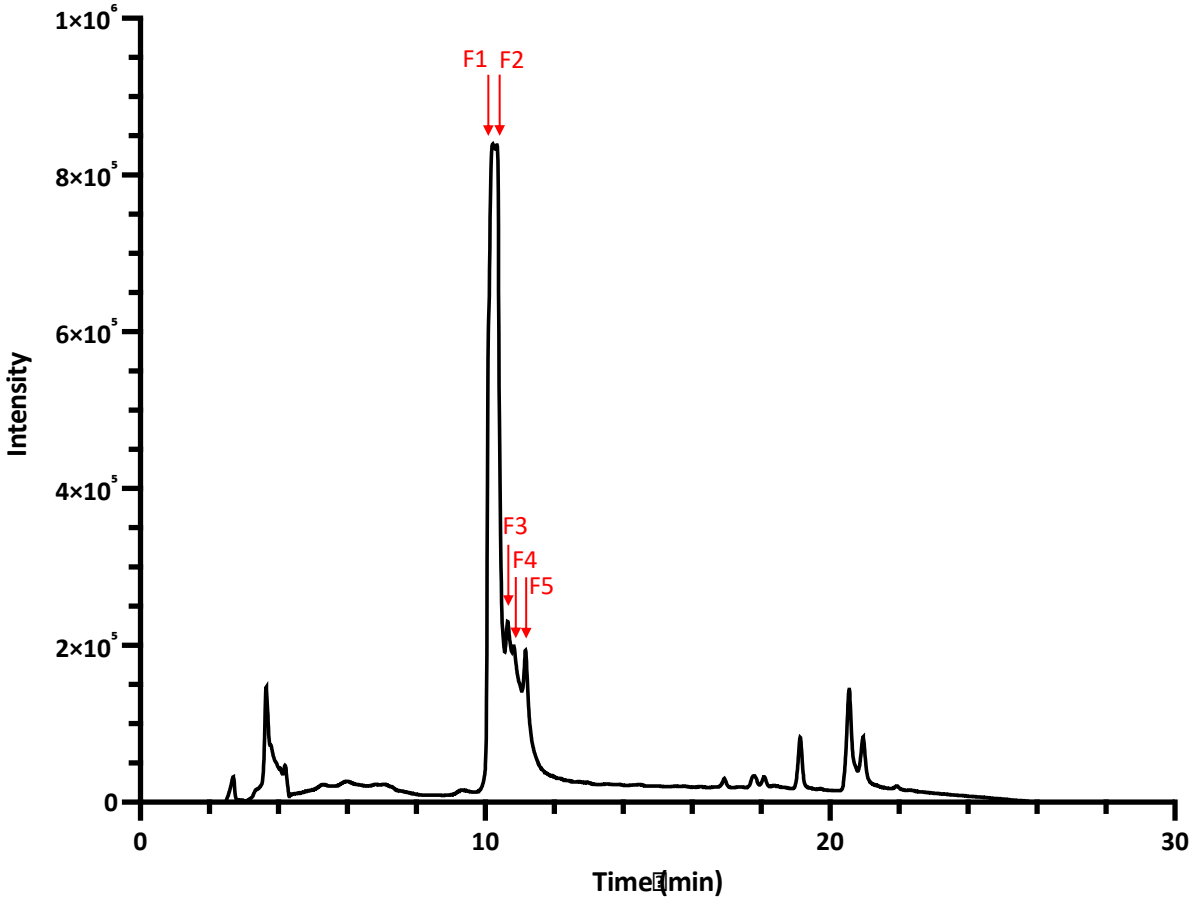

Figure 3.4: Preparative RF-HPLC spectrum for modification of arginine in GKGRG.

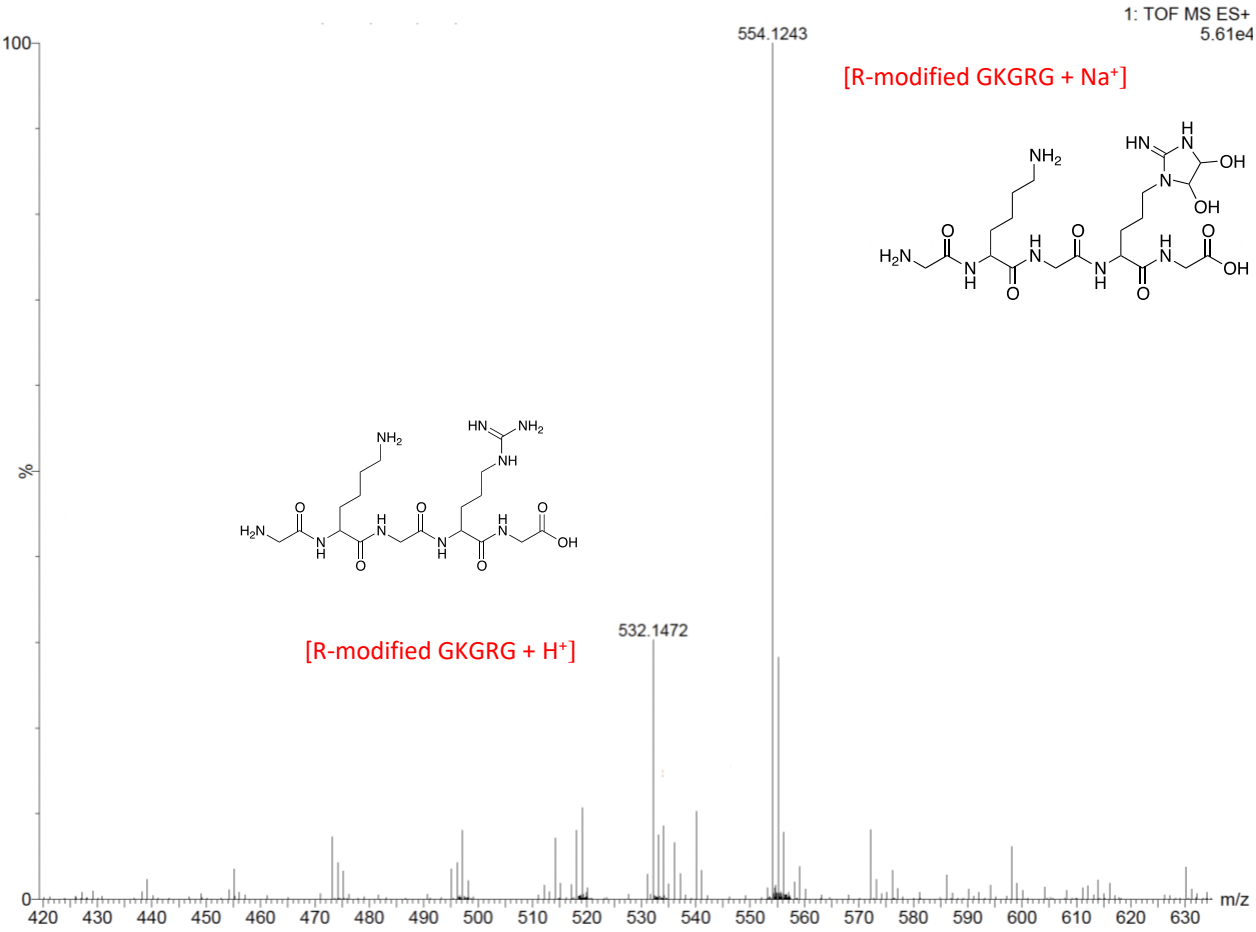

Figure 3.5: ESI-MS spectrum of modification of arginine in GKGRG.

3.2.3. Modification of lysine in ZY13 sequence

ZY13 (VKRWKKWRWKWKKWV) is a synthetic AMP in this project. Since ZY13 included both lysine and arginine in its sequence, it was a proper candidate to confirm the orthogonality in modification of lysine and arginine by *N*-hydroxyethyl acrylamide and glyoxal, respectively. After modification of lysine residues of ZY13 (Scheme 3.3), purification was performed by preparative mode of RF-HPLC (Figure 3.6). Four fractions were collected from RF-HPLC between 13.3 min to 15.5 min (F1:13.6, F2:14.3, F3:14.4 and F4:15 min). All four fractions showed the same peptide

composition after characterization by QTOF (Figure 3.7). Again, we attempted different RF-HPLC methods to be able to have one molecular weight for each fraction; however, even with more separate peaks still the same compounds appeared in all four fractions. As mentioned before, there were many molecular weight possibilities for the final compound in modification of lysines in ZY13. In fact, the primary amines on the lysine side chain can go through single or double addition with *N*-hydroxyethyl acrylamide. In addition, it is possible not all the lysine residues in the sequence go through the reaction because of steric hinderance. After purification of the final compounds, QTOF showed the peptide composition containing conjugation of 8, 9, 10 and 11 *N*-hydroxyethyl acrylamides out of 14 possible conjugations (Figure 3.7). For example, in Figure 3.4 in m/Z = 630.7743, Z = 5, m = 3153.8715 Da which is the molecular weight of 8 conjugations of *N*-hydroxyethyl acrylamides plus $5H^+$. m/Z = 653.9880, Z = 5, m = 3269.94 Da which is the molecular weight of 9 conjugations of *N*-hydroxyethyl acrylamides plus $5H^+$. m/Z = 676.9999, Z = 5, m = 3384.9995 Da which is the molecular weight of 10 conjugations of *N*-hydroxyethyl acrylamides plus $5H^+$. m/Z = 700.0115, Z = 5, m = 3500.0575 Da which is the molecular weight of 11 conjugations of *N*-hydroxyethyl acrylamides plus $5H^+$. And this pattern reaped throughout the QTOF spectrum with different values for Z. The weight average of the molecular weight = 3273.98 Da.

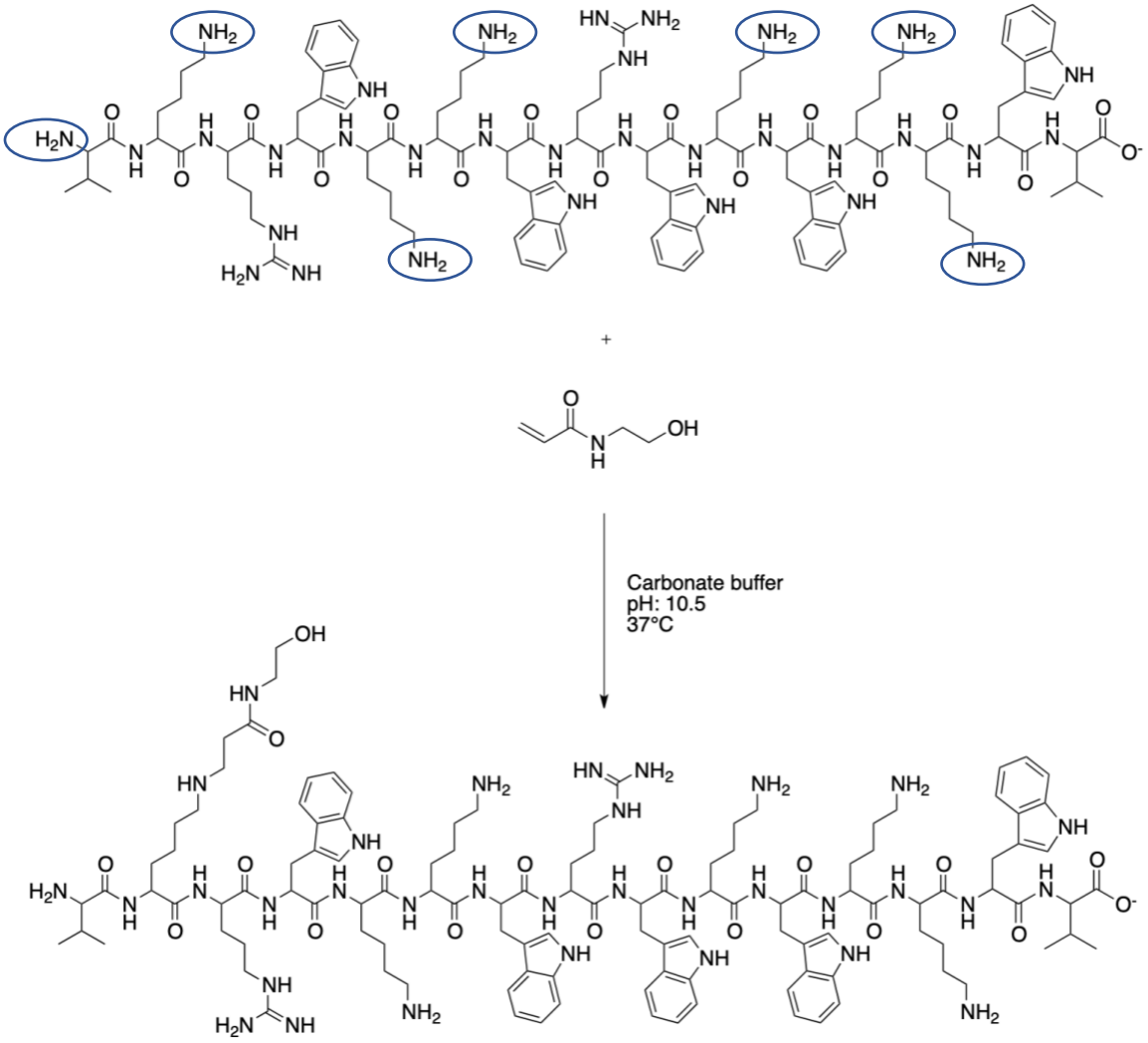

Scheme 3.3: Modification of lysine in ZY13.

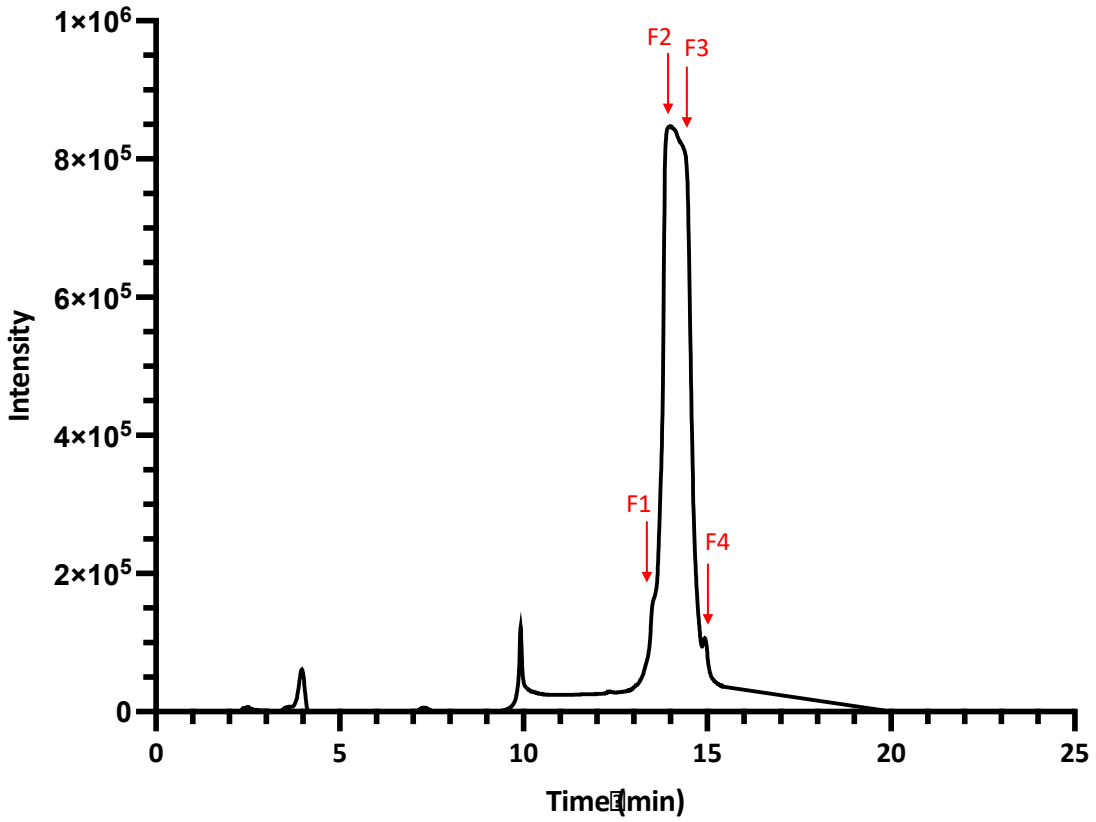

Figure 3.6: Preparative RF-HPLC spectrum for modification of lysine in ZY13.

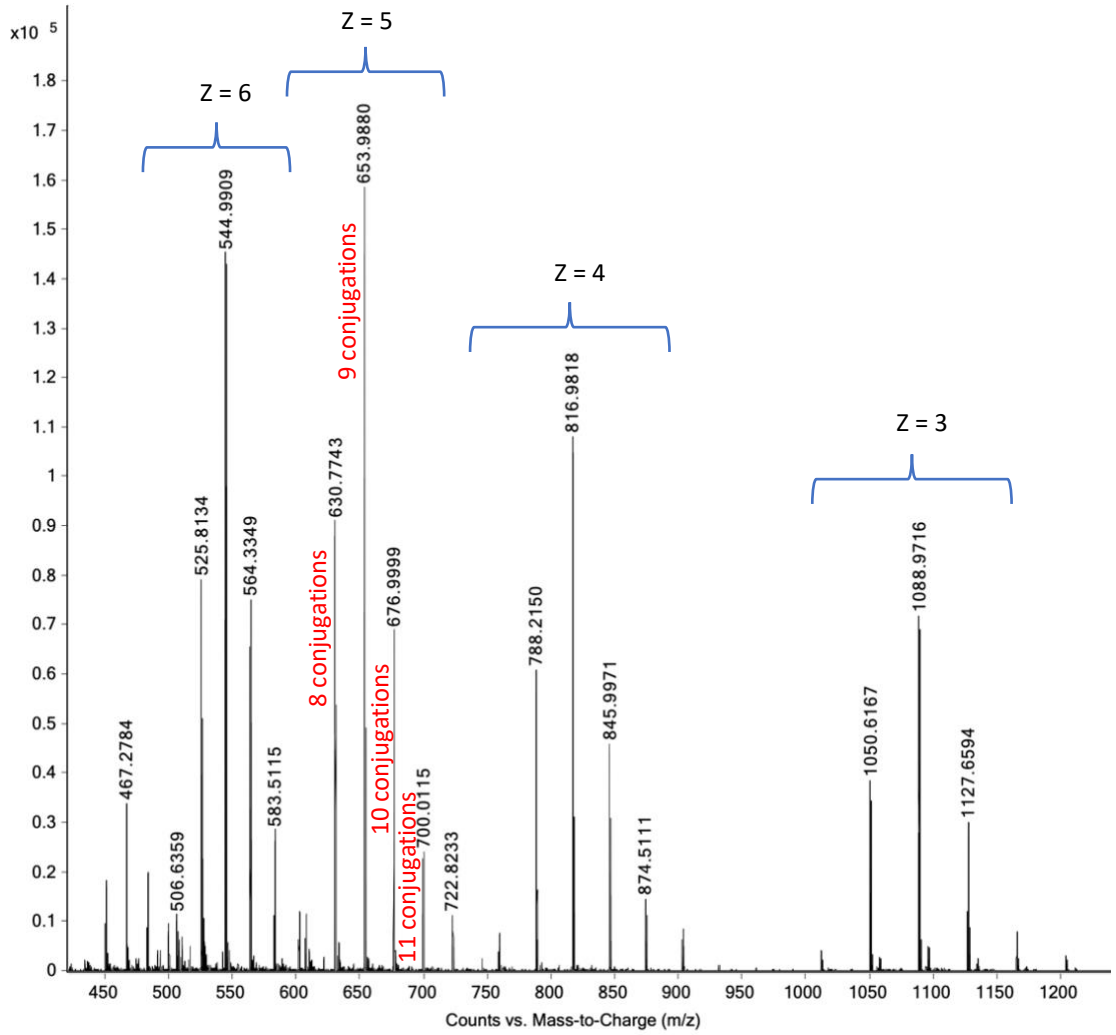

Figure 3.7: QTOF spectrum of K-modified ZY13.

3.2.4. Modification of arginine in ZY13 sequence

ZY13 included two arginines in its sequence which could be modified by glyoxal. After modification of arginine residues in ZY13 (Scheme 3.4), purification was performed by preparative mode of RF-HPLC (Figure 3.8). Here, we had a sharp peak (with a shoulder) at 13.5-15.2 min. Two fractions were collected from RF-HPLC (F1:14.2 and F2:14.6). F1 was collected to separate the shoulder compounds from the sharp peak compounds. However, both F1 and F2

showed the same peptide composition consisting of single and double conjugation of ZY13 with glyoxal (Figure 3.9). Once again, we attempted different RF-HPLC methods to be able to have one molecular weight for each fraction; however, even with more separate peaks still the same compounds appeared in both fractions. QTOF confirmed the conjugation of arginine with glyoxal. QTOF showed the conjugation of 1 and 2 glyoxal out of 2 possible conjugations (Figure 3.9). For example, in Figure 3.5 in m/Z = 462.6560, Z = 5, m = 2313.2800 Da which is the molecular weight of 1 conjugation of glyoxal plus $5H^+$. m/Z = 474.2569, Z = 5, m = 2371.2845 Da which is the molecular weight of 2 conjugations of glyoxal plus $5H^+$. This pattern reaped throughout the QTOF spectrum with different values for Z. The weight average of the molecular weight = 2307.28 Da.

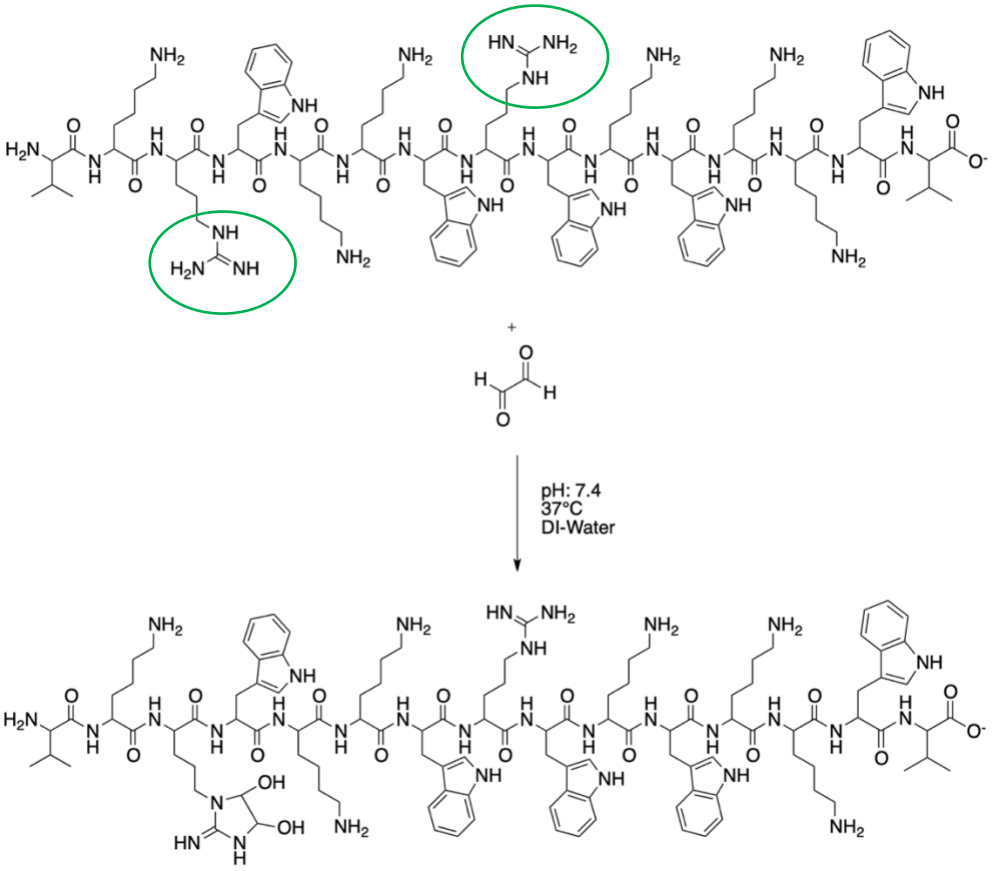

Scheme 3.4: Modification of arginine in ZY13.

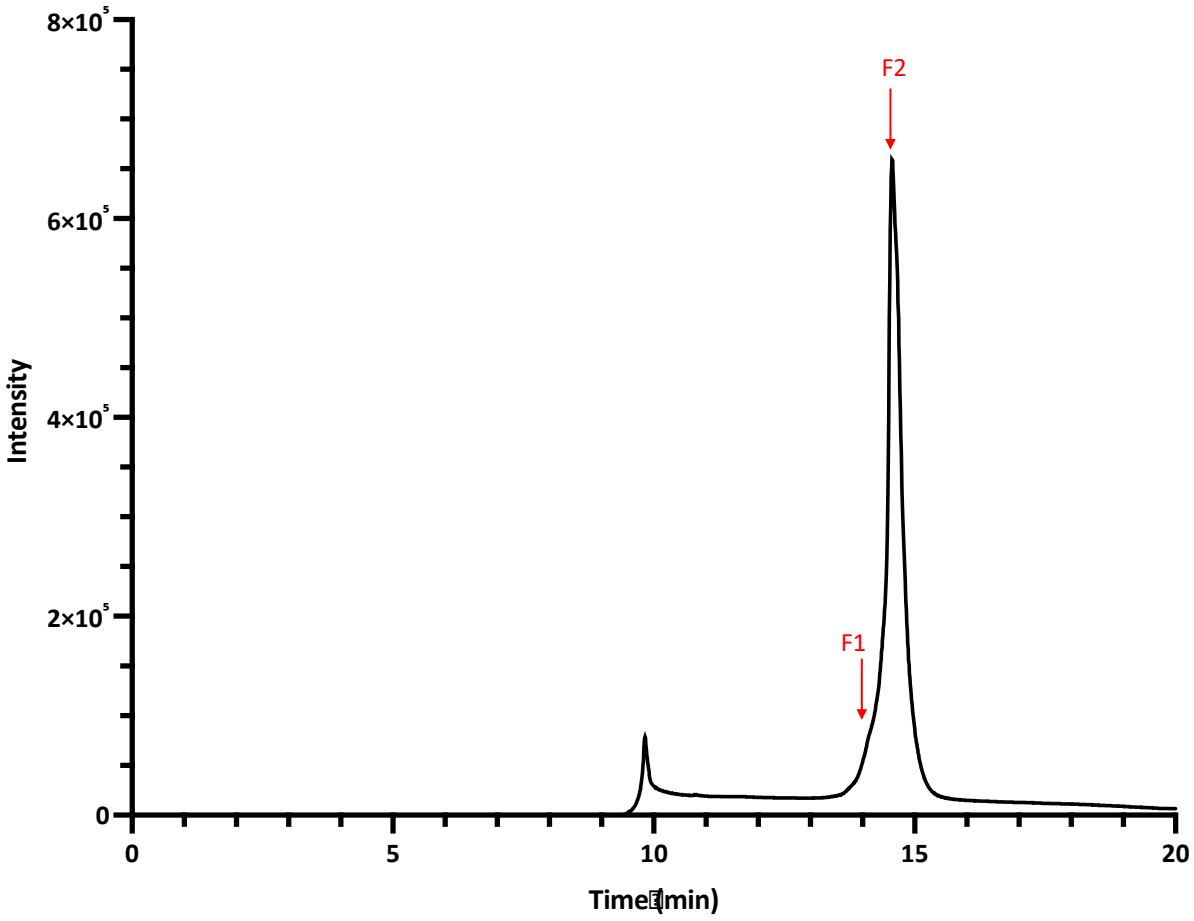

Figure 3.8: Preparative RF-HPLC spectrum for modification of arginine in ZY13.

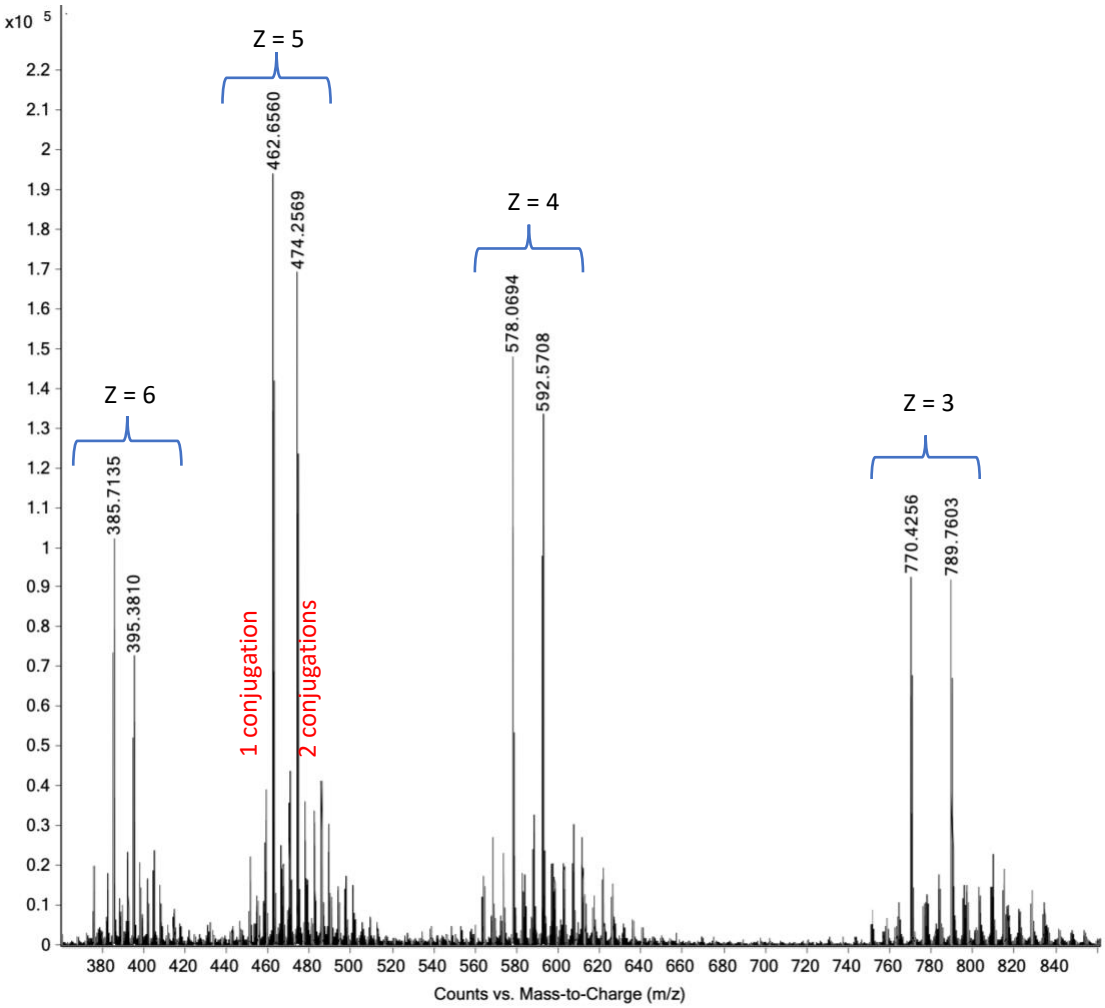

Figure 3.9: QTOF spectrum of R-modified ZY13.

Therefore, for modification lysines in ZY13 (K-modified ZY13), a peptide complex including 8,9,10 and 11 conjugations was obtained. In addition, for modification arginines in ZY13 (R-modified ZY13), a peptide complex including 1 and 2 conjugations was obtained.

3.2.5. Modification of lysine in Magainin 2 sequence

Magainin 2 (GIGKFLHSAKKFGKAFVGEIMNS) is a natural AMP in this project. Magainin 2 included four lysines its sequence which could be modified by *N*-hydroxyethyl acrylamide. After modification of lysine residues in Magainin 2 (Scheme 3.5), QTOF confirmed the conjugation of lysines and *N*-hydroxyethyl acrylamide. Again, there were 10 molecular weight possibilities for the final compound in modification of lysines in Magainin 2 (4 lysines in Magainin 2 sequence and 1 primary amine on *N*-terminal). After purification of the final compound by RF-HPLC, six fractions were collected between 14 min to 16.8 min (F1:14.3, F2:14.74, F3:14.76, F4:15, F5:15.41 and F6:15.43 min) (Figure 3.6). All six fractions showed the same peptide composition which belonged to 7, 8, 9 and 10 conjugations of *N*-hydroxyethyl acrylamide to Magainin 2 after characterization by QTOF (Figure 3.7). Again, we attempted different RF-HPLC methods to be able to have one molecular weight for each fraction; however, even with more separate peaks still the same compounds appeared in all four fractions. QTOF showed the conjugation of 7, 8, 9 and 10 *N*-hydroxyethyl acrylamides out of 10 possible conjugations (Figure 3.11). For example, in Figure 3.6 in m/Z = 819.1965, Z = 4, m = 3276.786 Da which is the molecular weight of 7 conjugations of *N*-hydroxyethyl acrylamides plus $5H^+$. m/Z = 848.2130, Z = 4, m = 3392.852 Da which is the molecular weight of 8 conjugations of *N*-hydroxyethyl acrylamides plus $5H^+$. m/Z = 876.7291, Z = 4, m = 3506.9164 Da which is the molecular weight of 9 conjugations of *N*-hydroxyethyl acrylamides plus $5H^+$. m/Z = 905.7467, Z = 4, m = 3622.9868 Da which is the molecular weight of 10 conjugations of *N*-hydroxyethyl acrylamides plus $5H^+$. And this pattern reaped throughout the QTOF spectrum with different values for Z. The weight average of the molecular weight = 3573.51 Da.

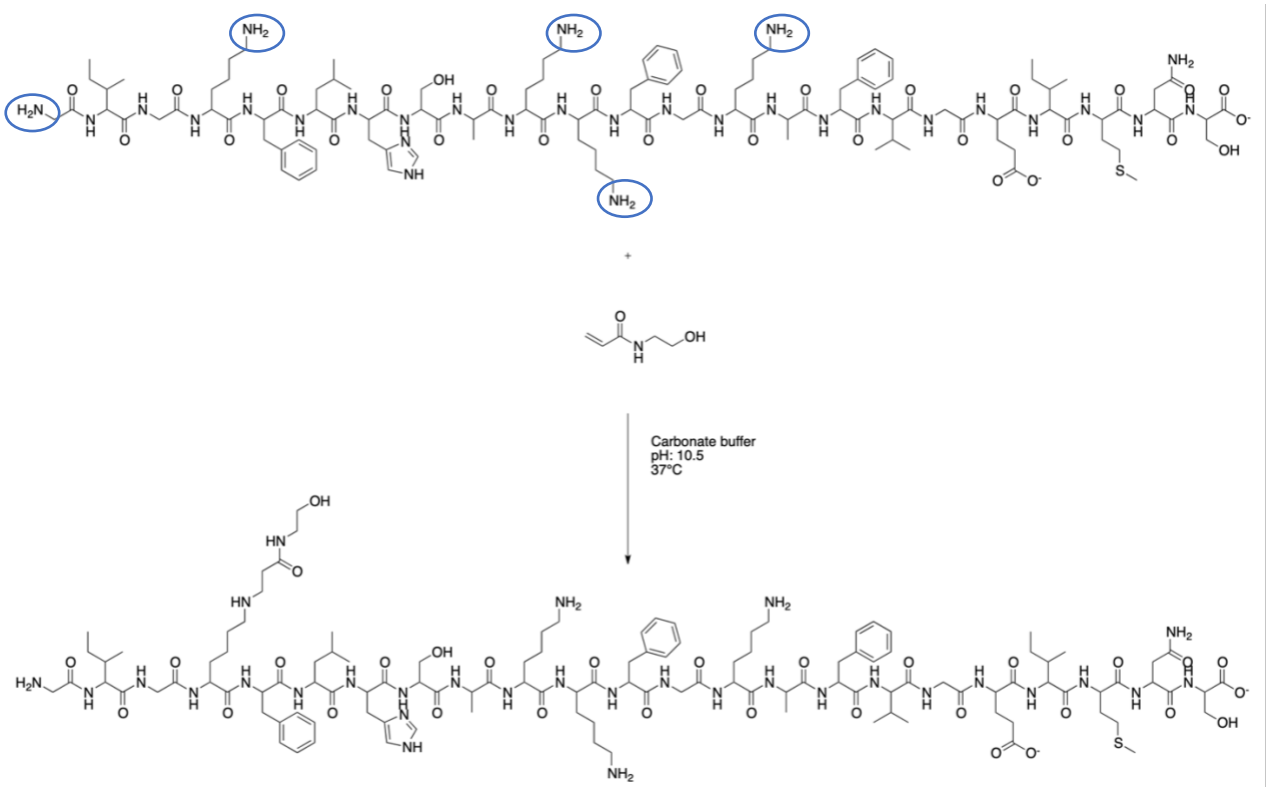

Scheme 3.5: Modification of lysine in Magainin 2.

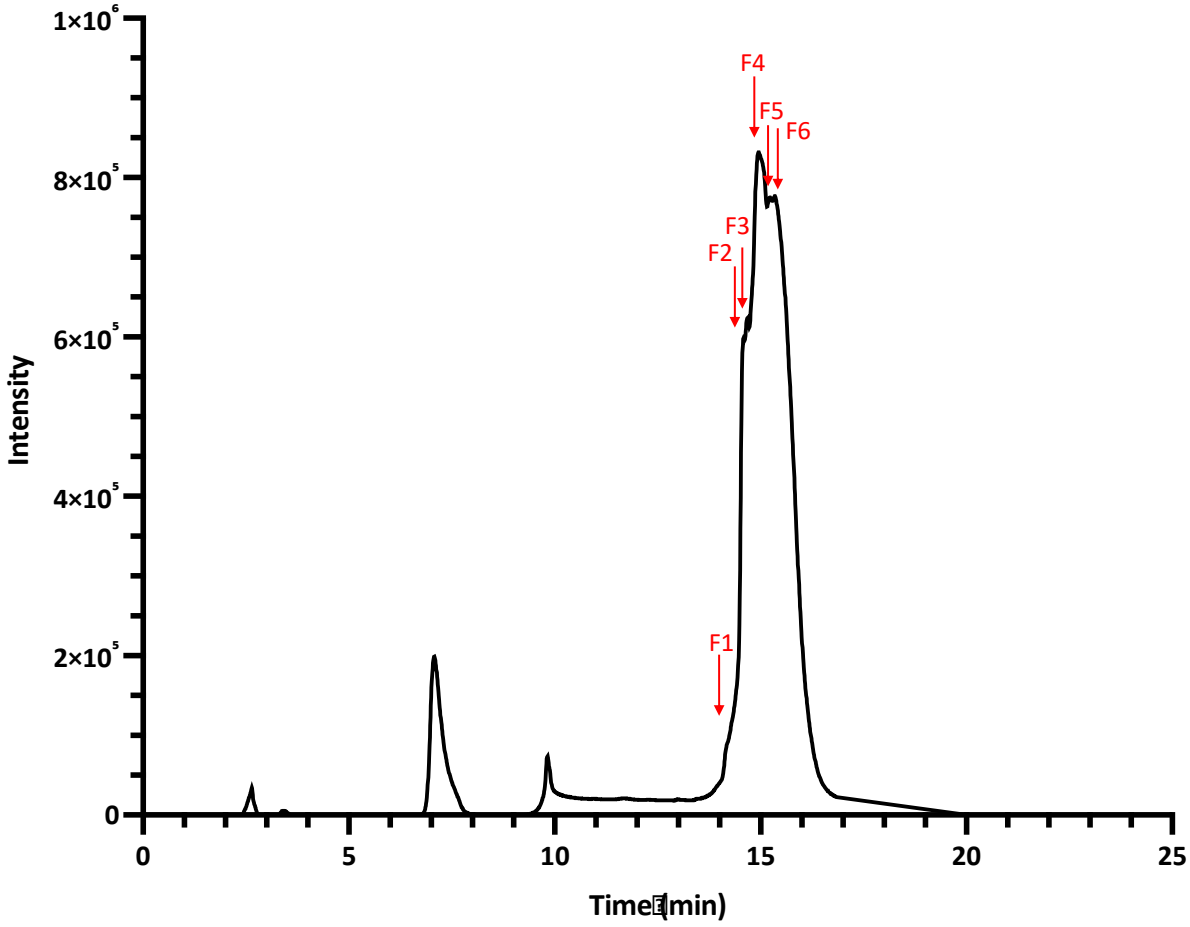

Figure 3.10: Preparative RF-HPLC spectrum for modification of lysine in Magainin 2.

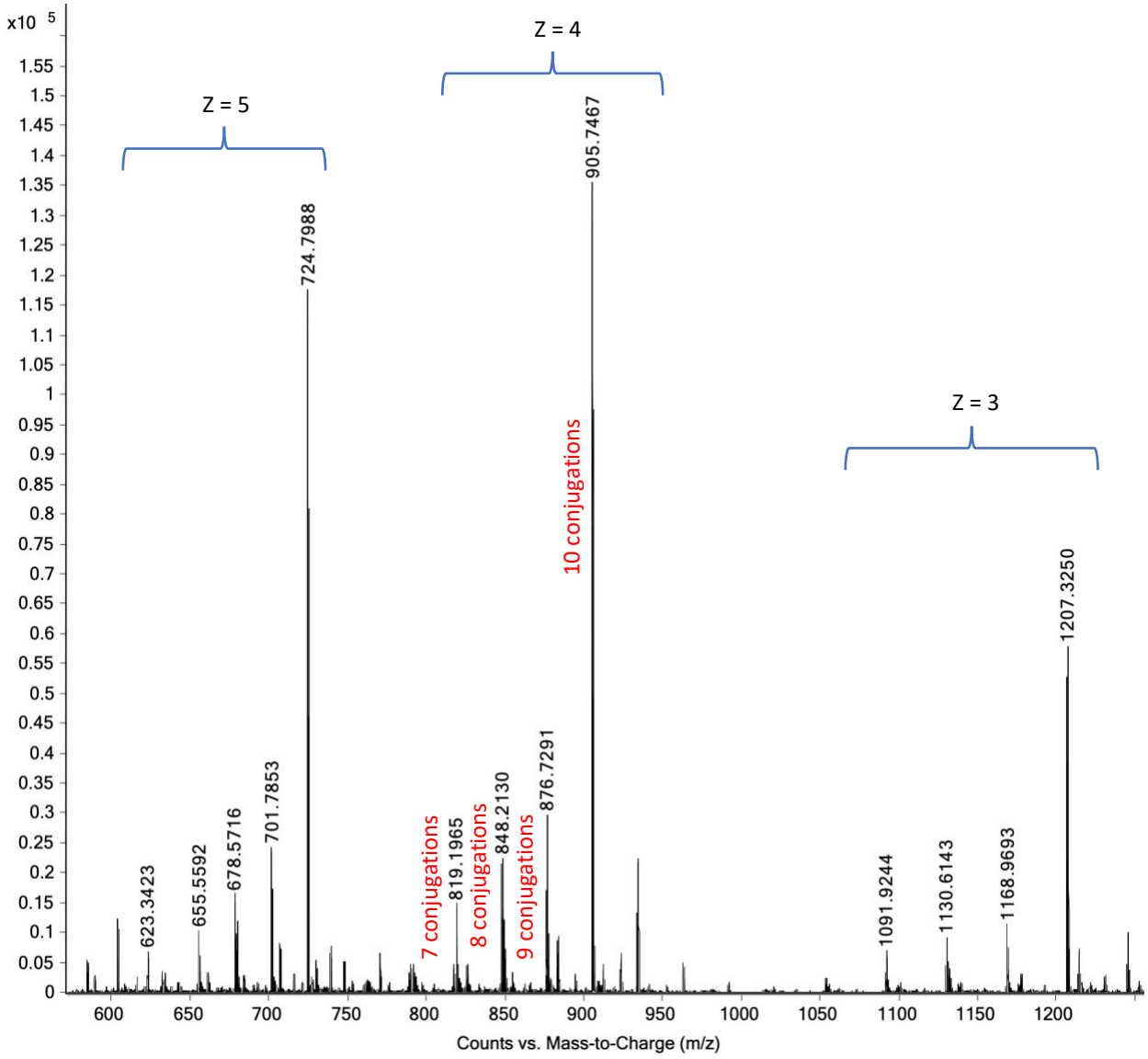

Figure 3.11: QTOF spectrum of K-modified Magainin 2.

3.3. Material and method

3.3.1. Material

Fmoc-Ser(tBu)-OH, Fmoc-Val-OH, Fmoc-Gly-OH, 2-(1H-Benzotriazol- 1-yl)-1,1,3,3-tetramethyluronium hexafluorophosphate (HBTU) (AnaSpec). Dichloromethane (DCM), acetonitrile (CH_3CN), Methanol (MeOH), HPLC-grade water, diethyl ether (Fisher Scientific). chlorotrityl chloride resin (ChemImpex). Hydroxybenzotriazole (HOBt) (ChemTech). Piperidine, *N,N*-diisopropyl-*N*-ethylamine (DIEA), triethylamine (TEA) (Alfa Aesar). phenol (Amresco). Trifluoroacetic acid (TFA), thioanisole, triisopropylsilane (TIS) (Acros Organics). *N*-hydroxyethyl acrylamide (Aldrich). Glyoxal, carbonate buffer (Sigma-Aldrich).

3.3.2. Synthesis of GKGRG

The GKGRG was synthesized by Fmoc/tbutyl batch solid-phase synthesis on an Applied Biosystems 433A automated peptide synthesizer, which allowed for direct conductivity monitoring of Fmoc deprotection. A 0.2 mmol scale synthesis was conducted using a preloaded 2-chlorotrityl resin.

3.3.2.1 Loading of the First Amino Acid.

A solution of Fmoc-Gly-OH (1 equiv) and DIEA (4 equiv) in dry DCM (10 mL) was added to 2-chlorotrityl chloride resin (1 equiv) and the reaction stirred for 4 hours. The resin was transferred into a peptide vessel fitted with a polyethylene filter disk and washed with a solution of DCM/MeOH/DIEA (17:2:1; 3 $\times$ 20 mL), DCM (3 $\times$ 20 mL), DMF (2 $\times$ 20 mL), and DCM (2 $\times$ 20 mL). The grafting yield was determined by measuring the absorbance of *N*-(9-fluorenylmethyl)

piperidine complex at 301 nm by UV−vis spectroscopy (after treatment with piperidine) and resulted 0.33 mmol/g.

3.3.2.2 Automatic Synthesis of Peptide.

Subsequent Fmoc amino acids were coupled using a "conditional double coupling" protocol on a 0.2 mmol scale. The Fmoc group was cleaved from the peptide-resin using a piperidine solution and monitored by conductivity. Subsequent amino acids (5 equiv amino acid) were activated with a mixture of HBTU/HOBt/ DIEA and attached to the *N*-terminal of the peptide-resin. Cleavage of the peptide from the resin with removal of the acid-labile protecting groups was achieved by using 10 mL of a scavenging mixture of TFA/phenol/water/thioanisole/TIS (10/0.75/0.5/0.5/0.25 v/w/v/v/v) for 3 hours. The resin was filtered out with a fritted filter, rinsed with 1 mL of TFA and 20 mL of DCM, the filtrate containing the unprotected peptide was concentrated to small volume, and the product was precipitated with cold diethyl ether, isolated by filtration, and dried under vacuum overnight. The peptide was purified by preparative RP-HPLC (JASCO system) at 17 mL/ min on a Waters C18 column (250 × 22 mm, 5 mm) using a gradient of A [H_2O + 0.1% TFA] and B [CH_3CN + 0.1% TFA]: 0% of B for 5 min, 0% → 100 for 37 min and 100% for 5 min; detection at 214nm. CH_3CN was evaporated under reduced pressure and the aqueous solution was freeze-dried to give a white solid (72%).

3.3.3. Modification of lysine in GKGRG

The pH of the reaction solution must be higher than 10.2 (amine pK_a on lysine residue) to generate the active amine. pH 10.5 carbonate buffer was utilized as the reaction solvent. The

Michael addition was attempted with *N*-hydroxyethyl acrylamide as the Michael acceptor based on the protocol for BOC-Lys-OH modification in chapter 2. According to the same protocol we started the reaction with 9 equiv of *N*-hydroxyethyl acrylamide. After 72 hours at 37°C, an aliquot was taken to check conversion to the desired product. Based on electro spray mass spectrometry data, the reaction was not complete. To increase conversion, additional 24 equiv. of *N*-hydroxyethyl acrylamide was added to the reaction mixture. After another 72 hours at 37°C, ESI-MS confirmed reaction completion, as unmodified GKGRG was no longer present in the reaction solution. The K-modified GKGRG was purified by preparative RP-HPLC (JASCO system) at 17 mL/ min on a Waters C18 column (250 × 22 mm, 5 mm) using a gradient of A [H_2O + 0.1% TFA] and B [CH_3CN + 0.1% TFA]: 0% of B for 5 min, 0% → 100 for 37 min and 100% for 5 min; detection at 214nm. CH_3CN was evaporated under reduced pressure and the aqueous solution was freeze-dried to give a white solid (81% yield).

3.3.4. Modification of arginine in GKGRG

The addition reaction with glyoxal was performed for modification of guanidinium on arginine side chain in GKGRG sequence. In neutral conditions, due to the modification of BOC-Arg-OH in chapter 2, 3 equiv of glyoxal was used to generate an imidazolidine-based heterocycle.[59] ESI-MS confirmed the addition of glyoxal to guanidinium in GKGRG after 24 hours at 37°C. The R-modified GKGRG was purified by preparative RP-HPLC (JASCO system) at 17 mL/ min on a Waters C18 column (250 × 22 mm, 5 mm) using a gradient of A [H_2O + 0.1% TFA] and B [CH_3CN + 0.1% TFA]: 0% of B for 5 min, 0% → 100 for 37 min and 100% for 5 min; detection at 214nm. CH_3CN was

evaporated under reduced pressure and the aqueous solution was freeze-dried to give a white solid (79% yield).

3.3.5. Synthesis of ZY13

The (VKRWKKWRWKWKKWV) peptide (ZY13) was synthesized by Fmoc/tbutyl batch solid-phase synthesis on an Applied Biosystems 433A automated peptide synthesizer, which allowed for direct conductivity monitoring of Fmoc deprotection. A 0.2 mmol scale synthesis was conducted using a preloaded 2-chlorotrityl resin.

3.3.5.1 Loading of the First Amino Acid.

A solution of Fmoc-Val-OH (1 equiv) and DIEA (4 equiv) in dry DCM (10 mL) was added to 2-chlorotrityl chloride resin (1 equiv) and the reaction stirred for 4 hours. The resin was transferred into a peptide vessel fitted with a polyethylene filter disk and washed with a solution of DCM/MeOH/DIEA (17:2:1; 3 $\times$ 20 mL), DCM (3 $\times$ 20 mL), DMF (2 $\times$ 20 mL), and DCM (2 $\times$ 20 mL). The grafting yield was determined by measuring the absorbance of *N*-(9-fluorenylmethyl) piperidine complex at 301 nm by UV−vis spectroscopy (after treatment with piperidine) and resulted 0.28 mmol/g.

3.3.5.2 Automatic Synthesis of Peptide.

Subsequent Fmoc amino acids were coupled using a “conditional double coupling” protocol on a 0.2 mmol scale. The Fmoc group was cleaved from the peptide-resin using a piperidine solution

and monitored by conductivity. Subsequent amino acids (5 equiv amino acid) were activated with a mixture of HBTU/HOBt/ DIEA and attached to the *N*-terminal of the peptide-resin. Cleavage of the peptide from the resin with removal of the acid-labile protecting groups was achieved by using 10 mL of a scavenging mixture of TFA/phenol/water/thioanisole/TIS (10/0.75/0.5/0.5/0.25 v/w/v/v/v) for 3 hours. The resin was filtered out with a fritted filter, rinsed with 1 mL of TFA and 20 mL of DCM, the filtrate containing the unprotected peptide was concentrated to small volume, and the product was precipitated with cold diethyl ether, isolated by filtration, and dried under vacuum overnight. The peptide was purified by preparative RP-HPLC (JASCO system) at 17 mL/ min on a Waters C18 column (250 × 22 mm, 5 mm) using a gradient of A [H_2O + 0.1% TFA] and B [CH_3CN + 0.1% TFA]: 0% of B for 5 min, 0% → 100 for 37 min and 100% for 5 min; detection at 214nm. CH_3CN was evaporated under reduced pressure and the aqueous solution was freeze-dried to give a white solid (63%).

3.3.6. Modification of lysine in ZY13

As mentioned before, in order to have an active amine the pH of the reaction solution must be higher than the pK_a of amin. There, pH 10.5 carbonate buffer was always utilized as the reaction solvent. However, in this case, ZY13 is not fully soluble in pH 10.5 carbonate buffer. The reaction solution color was opaque white. We continued the reaction with partially soluble ZY13 in 10.5 carbonate buffer. The Michael addition was performed with 54 equiv *N*-hydroxyethyl acrylamide as ZY13 had six lysine in its sequence. After 72 hours at 37°C, an aliquot was taken to check conversion to the desired product. Based on QTOF (Agilent system) data, the reaction was not complete. To increase conversion, additional 18 equiv of *N*-hydroxyethyl acrylamide was added

to the reaction mixture. After another 48 hours at 37°C, QTOF confirmed the reaction completion. The K-modified ZY13 was purified by preparative RP-HPLC (JASCO system) at 17 mL/ min on a Waters C18 column (250 × 22 mm, 5 mm) using a gradient of A [H_2O + 0.1% TFA] and B [CH_3CN + 0.1% TFA]: 0% of B for 5 min, 0% → 100 for 37 min and 100% for 5 min; detection at 214nm. CH_3CN was evaporated under reduced pressure and the aqueous solution was freeze-dried to give a white solid (87% yield).

3.3.7. Modification of arginine in ZY13

In neutral condition (pH 7.4), 6 equiv of glyoxal was added to ZY13 to generate an imidazolidine-based heterocycle.[59] QTOF confirmed the addition of glyoxal to guanidinium after 24 hours at 37°C. The R-modified ZY13 was purified by preparative RP-HPLC (JASCO system) at 17 mL/ min on a Waters C18 column (250 × 22 mm, 5 mm) using a gradient of A [H_2O + 0.1% TFA] and B [CH_3CN + 0.1% TFA]: 0% of B for 5 min, 0% → 100 for 37 min and 100% for 5 min; detection at 214nm. CH_3CN was evaporated under reduced pressure and the aqueous solution was freeze-dried to give a white solid (60% yield).

3.3.8. Synthesis of Magainin 2

The (GIGKFLHSAKKFGKAFVGEIMNS) peptide (Magainin 2) was synthesized by Fmoc/tbutyl batch solid-phase synthesis on an Applied Biosystems 433A automated peptide synthesizer, which allowed for direct conductivity monitoring of Fmoc deprotection. A 0.2 mmol scale synthesis was conducted using a preloaded 2-chlorotrityl resin.

3.3.8.1 Loading of the First Amino Acid.

A solution of Fmoc-Ser(tBu)-OH (1 equiv) and DIEA (4 equiv) in dry DCM (10 mL) was added to 2-chlorotrityl chloride resin (1 equiv) and the reaction stirred for 4 hours. The resin was transferred into a peptide vessel fitted with a polyethylene filter disk and washed with a solution of DCM/MeOH/DIEA (17:2:1; 3 × 20 mL), DCM (3 × 20 mL), DMF (2 × 20 mL), and DCM (2 × 20 mL). The grafting yield was determined by measuring the absorbance of *N*-(9-fluorenylmethyl) piperidine complex at 301 nm by UV−vis spectroscopy (after treatment with piperidine) and resulted 0.28 mmol/g.

3.3.8.2 Automatic Synthesis of Peptide.

Subsequent Fmoc amino acids were coupled using a “conditional double coupling” protocol on a 0.2 mmol scale. The Fmoc group was cleaved from the peptide-resin using a piperidine solution and monitored by conductivity. Subsequent amino acids (5 equiv amino acid) were activated with a mixture of HBTU/HOBt/ DIEA and attached to the *N*-terminal of the peptide-resin. Cleavage of the peptide from the resin with removal of the acid-labile grotecting groups was achieved by using 10 mL of a scavenging mixture of TFA/phenol/water/thioanisole/TIS (10/0.75/0.5/0.5/0.25 v/w/v/v/v) for 3 hours. The resin was filtered out with a fritted filter, rinsed with 1 mL of TFA and 20 mL of DCM, the filtrate containing the unprotected peptide was concentrated to small volume, and the product was precipitated with cold diethyl ether, isolated by filtration, and dried under vacuum overnight. The peptide was purified by preparative RP-HPLC (JASCO system) at 17 mL/ min on a Waters C18 column (250 × 22 mm, 5 mm) using a gradient of A [H_2O + 0.1% TFA] and B [CH_3CN + 0.1% TFA]: 0% of B for 5 min, 0% → 100 for 37 min and 100% for 5 min; detection at

214nm. CH_3CN was evaporated under reduced pressure and the aqueous solution was freeze-dried to give a white solid (49% yield).

3.3.9. Modification of lysine in Magainin 2

Reaction was performed in pH 10.5 carbonate buffer as the solvent. The Michael addition was attempted with *N*-hydroxyethyl acrylamide. Thirty-six equiv of *N*-hydroxyethyl acrylamide was added to the reaction solution. The reaction was complete after 96 hours at 37°C. The K-modified Magainin 2 was purified by preparative RP-HPLC (JASCO system) at 17 mL/ min on a Waters C18 column (250 $\times$ 22 mm, 5 mm) using a gradient of A [H_2O + 0.1% TFA] and B [CH_3CN + 0.1% TFA]: 0% of B for 5 min, 0% $\rightarrow$ 100 for 37 min and 100% for 5 min; detection at 214nm. CH_3CN was evaporated under reduced pressure and the aqueous solution was freeze-dried to give a white solid (67% yield).

3.4. Conclusion

It was concluded in chapter 2, that we achieved orthogonal modification of BOC-Lys-OH and BOC-Arg-OH by addition of *N*-hydroxyethyl acrylamide and glyoxal, respectively. In this chapter we showed that we can implement this orthogonal modification while lysine and arginine are in the sequence of an AMP. Both lysine and arginine exist in the sequence of ZY13. We successfully modified a lysine and arginine by *N*-hydroxyethyl acrylamide and glyoxal, respectively, orthogonally. This data was valuable since it makes the modification of lysine and arginine residues in peptide sequences possible in a one-pot process. In addition, the purification process for modification of lysine and arginine, while in the peptide sequence, is shorter therefore less expensive than modifying each basic amino acid individually and then use the modified amino acids in a peptide sequence.

Chapter 4: Evaluation of the effectiveness of basic amino acid modification by SAXS and bioassays

4.1. Introduction

After successful synthesis of K-modified ZY13, R-modified ZY13 and K-modified Magainin 2, bioassays were performed on the modified AMPs in order to confirm the impact of modification. As mentioned in chapter 1, The aim of our project was to narrow down the antibacterial activity of broad-spectrum AMPs by modifying the side chain functional groups. Hence, engineering pH-sensitive, more selective AMPs. In fact, most pathogenic conditions (e.g., dental cavities occur by *Streptococcus mutans*)[64] cause lower pHs. Therefore, to evaluate the effect of pH on the antibacterial activity of our modified AMPs, all prokaryotic cell related assays were performed in two different pHs to mimic biological and pathogenic conditions. SAXS on small unilamellar vesicles, which are able to mimic prokaryotic and eukaryotic cell membranes, was also done in both biological and pathogenic pHs. LIVE/DEAD assay, which is a mammalian cell assay was done just in biological pH.

4.2. Results and discussion

4.2.1. SAXS analysis

We investigated the membrane restructuring ability of K-modified Magainin 2, K-modified ZY13 and R-modified ZY13 by SAXS to determine if our modified AMPs generate the negative Gaussian membrane curvature necessary for membrane permeabilization. SAXS spectra showed that K-modified Magainin 2 significantly restructured SUVs composed of PG/PE=20/80 mimicking prokaryotic cell membrane at pH 5 (Figure 4.1A). However, at pH 7.4, K-modified Magainin 2 left the PG/PE=20/80 SUVs intact. These results confirm the pH sensitivity in antibacterial activity of Magainin 2. This modified AMP was able to create NGC on bacterial mimicking vesicles at pH 5 but not at pH 7.4. In addition, K-modified Magainin 2 did not create NGC on eukaryotic mimicking membrane at pH 5 and pH 7.4 which confirms the low cytotoxicity of this modified AMP. Similar results were observed for K-modified ZY13 (Figure 4.1B) and R-modified ZY13 (Figure 4.1C). In another data set, each modified AMP was compared to the intact version of the same AMP against bacterial membrane mimicking vesicles (PG/PE=20/80) at pH 5 and pH 7.4. In comparison of K-modified Magainin 2 with unmodified Magainin 2, it was observed that K-modified ZY13 selectively creates NGC only at pH 5 and not at pH 7.4 (Figure 4.2A). In addition, our experiment was performed at P/L of 1/40 and at this P/L ratio unmodified Magainin 2 does not show any cubic phase or inverted hexagonal phase. In case of K-modified ZY13 and unmodified ZY12 (Figure 4.2B), while the unmodified ZY13 can create NGC on PG/PE=20/80 vesicles at both pH 5 (a = 141.7 A°, $<k>=0.0326\ nm^{-2}$) and pH 7.4 (a = 200.4 A°, $<k>=0.0163\ nm^{-2}$), K-modified ZY13 selectively creates NGC only at pH 5. Similar result was observed in comparing R-modified ZY13 and ZY13 (Figure 4.2C). For K-modified Magainin 2, against PG/PE=20/80 at pH5, with lipid molar ratio, P/L,

of 1/40, diffraction peaks at measured Q-positions are observed with characteristic ratios, √2:√3:√4 and √2:√4:√6, indicating the presence of a Pn3m cubic phase (a = 242.8 A°, <k> = 0.0111 nm^{-2}) and Im3m cubic phase (a = 312.6 A°, <k> = 0.0111), respectively. For K-modified ZY13, against PG/PE=20/80 at pH5, with lipid molar ratio, P/L, of 1/40, diffraction peaks at measured Q-positions were again observed with characteristic ratios, √2:√4:√6, indicating the presence of a Im3m cubic phase (a = 285.4 A°, <k>=0.0132 nm^{-2}). For R-modified ZY13, against PG/PE=20/80 at pH5, with lipid molar ratio, P/L, of 1/40, diffraction peaks at measured Q-positions were observed with characteristic ratios, √2:√3:√4 and √2:√4:√6, showed the presence of a Pn3m cubic phase (a = 230.4 A°, <k>=0.0123 nm^{-2}) and Im3m cubic phase (a = 295.7 A°, <k> = 0.0123), respectively. The Pn3m and IM3m are bulk bicontinuous phases composed of two nonintersecting water channels separated by the membrane.[68,69] The bilayer midplane traces out a surface with principal axes of curvature, c1 and c2, equal and opposite everywhere, $c_1 = -c_2$. These surfaces are known as minimal surfaces, and they have zero mean curvature, $H = 1/2(c_1 + c_2) = 0$, and negative Gaussian curvature (NGC), $K = c_1c_2 < 0$, at every point.[69] Geometrically, everywhere on the surface is locally shaped like a saddle. Observation of K-modified Magainin 2, K-modified ZY13 and R-modified ZY13 inducing NGC on bacterial membrane mimicking vesicle at pH 5 but not pH 7.4 is significant as it means that our modified AMPs are able to target pathogenic bacteria at pH 5 but leave the beneficial bacteria intact in physiological pH.

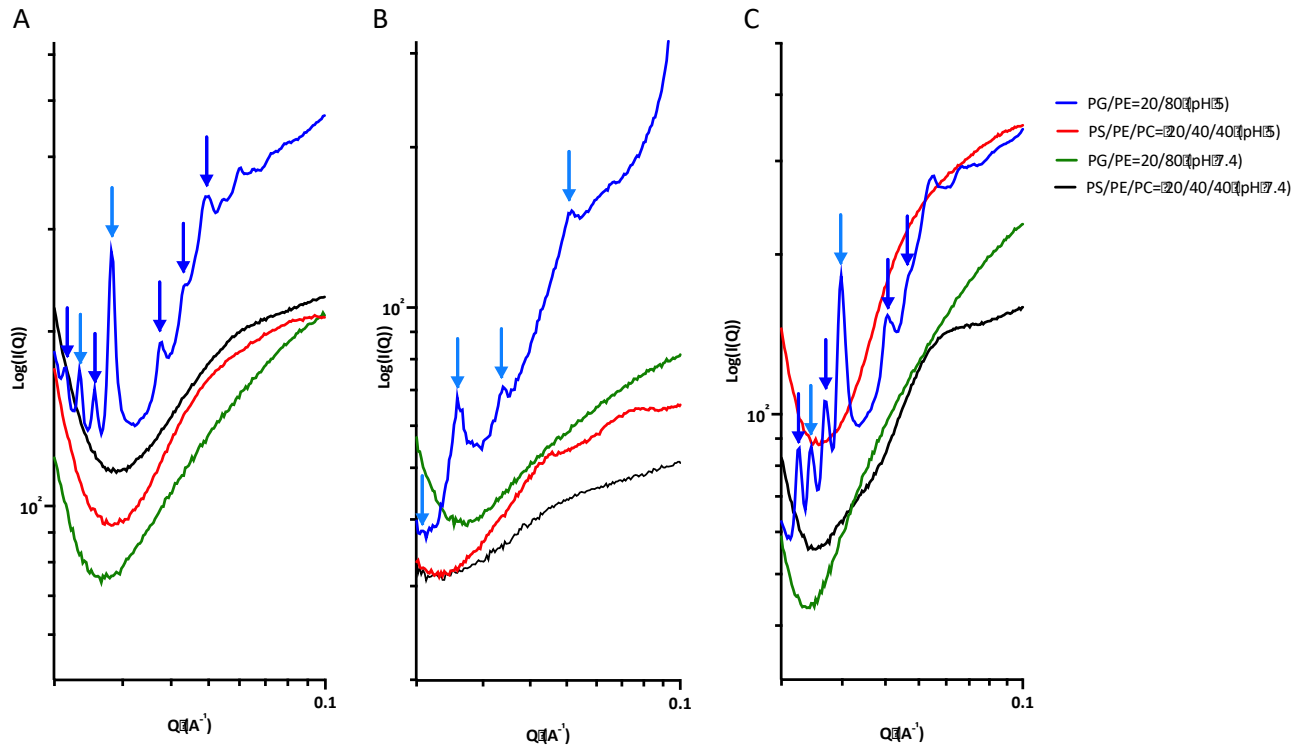

Figure 4.1: SAXS spectra for (A) K-modified Magainin 2 (B) K-modified ZY13 and (C) R-modified ZY13 against PG/PE=20/80 and PS/PE/PC=20/40/40 lipid compositions at pH 7.4 and pH 5.

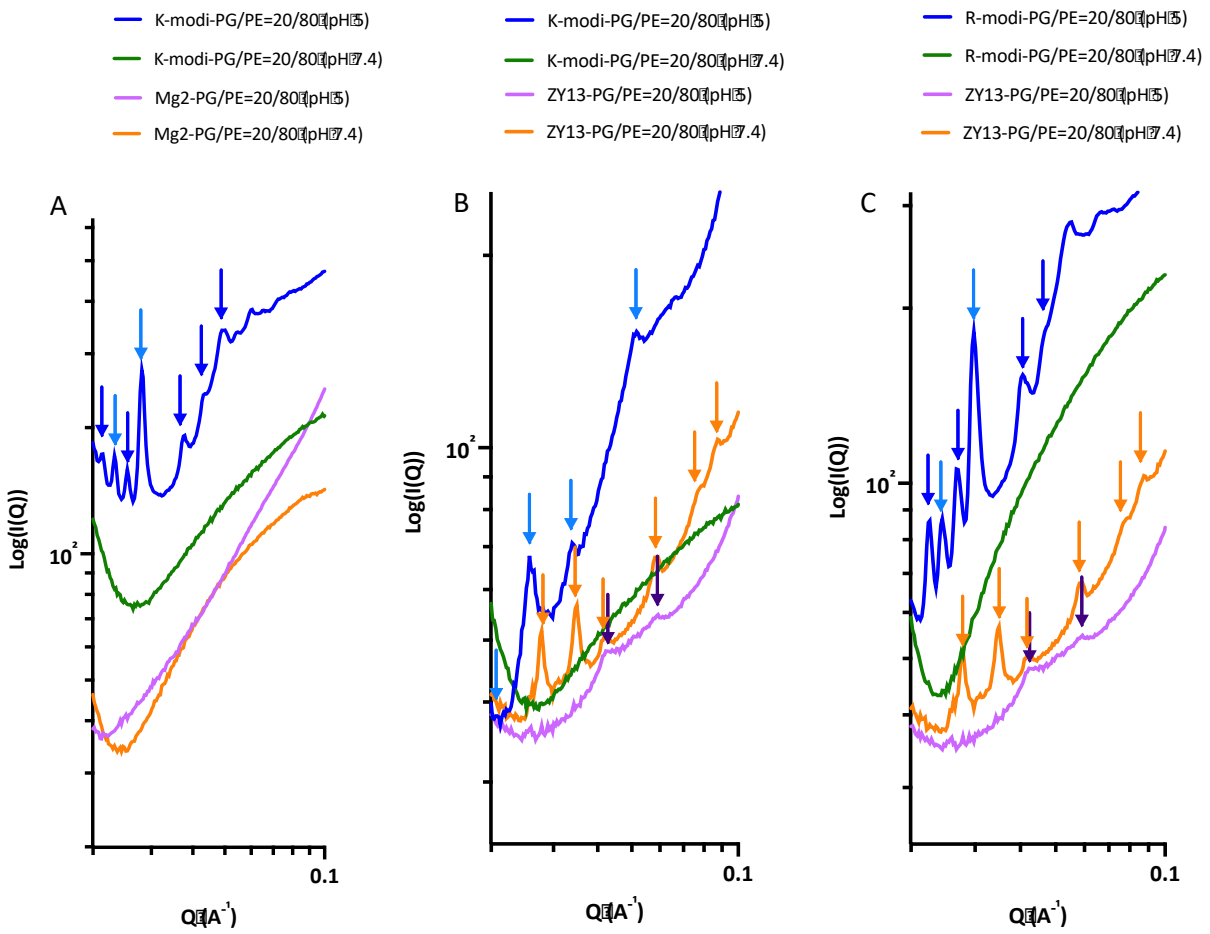

Figure 4.2: SAXS spectra of (A) K-modified Magainin 2 versus Magainin 2 (B) K-modified ZY13 versus ZY13 and (C) R-modified ZY13 versus ZY13 against PG/PE=20/80 at pH 7.4 and pH 5.

4.2.2. Minimum inhibitory concentration (MIC) and Minimum bactericidal concentration (MBC)

We investigated the antimicrobial potency of these K-modified ZY13, R-modified ZY13 and K-modified Magainin 2 by determining their MIC and MBC against Gram-negative *Pseudomonas aeruginosa* (PAO1) and Gram-positive *Staphylococcus aureus* (SA113) pathogens with a turbidity-based microdilution broth assay (Table 4.1). The most important findings of MIC assay were about K-modified ZY13. While intact ZY13 is very active in both pH 7.4 and 5 against both PA and

SA, K-modified ZY13 showed no antimicrobial potency at biological pH 7.4 against PA and SA. However, at pH 5, it displayed good antibacterial activity against both PA and SA (MIC: 55.5 μM and 27.8 μM, respectively). In addition, while intact Magainin 2 is very active in both pH 7.4 and 5 against both PA and SA, K-modified Magainin 2 showed no potency at pH 7.4 against PA, but at pH 5 a good antimicrobial activity was observed against PA (MIC: 27.8 μM). Overall, all our modified AMPs the MIC dropped significantly at pH 5, which suggested that lower dose of our modified AMPs would not be active at biological pH but very active at acidic pathogenic conditions (specially for ZY13). Moreover, the MBC values of our modified AMPs are either equal to or slightly higher than their respective MIC values at pH 5, suggesting that the compounds not only are inhibiting bacterial growth but are also bactericidal.

Table 4.1: MIC and MBC values of ZY13, Magainin 2, K-modified ZY13, R-modified ZY13 and K-modified Magainin 2 against *P.aeruginosa* and *S.aureus* (MIC and MBC are reported in mM) .

	***P.aeruginosa* (PAO1)**				***S. aureus* (SA113)**			
	pH 5		**pH 7.4**		**pH 5**		**pH 7.4**	
	MIC	**MBC**	**MIC**	**MBC**	**MIC**	**MBC**	**MIC**	**MBC**
ZY13	55.5	111.1	27.8	27.8	6.9	13.9	6.9	13.9
K-modified ZY13	55.5	55.5	>111.1	>111.1	27.8	27.8	>111.1	>111.1
R-modified ZY13	6.9	13.9	27.8	27.8	1.2	3.5	6.9	13.9
Magainin 2	3.5	3.5	13.9	13.9	13.9	27.8	27.8	>111.1
K-modified Magainin 2	27.8	27.8	>111.1	13.9	1.2	27.8	27.9	27.8

4.2.3. LIVE/DEAD assay

K-modified ZY13, R-modified ZY13 and K-modified Magainin 2 did not show cytotoxic effect on NIH/ 3T3 mouse fibroblast cells even after 24 h incubation at 10X more concentrated doses than MIC (Figure 4.3-Figure 4.4). Moreover, by LIVE/DEAD assay it was possible to assess the effect of our modified AMPs on the cell membrane integrity. LIVE/DEAD cell viability assay determined intracellular esterase activity by using calcein, a membrane-permeable polyanionic dye. Calcein can be hydrolyzed by intracellular esterases. While the dead cells lack active esterases, calcein produce a green fluorescence in alive cells. LIVE/DEAD assay can also evaluate plasma membrane integrity by using ethidium homodimer, a membrane-impermeable red fluorescent dye which

only penetrates cells with compromised membranes. Treatment of the cells with Magainin 2 and K-modified Magainin 2 resulted in significant difference in cytotoxicity (Figure 4.3 and Figure 4.4). While naturally occurring Magainin 2 kills almost all 3T3 cells (<10% viability) after 8 hours, at 10X concentration (X: MIC concentration), treatment with K- modified Magainin 2 shows more than 98% cell viability after 8 hours for 10X concentration. Similar results were observed even after 24 hours. Naturally, at 5X concentration, Magainin 2 cell viability was higher than 10X (36% cell viability); however, again, treatment with K-modified Magainin 2 showed significantly higher cell viability compared to Magainin 2 after 8 hours and 24 hours (>93% cell viability). While in both time points and concentrations viability of cells treating with K- modified Magainin 2 was significantly high, naturally occurring Magainin 2 showed poor cell viability in all the conditions (p <0.0001).

While the difference between the cell viability of synthetic peptide, ZY13, with it modified versions (K-modified ZY13 and R-modified ZY13) is not as significant as Magainin 2, still in ZY13 case, treatment with K- and R-modified ZY13 showed higher cell viability at 10X after 8 hours (p=0.0068 and p=.0013, respectively) (Figure 4.3 and Figure 4.4). Furthermore, in our counting process no cells were doubly labeled. This indicated that the cells retain their membrane integrity.

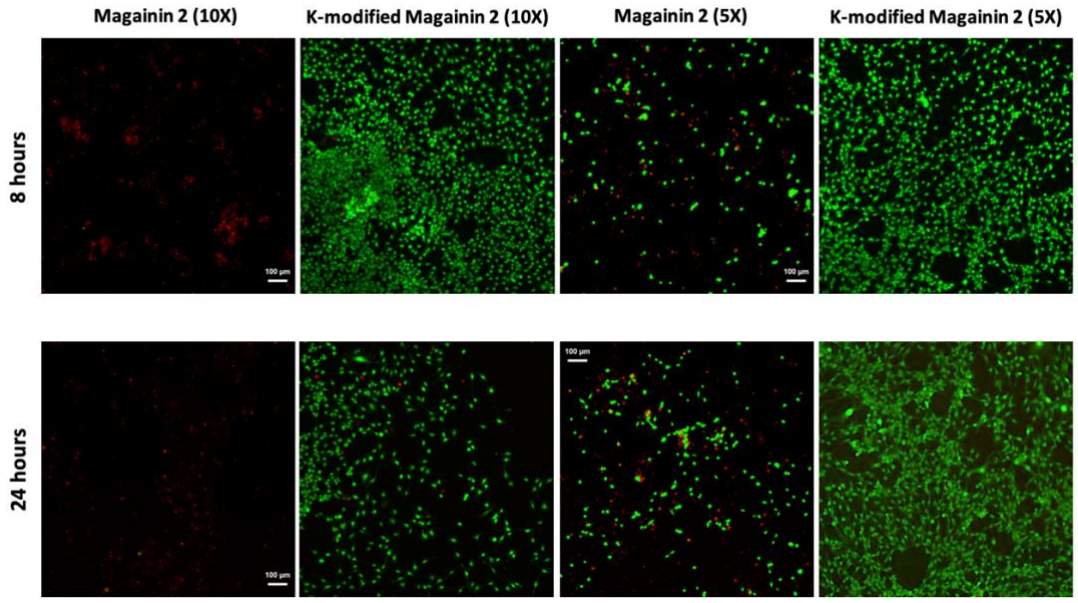

Figure 4.3: Fluorescence images of LIVE/DEAD cell viability assay incubated with Magainin 2 and K-modified Magainin 2 after 8 hours and 24 hours of incubation in two different concentrations (10X and 5X of MIC values)

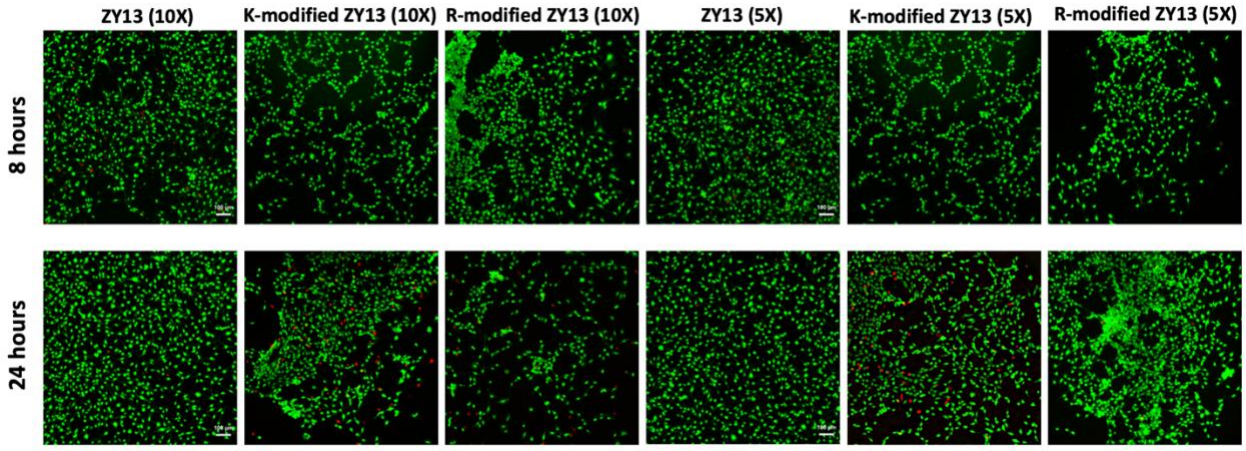

Figure 4.4: Fluorescence images of LIVE/DEAD cell viability assay incubated with ZY13 and K-modified ZY13 and R-modified ZY13 after 8 hours and 24 hours of incubation in two different concentrations (10X and 5X of MIC values).

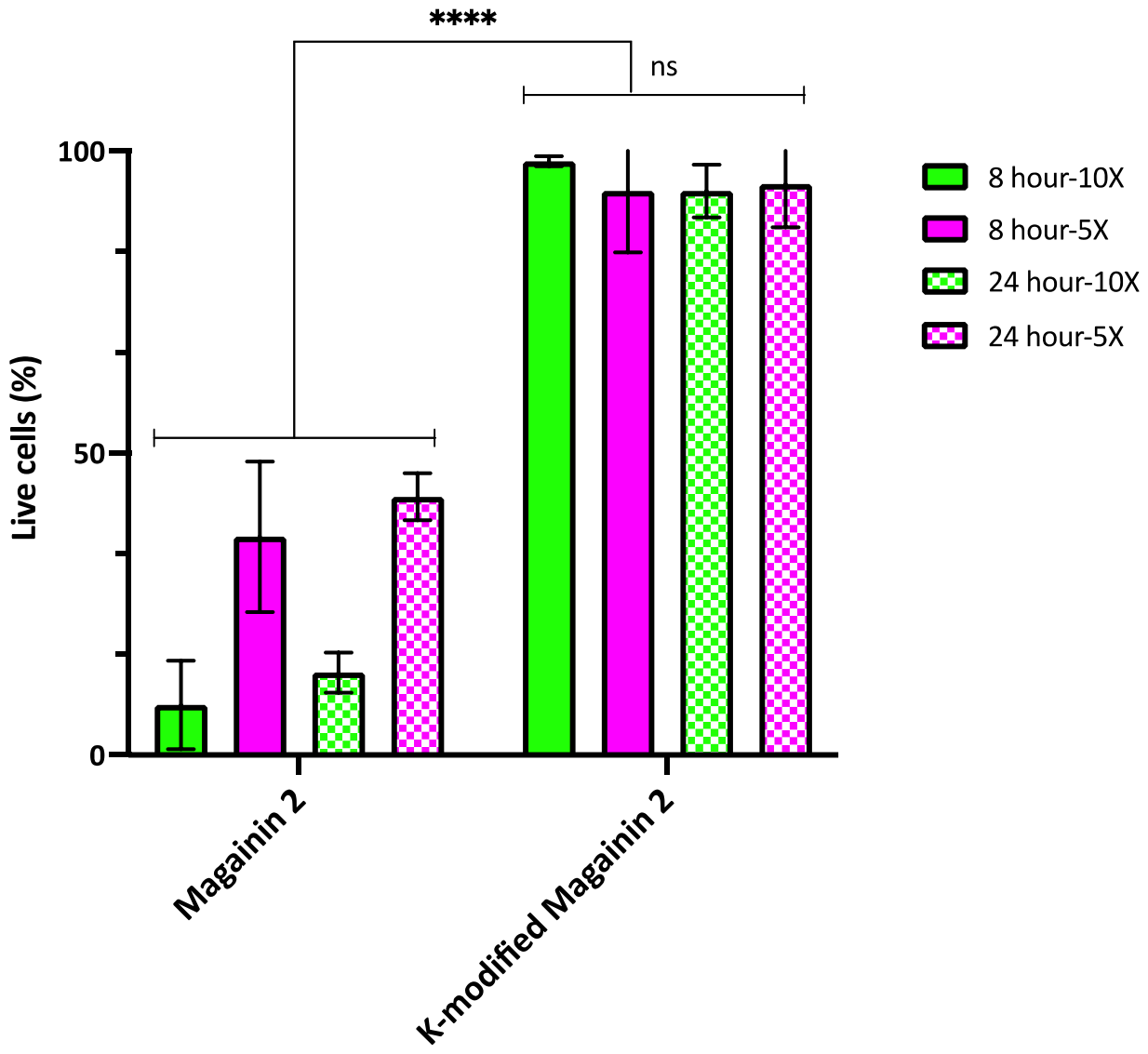

Figure 4.5: Live cell percentage for treating the 3T3 cells with magainin2 versus K-modified Magainin 2 in LIVE/DEAD cell viability assay.

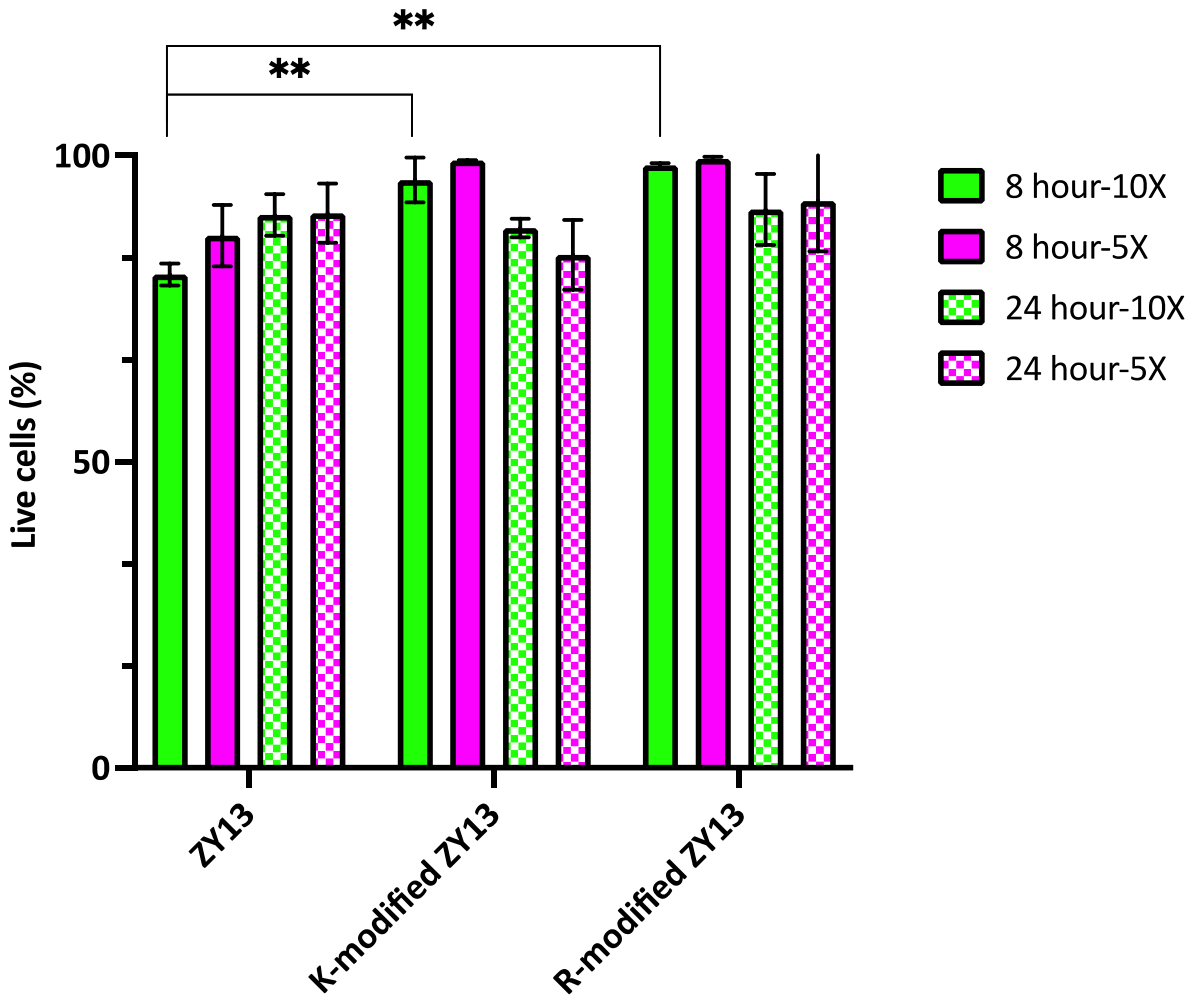

Figure 4.6: Live cell percentage for treating the 3T3 cells with ZY13 versus K-modified ZY13 and R-modified ZY13 in LIVE/DEAD cell viability assay.

4.3. Material and method

4.3.1. Material

Lysogeny broth (LB) (Fisher Scientific). Tryptic soy broth (TSB), agar, M9 minimal salts (Difco Laboratories). 3T3 cells (Sigma-Aldrich), T25 flask (Fisher Scientific), Dulbecco's Modified Eagle Medium (DMEM) complete (Thermo Fisher), LIVE/DEAD solution (Thermo Fisher kit), tissue culture–grade D-PBS (Thermo Fisher), 1,2-dioleoyl-*sn*-glycero-3-phosphoethanolamine (DOPE), 1,2-dioleoyl-*sn*-glycero-3-phospho-L-serine (DOPS) 1,2-Dioleoyl-*sn*-glycero-3-phosphocholine (DOPC) and 1,2-Dioleoyl-*sn*-glycero-3-phospho-*rac*-(1-glycerol) (DOPG) lyophilized lipids (Avanti Polar Lipids), quartz-glass capillaries (Hilgenberg GmbH).

4.3.2. Minimum inhibitory concentration (MIC) determination

Standard lab strains *E. coli* MG1655 and *S. aureus* SA113 are used as Gram-negative and Gram-positive strain, respectively. *E. coli* MG1655 were grown in (LB), and SA113 were grown in Tryptic (TSB) at 37 °C. Both bacterial strains are grown under aerobic condition. MICs of Magainin 2, ZY13, K-modified Magainin 2, K-modified ZY13 and R-modified ZY13 were determined in a standard microbroth dilution assay in accordance with the guidelines of the Clinical and Laboratory Standards Institute guidelines (CLSI)[65] with suggested modifications by Hancock group.[66] An overnight culture of bacterial strains was diluted with the appropriate media and grown to mid log phase (OD600 of 0.5−0.6), then diluted 50 times before added to a 96-well microplate containing 2× serial dilutions of Magainin 2, ZY13 as the positive controls, no drug as negative control, K-modified Magainin 2, K-modified ZY13 and R-modified ZY13 for a final count of 5×10^4 cfu/well. The plates were incubated at 37 °C for 18 hours in an ambient air incubator

and read for turbidity in each well. The MIC values were determined as the lowest concentration that completely inhibited bacterial growth. Assay was performed in triplicate.

4.3.3. Minimum bactericidal concentration (MBC) determination

For the determination of MBCs, 5 µL of bacterial suspension from each well of the MIC plate were then transferred into 100 µL of LB or TSB in a 96-well plate and incubated for 18 hours at 37 °C. The lowest concentration that revealed no visible bacterial growth after subculturing was taken as MBC. Assay was performed in triplicate.

4.3.4. LIVE/DEAD Viability/Cytotoxicity for mammalian cells

3T3 cells were thawed at 37°C and immediately cultured in a T25 flask containing 10 ml (DMEM) complete (DMEM + 10% Fetal bovine serum (FBS) + 1% Antibiotic-Antimycotic (ABAM)). Cells were cultured at 37°C with 5% CO_2 until 90% confluency. Then, cells were removed from the flask, counted, and plated in a 96 well plate at 5000 cell/well density with 100ul complete media. 24 hours later, cell adherence was confirmed under microscope (Zeiss Axio.Z1 Observer microscope). The cells were treated with Magainin 2 and ZY13 as the positive controls, no drug as negative control, K-modified Magainin 2, K-modified ZY13 and R-modified ZY13 (the concentration of compounds are 10 times more than their MIC values). After 24 hours, media was completely removed and 100ul LIVE/DEAD solution was added to each well.

4.3.4.1 LIVE/DEAD solutions preparation and assay

10 mL of 2 µM calcein AM and 4 µM EthD-1 solution was made. Based on Thermo Fisher protocol these dye concentrations are suitable for NIH 3T3. After the LIVE/DEAD reagent stock solutions were warmed up at room temperature, 20 µL of the 2 mM EthD-1 stock solution were added to 10 mL of sterile, tissue culture–grade D-PBS and vortexed to give us 4 µM EthD-1 solution. Then, 5 µL of 4 mM calcein AM stock solution was added to the 10 mL EthD-1 solution and vortexed. The 2 µM calcein AM and 4 µM EthD-1 working solution was then added directly to cells. 100 µL of the combined LIVE/DEAD assay reagents, using optimized concentrations was added to the wells containing the cells in a way that all cells are covered with solution. Cells were incubated for 30–45 minutes at room temperature. The assay was done in triplicate. The imaging was performed fluorescence microscope (Zeiss Axio.Z1 Observer microscope). Cell counting was performed by imageJ software (cell counter option).

4.3.5. SAXS Studies

4.3.5.1. Liposome Preparation for X-ray Measurements.

DOPE, DOPS, DOPC and DOPG lyophilized lipids were used. Small unilamellar vesicles (SUVs) were prepared by sonication. Stock solutions of DOPS, DOPE and DOPC were prepared in chloroform at ∼20 mg/g. Mixtures of these lipids were prepared at molar ratio of DOPS/DOPE/DOPC = 20/40/40 (eukaryotic mimicking SUV) and DOPG/DOPE = 20/80 (prokaryotic mimicking SUV). Chloroform was evaporated under N_2, and the mixtures were dried further by overnight desiccation under vacuum. The dried lipids were resuspended the next day in in aqueous buffer solution at two different pH levels: 1) 140 mM NaCl + 10 mM HEPES (pH 7.4); 2) 140 mM NaCl,

10 mM sodium acetate (pH 5.0). Solutions were incubated at 37 °C for 18 hours and then sonicated until clear. SUVs were obtained by extrusion (0.2 μm pore Nucleopore filter).

4.3.5.2. SAXS Experiments.

Magainin 2, ZY13, K-modified Magainin 2, K-modified ZY13 and R-modified ZY13 stock solutions were prepared by dissolving the molecules in 10mM HEPES, 140 mM NaCl for pH 7.4 and 10mM acetate, 140 mM NaCl for pH 5. Lipids were thoroughly mixed with modified AMPs at specific molecule to lipid ratios (P/L) in pH 5 and pH 7.4 buffers. Sample solutions were hermetically sealed in quartz-glass capillaries. Synchrotron SAXS experiments were conducted at the Stanford Synchrotron Radiation Laboratory (BL 4-2). Monochromatic X-rays with 9 keV energy were used. Scattering was collected using a Rayonix MX225-HE detector (pixel size 73.2 μm). The 2D SAXS powder patterns were integrated using the Nika 1.48 package for Igor Pro 6.21 and FIT2D.[67]

4.4. Conclusion

MIC dropped significantly for all modified AMPs at pH 5, which suggested that lower dose of our modified AMPs would not be active at biological pH but very active at acidic pathogenic conditions (specially for ZY13). K- modified ZY13 showed no antibacterial activity at pH 7.4 against both PA and SA. However, it showed a good MIC value at pH 5 against PA and SA. K- modified Magainin 2 showed no antibacterial activity at pH 7.4 against PA but showed a good MIC value at pH 5 against PA against the same bacterial strain. MBC values of our modified AMPs are similar to their respective MIC values at pH 5, indicating that the compounds not only are inhibiting bacterial growth but are also bactericidal. Bioassays and SAXS consistently confirmed pH sensitivity of K-modified ZY13, R-modified ZY13 and K-modified Magainin 2. None of our modified antimicrobial peptides showed any antibacterial activity against eukaryotic mimicking SUVs (PS/PE/PC:20/40/40) at both pH 5 and pH 7.4. However, they all induced cubic phase, necessary for bacterial membrane disruption, on prokaryotic mimicking SUVs (PG/PE:20/80) at pH 5. The significance of these was revealed when the modified AMPs could not induce cubic phase on prokaryotic mimicking SUVs at pH 7. Another significant feature of our modified AMPs is none of them showed toxicity toward 3T3 mammalian cells in LIVE/DEAD assay even after 24 hours in concentration ten times more than their MIC value.

Chapter 5: Hybrid antibiotic peptide conjugates to cross bacterial membranes

(This work is already published in Bioconjugate chemistry journal in 2017. My contribution to this work was synthesis of and purification peptide transporters and performing MIC and MBC assays)

5.1. Introduction

Aminoglycosides are a family of commercially available antibiotics. The most therapeutically used antibiotic in this family are tobramycin, gentamicin, kanamycin, amikacin and neomycin. Streptomycin is the first antibiotic discovered in the aminoglycoside family. This medicine, which was the first effective antibiotic against tuberculosis, was isolated from the actinobacterium *streptomyces griseus* in 1943. Aminoglycosides mechanism of action is to bind 30S subunit of bacterial ribosome and block protein synthesis[70,71,72]. This family of antibiotics are mostly potent against aerobic Gram-negative bacteria but can also show moderate potency against Gram-positive bacteria[73]. Unfortunately, even with high potency of aminoglycosides, antibiotic resistance in bacteria against this family of antibiotics has drastically increased[74,75,76]. To combat this problem, we should focus on the main mechanisms of aminoglycosides resistance. Bacteria can become resistant against aminoglycosides mostly by one of these three mechanisms: 1) uptake and drug efflux reduction 2) inactivation of aminoglycosides via enzymatic reactions, such as acetylation, phosphorylation and adenylation 3) modification of ribosomes like mutation and methylation[70,76]. For example, counteracting the enzymatic inactivation of aminoglycosides is one of the approaches to prevent bacterial resistance. In this method articular inhibitors are used to compete with aminoglycoside-modifying enzymes[77,78,79]. However, the side effects of these inhibitors outweigh their effectiveness on bacterial resistance. Recently, chemical modification

of aminoglycosides to prevent bacterial resistance has been drawn significant attention[80,81,82,83]. Since 1990s various analogs of aminoglycosides have been produced by chemical modification. However, only a few products reached clinical trials like Plazomicin. This antibiotic, which is been introduced by Achaogen Inc, is a semisynthetic aminoglycoside derived antibiotic from sisomoci. Plazomicin was approved for medical use in the United States in 2018. It is used to treat complicated urinary tract infection and shown good activity against Gram-positive and Gram-negative bacteria[84,85]. As of 2019 it is recommended only for those in whom alternatives are not an option due to side effects including kidney problems, diarrhea, nausea, and blood pressure changes, hearing loss, *Clostridium difficile*-associated diarrhea, anaphylaxis and muscle weakness.

The balance between the amount of antibiotic influx and efflux determines the amount of drug accumulating in the bacterial cells. Another method to prevent antibiotic resistance is to increase the influx of antibiotics through the bacterial cell membrane barrier. This approach increases the activity of antibiotics against resistant strain of bacteria. Recent technology advancements help scientists to understand the membrane mechanism of drug uptake and extrusion by much better[86].

There is a strong correlation between bacterial efflux system overexpression and multidrug resistance[86]. Efflux pumps exist in nearly all bacteria. This efflux system in bacteria constantly pumps antibiotics out of the cell to decrease the amount of drug within the cell; hence, helping the bacterial survival. Reduced amount of antibiotic inside bacteria not only effects the bacteria susceptibility toward drugs but also causes the acquisition of additional resistance mechanisms. In addition, efflux pumps can contribute to the appearance of drug-tolerant persister bacteria. In

Gram-negative bacteria the pours of the cell membrane is full of water. Therefore, small hydrophilic compounds like b-lactams can easily enter the cell. However, hydrophobic drugs, which cannot pass through the water pours, gain access to the inside of the bacteria cells by a slow metabolic activity-dependent mechanism. This outer membrane (OM) structure of the Gram-negative bacteria works as a significant barrier for hydrophobic drugs to get into the cell and provides an extra layer of defense[87]. In multidrug resistant strains of bacteria the permeability of drug may be reduced[87,88] by the cell via different mechanisms, such as modification or reduction of the porins or adjustment on phospholipid composition of the outer membrane. In addition, the reduced rate of antibiotic permeation into the bacteria leads to less accumulation of antibiotics in persister cells. Neutral and hydrophobic drugs pass through the membrane of bacteria much easier than positively charged antibiotics. The reason is that, positively charged antibiotics, such as aminoglycosides, have a large electrostatic self-energy compared to the lipid as a low electric constant media.

In general, aminoglycosides are inactive against different kinds of microbes, such as anaerobic bacteria and persister cells[80,89,90,91,92]. To investigate the reason behind such inactivity we need to pay attention to the aminoglycosides uptake mechanism in these species. The proposed aminoglycosides uptake mechanism is this family of drugs can gain access to the cell interior based on an active-transport mechanism. This active-transportation mechanism is an energy dependent phenomenon based on the generation of proton-motive force (PMF)[93,89]. The challenge about this mechanism is that PMF can be shut down by persiter cells which blocks the influx of aminoglycosides[93]. Therefore, the efflux pumps can counteract the influx pumps and

significantly reduce the aminoglycoside concentration in the cell. In addition, the active-transport mechanism is very slow compared to the diffusive transport.

Antimicrobial peptides (AMPs) are an important part of part of innate immunity in human beings, animals, plants and microorganisms. In the past few decades, AMPs gained significant attention as potential antibiotics to treat resistant bacteria. AMPs are broad-spectrum antibiotics[15,16,11,18], which can kill the bacteria by a non-specific interaction that targets the generic features of the outer membrane in different kinds of pathogens. Therefore, unlike conventional antibiotic, development of resistance against antimicrobial peptides is less common[15]. The most important drawback with AMPs is, compare to conventional antibiotics, they have moderate potency[94].

AMPs share two common features: they are cationic and amphiphilic. In fact, both positive charge and hydrophobicity are necessary to introduce negative Gaussian curvature on the membrane of the bacteria[46]. Formation of negative Gaussian curvature on the bacterial membranes leads for membrane destabilization processes such as budding, blebbing and pore formation[95].

In order to overcome aminoglycoside uptake issue, we engineered a membrane-active antibiotic-peptide conjugate (MAAPC), Pentobra. Pentobra consist of a short peptide (derived from penetratin) as the cell-penetration peptide (CPP) and tobramycin from aminoglycoside family. Hence, it owns a higher molecular weight than aminoglycoside alone. This higher molecular weight help the drug to accumulate in higher concentrations within the bacterial cell due to the less efficiency of the efflux pumps against higher molecular weight compounds. In addition, the peptide-conjugate target the membrane of the bacteria and facilitates the aminoglycoside uptake. Therefore, with this new engineered molecule, we can tackle the uptake and efflux

problems, simultaneously. Moreover, Pentobra kills the bacteria in two different but mutually amplifying ways. 1) The CPP part of the drug disrupts the bacterial cell membrane integrity and 2) The aminoglycoside tobramycin part targets the protein synthesis in the cell. This peptide-aminoglycoside conjugation also promotes more rapid drug uptake into persistant cells via AMP-like membrane permeation mechanism. In addition, the mistranslation of proteins, caused by the aminoglycoside part, stress the membrane barrier function even more. Therefore, Pentobra has a potential antimicrobial activity against bacteria that aminoglycoside cannot target alone.

Previously, Pentobra was synthesized and its antimicrobial activity evaluated in our group. The data showed that Pentobra is a broad-spectrum, potent antibiotic against persistant cells and anaerobic *Propionibacterium acne*[96].

The Pen peptide in Pentobra has a sequence containing twelve amino acids (RQIKIWFQNRRW). As mentioned before Pen peptide is a derivative of Penetratin (RQIKIWFQNRRMKWKK) with sixteen amino acids. In this chapter, we engineer a library of MAAPCs derivatives of Pen peptide with different variations in the peptide sequence, hydrophobicity, helical amphiphilicity, the conjugation site tobramycin and linker chemistry. All these factors are important in antimicrobial activity of the final drug. These experiments result in a platform of novel, broad-spectrum MAAPCs which distinct and synergistic mechanisms of killing.

5.2. Result and discussion

5.2.1. Synthesis of MAAPC

As mentioned above, membrane activity of the AMP part of MAAPCs helps the traditional antibiotics access the bacterial cell interior. MAAPCs contain a potent antibiotic, which has difficulty to cross the bacterial cell wall, and a peptide transporter conjugated to the potent antibiotic and facilitates bacterial membrane entry. It is important to keep in mind that conjugation of a potent antibiotic and a peptide with high antimicrobial activity does not necessarily lead to a potent hybrid antibiotic. In fact, if the mechanism of membrane activity in molecules such as AMPs gets neglected, the activity of both the traditional antibiotic and the peptide transporter can decrease by functional interference. To engineer, these diverse antibiotics a specific methodology is needed. Schmidt et al. discovered sequence principals to design peptides which are able to induce negative Gaussian curvature on the bacterial membrane[18,31,46,97,98,99]. As mentioned in chapter 1, there is a trend observed in the sequence of 1080 cationic AMPs in which the lysine/arginine ratio increases with the hydrophobic content of an AMP[100]. Creation of negative Gaussian curvature and therefore membrane disruption depends on both positively charged residues such as lysine and arginine and hydrophobic content of the AMP sequence. These requirements put a constraint on the designing of the AMP sequence. Therefore, these sequence constraints under-determine the full sequence. On the other hand, they enable the same sequence blend different functions in the antimicrobial activity. Based on this reason, it is possible to deliver molecules like polycationic aminoglycosides by utilizing the membrane activity of AMPs[101].

We chose tobramycin, a polycationic aminoglycoside, as the conventional antibiotic part since: 1) it has only one primary hydroxyl group in its structure which helps the selective conjugation. Compared to the secondary hydroxyl group in tobramycin structure, the primary hydroxyl is a stronger nucleophile and less sterically hindered. These features of the primary hydroxyl eliminate the need for orthogonal protection of the secondary hydroxyl group exists in tobramycin structure. 2) The primary hydroxyl group, as the conjugation site, does not interact with ribosome of the bacteria and leaves the antibiotic activity of tobramycin intact after conjugation with the peptide[102,103]. 3) Tobramycin is the most common antibiotic to treat many types of *Pseudomonas aeruginosa* infections like pulmonary infections caused by cystic fibrosis[104]. A selective membrane permeation by the peptide transporters is a result of a proper ratio in the number of cationic charges and hydrophobic content of the peptide sequence. Therefore, we are able to tune the antimicrobial activity by adjusting peptide hydrophobicity and cationic charge. In this chapter we designed peptides transporters (MAAPCs), paying attention to the sequence patterns in natural AMPs and the rules of saddle-splay curvature creation on bacterial membranes (Table 5.1).

Table 5.1: Designed MAAPCs based on induced saddle-splay curvature

MAAPC	Other name	Peptide sequence	*N*- or *C*- terminal conjugation
	Penetratin	RQIKIWFQNRRMKWKK	
MAAPC01	Pentobra	RQIKIWFQNRRW	*N*-terminal
MAAPC02		GWIRNQFRKIWQR	*N*-terminal
MAAPC03		GWRRNQFWIKIQR	*N*-terminal
MAAPC04		GWRNQIRKGWQR	*N*-terminal
MAAPC05		RQIKIWFQNRRW	*C*-terminal

MAAPC01 (Pentobra) has been designed inspired by natural AMP, Penetratin. In MAAPC02, MAAPC03 and MAAPC04, just as Pentobra, tobramycin is attached to the *N*-terminus of the peptides by a short amide bond linker (Figure 5.1)[92]. MAAPC05 and MAAPC01 have the same peptide sequence; however, in MAAPC01 tobramycin is attached to the *C*-terminus of the peptide by a synthetic amino acid, L -propargylglycine, via click chemistry (Scheme 5.1). As a

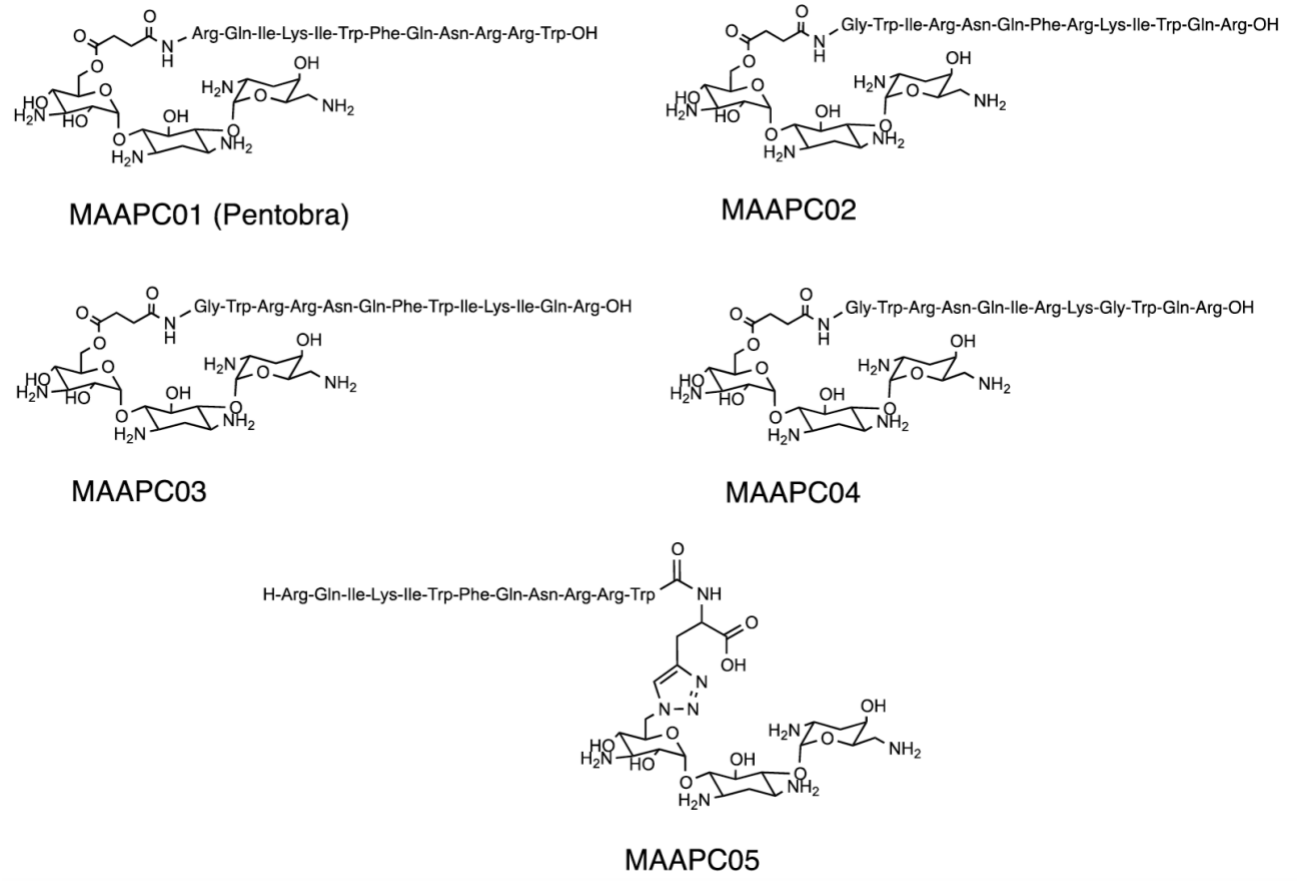

Figure 5.1: Chemical structures of MAAPC01, MAAPC02, MAAPC03, MAAPC04, MAAPC05.

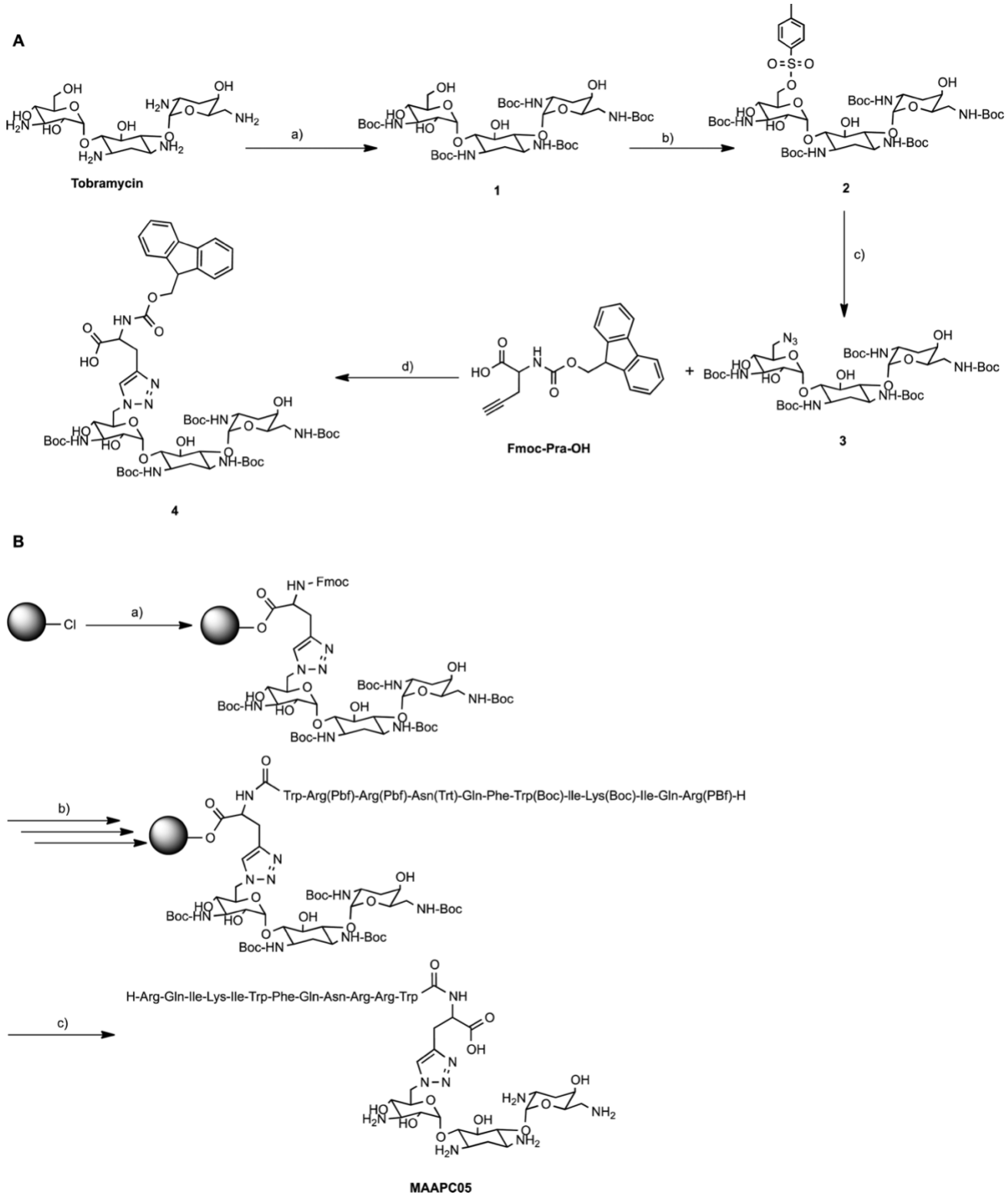

Scheme 5.1: Synthesis of Fmoc-Pra(BocTobra)-OH (4): (a) Boc2O, TEA, H2O/DMF (1:4), 5 hours, 60 °C, 93%[92] (b) TsCl, pyridine, 12 hours, 23 °C, 36% (c) NaN3, DMF, 12 hours, 80°C, 99% (d)

CuSO4, sodium ascorbate, DMF, 24 hours, 40°C, 61% (B) Grafting of Fmoc-Pra(BocTobra)-OH to 2-chlorotrityl chloride resin ((a) compound 4, DIEA, DCM, 4 hours, 23°C followed by peptide synthesis on solid support using Fmoc strategy ((b) Fmoc cleavage using piperidine and coupling using DIEA, HOBt and HBTU), and final cleavage and deprotonation of the peptide using a mixture of trifluoroacetic acid (TFA) and scavengers ((c) TFA/phenol/water/thioanisole/TIS (10:0.7:0.5:0.5:0.25 v/w/v/v/v), 3 h, 23 °C, 46%). The gray sphere represents the 2-chlorotrityl chloride resin.

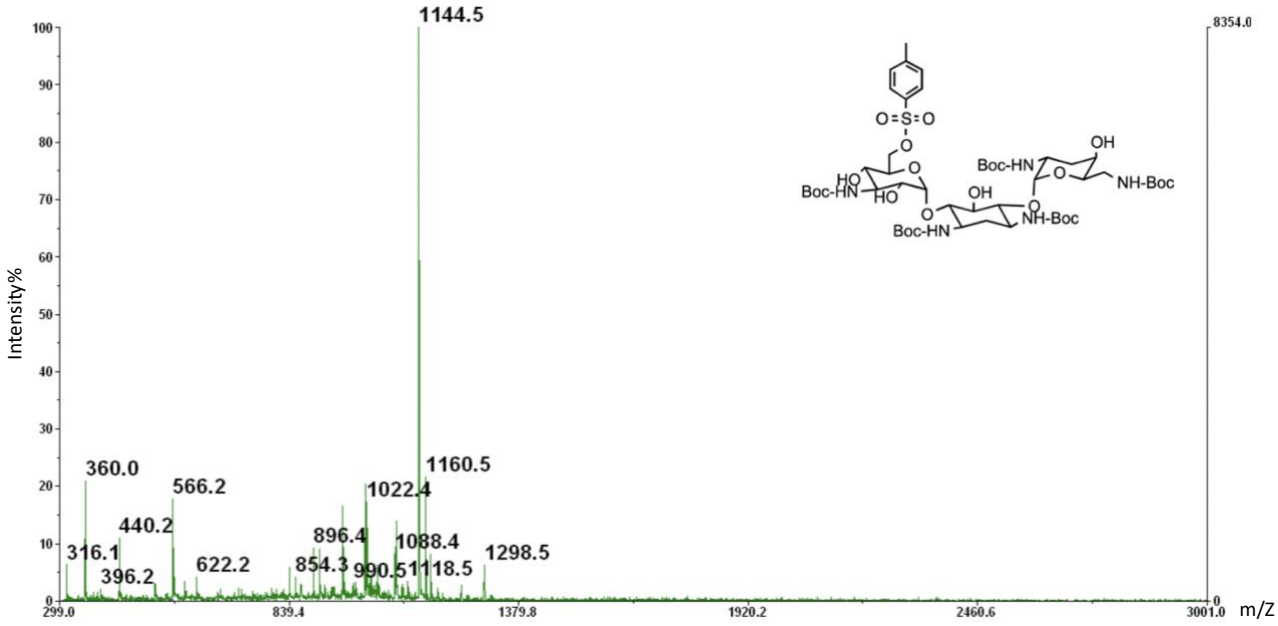

Figure 5.2: MALDI Spectrum of Tosyl-Boc5-tobramycin

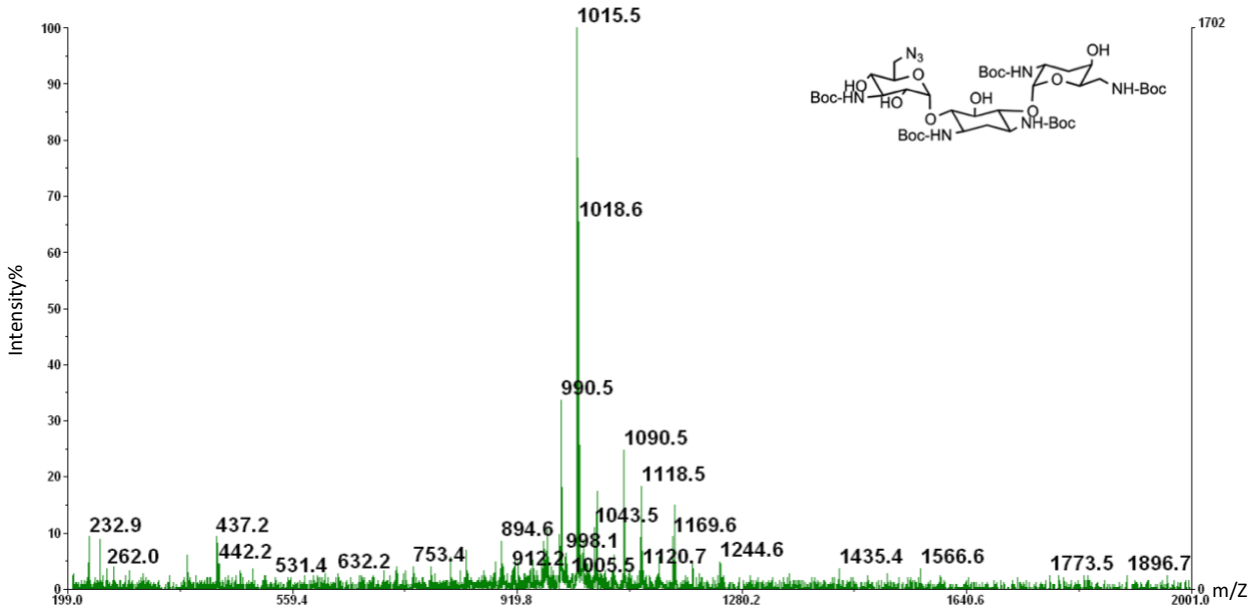

Figure 5.3: MALDI Spectrum of Azido-Boc5-tobramycin

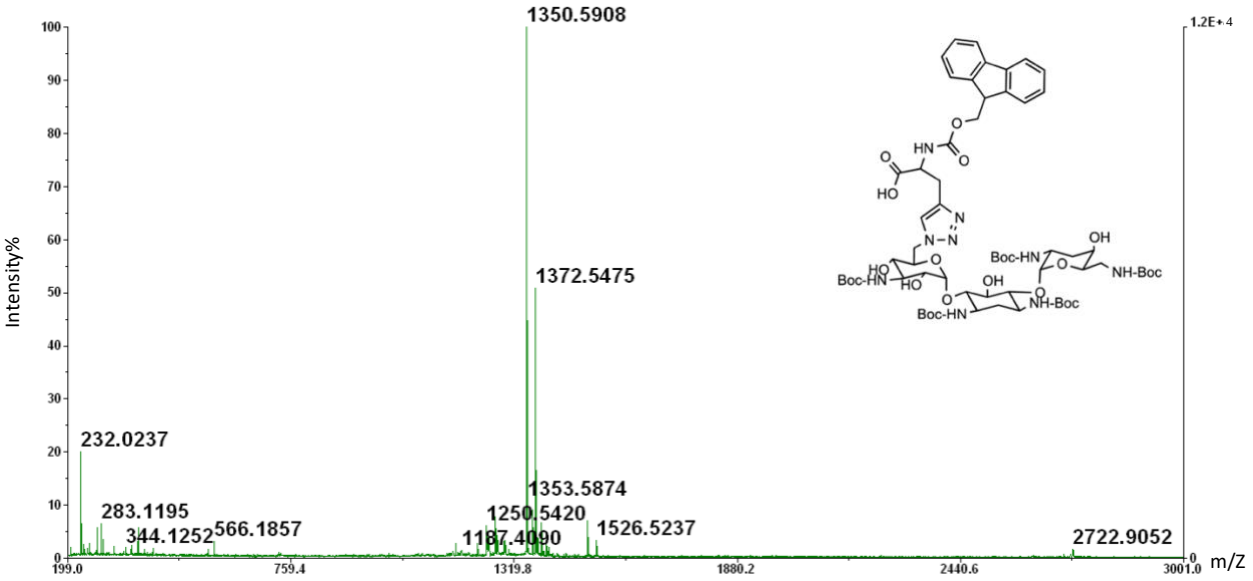

Figure 5.4: MALDI Spectrum of Fmoc-Pra(BocTobra)-OH

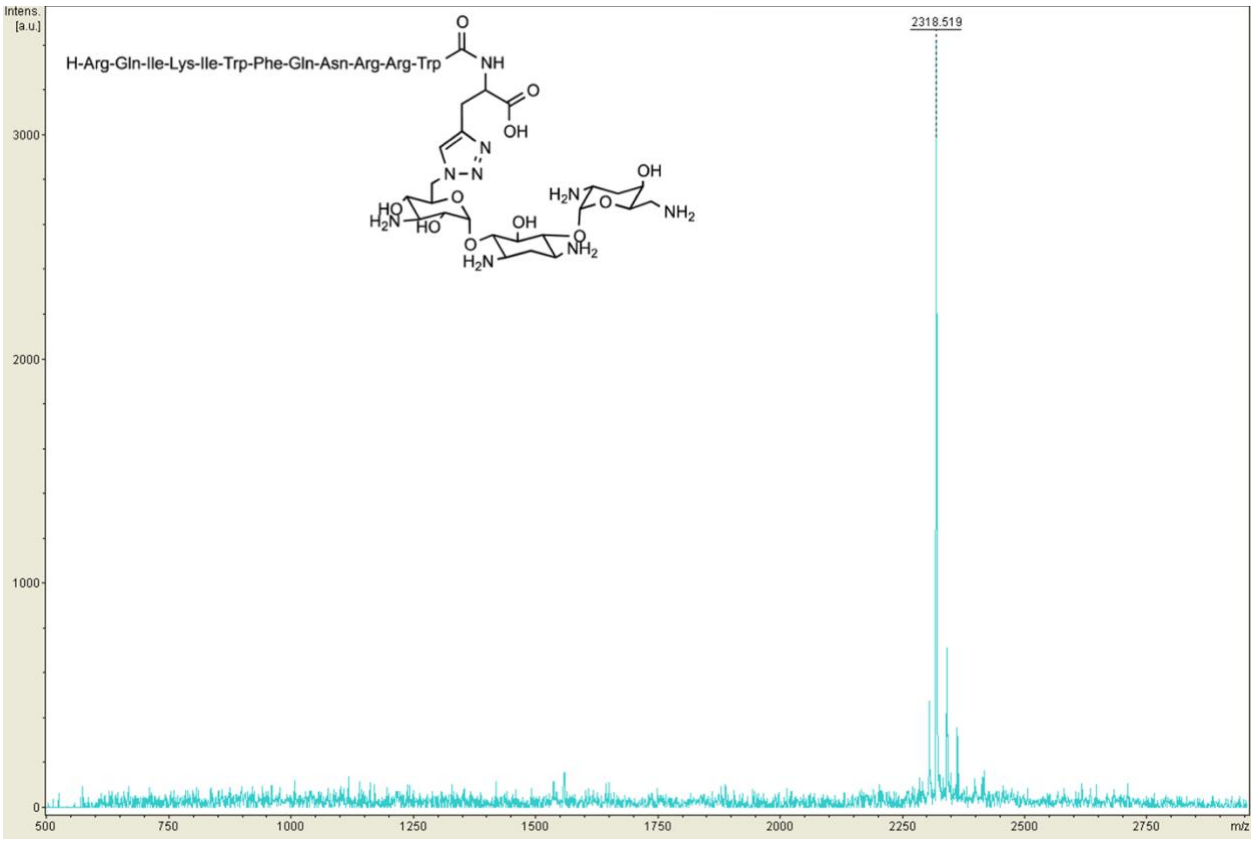

Figure 5.5: MALDI spectrum of Pra (Tobra)Pen (cPentobra)

result, in MAAPC05, tobramycin is attached to the peptide sequence by a triazole ring which is more stable against hydrolysis than the ester bond in MAAPC01. To achieve click chemistry, the amine groups in tobramycin were first protected by *tert*-butoxycarbamates (BOC) protecting group (compound **1**). In the next step, the hydroxyl group at C6" position of BOC protected tobramycin was activated via the reaction with *p*-toluenesulfonyl (TsCl) in pyridine, resulting the monotosylated BOC protected tobramycin (compound **2**) (Figure 5.2). Then, to introduce azide function, essential for "click" reaction, on monotosylated BOC protected tobramycin, it went through the reaction with soduim azide (NaN_3) in DMF at 80°C to produce azido-Boc_5-tobramycin (compound **3**) (Figure 5.3). For the final step, "click" reaction was performed to produce Fmoc-

Pra (BocTob)-OH (compound **4**) (Figure 5.4). In this final step, compound **3** clicked with Fmoc-protected ^{L}-propargylglycine (Fmoc-Pra-OH) by copper(I)-catalyzed azide-alkyne 1,3-dipolar cycloaddition reaction (Scheme 5.1A). To be able to perform solid-phase peptide synthesis, compound **4,** as the first peptide residue, was grafted to 2-chlorotrytil chloride resin. The rest of the peptide sequence was synthesized by peptide synthesizer due to standard Fmoc strategy. Finally, the peptide was cleaved from the resin and fully deprotected using a mixture of trifluoroacetic acid (TFA) and scavengers to yield MAAPC05 (Scheme 5.1B) (Figure 5.5).

The MAAPC peptide designs are based on penetratin, a cell penetrating peptide (CPP) isolated from the homeobox domain of the ANTP protein. CPPs, like AMPs, interact strongly with membranes and are cationic and amphiphilic. There is no strict distinction between the two peptide classes, although CPPs are generally less hydrophobic than AMPs.[105] Many AMPs have been shown to cross bacterial membranes in the CPP-like manner and exert antimicrobial activity by binding intracellular targets, and certain CPPs are antibacterial in vitro.[106] All MAAPCs in this project contain tobramycin, which binds to the tRNA decoding A-site in prokaryote ribosomes.[71,72,74] The first MAAPC, Pentobra (MAAPC01) and the other peptide sequences were selected in concert with the physicochemical properties of tobramycin such that the conjugate possesses a specific total cationic charge that favors membrane penetration and permeabilization in bacteria. The new MAAPCs share many similarities in sequence and amino acid composition (Table 5.1 and 5.2), but were designed to differ in important ways, in order to examine how specific peptide characteristics affect the ability of MAAPCs to target bacteria and optimize activity. We focused on the effects of peptide sequence, hydrophobicity, helix amphiphilicity, the linker used to connect the peptide with tobramycin, and *N*-terminal vs *C*-

terminal conjugation. Penetratin comprises 16 amino acids, whereas all the transporter sequences are shorter, with 12 or 13 amino acids (Table 5.2). Penetratin and each of the transporter sequences each possess the same number of arginine, glutamine, asparagine, and tryptophan residues (Table 5.2).

Table 5.2: Composition of Peptide Transporter Sequences

	R	Q	K	N	W	I	F	G	M	Net charge
Penetratin	3	2	4	1	2	2	1	0	1	+7
MAAPC 01/05	3	2	1	1	2	2	1	0	0	+9
MAAPC 02/03	3	2	1	1	2	2	1	1	0	+9
MAAPC4	3	2	1	1	2	1	0	2	0	+9

The net charge of penetratin is +7, whereas the peptide−tobramycin conjugates have a net charge of +9. Figure 5.2 depicts the helical wheel projections of the MAAPCs in comparison to penetratin. It is important to note that (a) rotational freedom along σ bonds means the

tobramycin may not sit exactly where depicted in this figure and (b) the size of the helical wheel is not depicted to the scale of the aminoglycoside. Despite these limitations, Figure 5.2 does allow us to compare structures of the MAAPCs to penetratin. Penetratin has a cluster of mostly cationic residues (RKKQR) flanked by multiple hydrophobic residues on either side (FWIRW and MI). MAAPC01 shows the greatest clustering of cationic character when the cationicity of tobramycin is included in addition to the cationic residues (RKQR-tobramycin). The amino acid composition MAAPC02 differs from MAAPC01 by the addition of a single glycine at the *N*-terminus, and the residues in MAAPC02 are rearranged to create a sequence in which the cationic and hydrophobic residues cluster on opposing sides of the peptide helical wheel diagram (Figure 5.2).

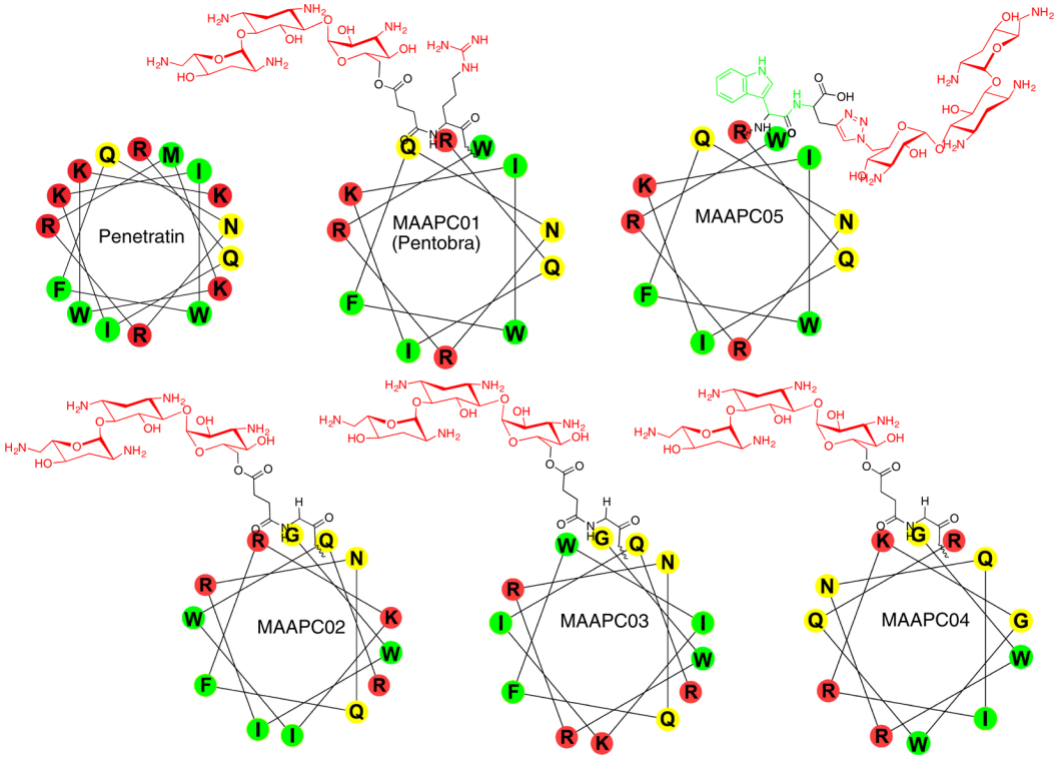

Figure 5.6: Helical wheel projections of MAAPCs. Cationic residues are represented in red, hydrophobic residues are represented in green, and neutral amino acids are in yellow.

This type of amphiphilicity is observed in α-helical AMPs sequences and is often important for antibacterial activity.[107] MAAPC03 has the reverse sequence of MAAPC01 and has identical amino acid composition to MAAPC02 but the amino acid residues are in a different sequence to exhibit greater amphipathicity. A reverse peptide sequence, in principle, is expected to have equivalent antibacterial activity as the original if activity is derived solely from nonspecific interactions with bacterial membranes. Helical amphiphilicity is also present in MAAPC04, but the hydrophobic content of the peptide is reduced from 38.5% to 25% (Table 5.3) by removing one isoleucine and the phenylalanine and replacing these bulky hydrophobic residues with glycines (Table 5.2).

Table 5.3: Hydrophobicity of Peptide Transporter Sequences

	%hydrophobic	Eisenberg consensus	Kyte Doolittle (GRAVY)	Wimley-White	N_K/N_R	$N_{Primary\ amines}/N_R$
Penetratin	37.5	-0.54	-1.73	-1.50	0.75	0.75
MAAPC 01/05	41.7	-0.47	-1.49	-1.36	0.33	2
MAAPC 02/03	38.5	-0.42	-1.41	-1.31	0.33	2
MAAPC4	25	-0.55	-2.17	-1.55	0.33	2

A comparison of MAAPC04 with the more hydrophobic MAAPC01 allows us to investigate the effects of reducing peptide hydrophobicity on membrane permeation and antibacterial activity. To explore the additional degree of freedom afforded by conjugation chemistry we connected tobramycin to the C-terminus of the Pen peptide from MAAPC01. The resulting MAAPC05 has a different chemical structure in the linker that is proximal to tobramycin. The arrangement of a cationic patch flanked by hydrophobic residues (as seen in penetratin) is best replicated by MAAPC01, where the aminoglycoside is located near the cluster of cationic residues. MAAPC05 also colocalizes the aminoglycoside with the cationic residues, but the overlap is not as great since attachment to the tryptophan residue orients it away from the cationic face. In this instance, however, rotation about the N−C bond of the tryptophan carbon would bring the aminoglycoside closer to the cationic face. MAAPC02 has a hydrophobic face and a cationic face, but the cationic face has neutral residues on one site, in contrast to penetratin. MAAPC03 is similar to MAAPC05; however, the rigidity of the peptide bond will direct the aminoglycoside chain such that it cannot sit directly over the neutral residues. Finally, MAAPC04 has a large cationic side, and only a small patch of hydrophobic residues. MAAPC01 and 05 have the highest percentage of hydrophobic residues at 41.7% (Table 5.3); MAAPC02 and 03 are comparable to Penetratin (38.5% and 37.5%, respectively), while MAAPC04 has the lowest number of hydrophobic residues (25%). The hydrophobicity of the MAAPCs in comparison to penetratin and other AMPs can also be observed in plots of the ratio of lysines to total cationic charge versus average molecule hydrophobicity (Figure 5.3). The peptide “transporter” sequences clearly lie along the AMP sequence trendline (Figure 5.3), with the MAAPCs 01 and 05 having the greatest average hydrophobicity, followed by MAAPCs 02 and 03, and finally MAAPC04. Their positions

demonstrate that all MAAPC peptides except MAAPC04 are more hydrophobic and arginine-rich than the parent penetratin peptide. Moreover, penetratin is less hydrophobic than AMPs with comparable lysine/cationic charge ratio, which is consistent with its classification as a CPP. If we account for the presence of tobramycin in the MAAPCs by considering its entire contribution to be charged from the five amine groups, then the molecules are located closer to penetratin on the plot and are expected to behave more like cell-penetrating peptides. This simple characterization of the physicochemical properties of tobramycin does not account for pKa differences in the amino groups and the influence of other chemical moieties in tobramycin, however, and the actual locations of the MAAPCs are likely to be between the peptide only and peptide + amine positions. The MAAPCs are therefore expected to possess membrane permeabilization and drug transporter abilities, the desired attributes of multifunctional antibiotics that act on both bacterial membranes and ribosomes. Together, these five MAAPCs provide insight into the effects that sequence, hydrophobicity, amphiphilicity, and linker chemistry have on antibacterial activity.

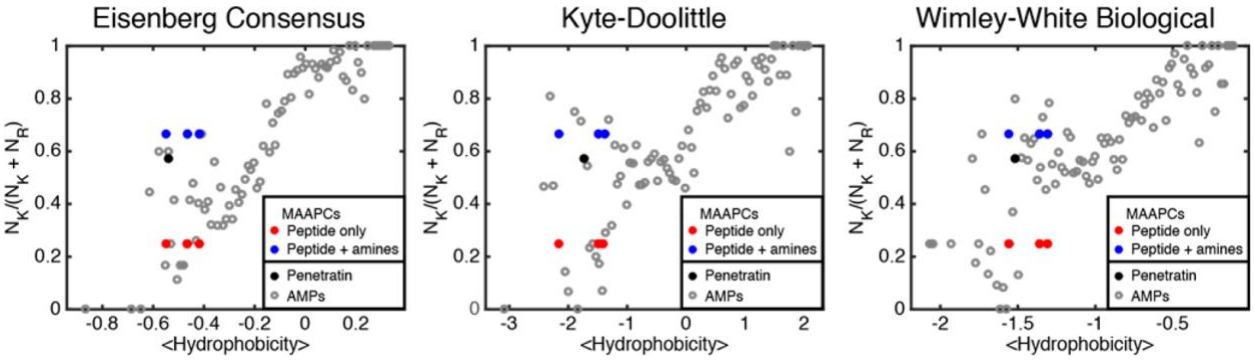

Figure 5.7: Cationic behavior of MAAPCs, plotted as the ratio of the number of amines in each molecule to its total cationic charge, as a function of average peptide hydrophobicity calculated with Eisenberg Consensus,[48] Kyte-Doolittle,[47]and Wimley-White[49] amino acid hydrophobicity scales. AMPs are represented by unfilled gray circles, MAAPC peptides by red circles, MAAPCs plus the charge contribution of the five amine groups in tobramycin by blue circles, and the black circle represents penetratin CPP.

5.2.2. MIC and MBC measurement

To evaluate the activity spectrum, we first investigated the antimicrobial potency of these new MAAPCs by determining their minimum inhibitory concentration (MIC) and minimum bactericidal concentration (MBC) against *Escherichia coli* (*E. coli* MG1655) and *Staphylococcus aureus* (SA113) pathogens with a turbidity-based microdilution broth assay (Table 5.4). Overall, all the MAAPCs display good antimicrobial activity and tend to be more selective to *E. coli* (MIC range 3.1−12.5 μM) over *S.aureus* (MIC range 12.5−25 μM), which follows the general observation that tobramycin is particularly active against Gram negative organisms.[108] Their MBC values are either equal to or slightly higher than their respective MIC values suggesting that the compounds not only are inhibiting bacterial growth but are also bactericidal. In contrast, the unconjugated

peptides (P1− P4) exhibited no or little antimicrobial activity against *E. coli* and *S. aureus*. However, the MAAPCs did not show better activity than tobramycin, which is expected because our conjugates are not designed to target lab strains but instead to have high efficacy against clinically relevant pathogens such as persisters, resistant bacteria, and anaerobes that are impermeable to existing antibiotics. It should be noted that a mixture of the peptide itself with tobramycin does not enhance the antimicrobial activity compared to tobramycin alone, indicating there is no synergistic effect between the two entities when simply mixed. Whereas MAAPC05 showed similar activity against *S. aureus* in comparison to MAAPC01 (indicating that the terminus of conjugation did not greatly impact activity), it displayed a 2-fold increase of the MIC against *E. coli*. In contrast, MAAPC02, MAAPC03, and MAAPC04 displayed improved activity compared to MAAPC01. These results indicate the importance of the peptide transporter sequence as well as the conjugation site for tobramycin. Interestingly, MAAPC02 and MAAPC03 have nearly identical amino-acid composition as MAAPC01 (the only difference is a single glycine), but the amino acids are in a different sequence. In the MAAPC02 analog, the hydrophobic amino acids are clustered along one side of the α-helical wheel of the peptide, which confers higher amphiphilic character and greater helical propensity. In the MAAPC03 analog, the peptide has the reversed sequence of MAAPC01. There are examples in the literature that the reversed analogs of antimicrobial peptides possess equal or enhanced antimicrobial activities.[109,110] The amphiphilicity and peptide sequence orientation might play a role on the membrane−peptide interaction. However, further experiments are required to elucidate the reasons for this improved antibacterial activity.

5.2.3. Hemolysis determination

One of the limitations to the clinical use of AMPs as antimicrobial agents is their hemolytic activity which is associated with increased toxicity.[111] Thus, as a first assessment of the MAAPC toxicity, we investigated whether the conjugates may cause lysis of human red blood cells (hRBCs). Notably, all MAAPCs exhibited negligible hemolytic activity against hRBCs (HC50 > 500 μM), which is the first indicator of the MAAPC safety toward eukaryotic cells (Table 5.4). Bacterial and animal cell membranes significantly differ in composition. Indeed, microbial cell surfaces contain more anionic lipids (overall negatively charged) whereas mammalian cell membranes have more lipids with neutral zwitterionic head groups (overall neutrally charged). The MAAPCs were designed to selectively discriminate between bacterial and mammalian cells. The selectivity indexes (SIs), defined as HC50/MIC, for *E. coli* and *S. aureus* demonstrated great selectivity of all MAAPCs to bacteria over hRBCs (Table 5.5), which implies that the MAAPCs are effective against bacteria without causing harm to human cells. MAAPC04 displayed the highest bacterial selectivity (SI > 640 and SI > 160 against E. coli and S. aureus, respectively) likely due to its reduced hydrophobic content.[112]

Table 5.4: MIC and MBC of MAAPCs, Unconjugated Peptides (P1−P4), Mixture of Unconjugated Peptide and Tobramycin (P1−P4+Tobramycin), and Tobramycin Alone on E. coli MG1655 and S. aureus S113.

	E. Coli MG1655		S. aureus S113	
	MIC μM	**MBC μM**	**MIC μM**	**MBC μM**
MAAPC01	6.3±0.0	6.3±0.0	25±0.0	33.3±14.4
MAAPC02	3.1±0.0	3.1±0.0	12.5±0.0	20.8±7.2
MAAPC03	<1.6	3.1±0.0	12.5±0.0	25±0.0
MAAPC04	3.1±0.0	4.2±1.8	12.5±0.0	14.6±9.5
MAAPC05	12.5±0.0	12.5±0.0	25±0.0	25±0.0
P1	12.5±0.0	12.5±0.0	50±0.0	50±0.0
P2	41.7±14.4	41.7±14.4	33.3±14.4	>100
P3	16.7±7.2	16.7±7.2	100.0±0.0	>100
P4	>100	>100	100.0±0.0	>100
P1+tobramycin	<1.6	3.1±0.0	3.1±0.0	5.2±1.8
P2+tobramycin	<1.6	2.1±0.9	6.3±0.0	12.5±0.0
P3+tobramycin	2.1±0.9	2.6±0.9	6.3±0.0	12.5±0.0
P4+tobramycin	<1.6	3.6±2.4	3.1±0.0	6.3±0.0
Tobramycin	<1.6	3.1±0.0	6.3±0.0	6.3±0.0

Table 5.5: Hemolytic Activity Against hRBCs and Bacterial Selectivity of MAAPCs

		Selectivity index (HC_{50}/MIC)	
	HC_{50} (μM)	*E. coli* MG1655	*S. aureus* S113
MAAPC01	516.50	82.64	20.66
MAAPC02	>1000	>320	>80
MAAPC03	>1000	>320	>80
MAAPC04	>2000	>640	>160
MAAPC05	676.70	54.14	27.07

5.2.4. Membrane Permeabilization

In order to better understand the mode of action of our conjugates, we probed the effect of the MAAPCs on the permeability of the outer (OM) and inner (IM) membranes of *E. coli*. The assays rely on the ability of a chromogenic agent to cross the membrane only when the membrane has been compromised. In the OM permeability assay, nitrocefin, a chromogenic cephalosporin is used. Nitrocefin cannot cross the OM and is excluded from the periplasmic space. If the OM is permeabilized and nitrocefin crosses, it is cleaved by a periplasmic β-lactamase inducing a color change that can be monitored with a spectrophotometer at 486 nm. In the IM permeability assay, the chromogenic substrate ortho-nitrophenyl-β-galactoside (ONPG) is used. Since there is no lactose permease in *E. coli* ML35 strain, ONPG cannot diffuse into the bacterial cell cytoplasm unless the IM is compromised. Upon membrane permeabilization, ONPG is cleaved by cytoplasmic β-galactosidase into onitrophenol onitrophenol and galactose, inducing a color

change that can be monitored spectrophotometrically at 400 nm. While MAAPC01 induced significant permeabilization of the OM of *E. coli* D31 at a concentration lower than MICs (2 μM), the other MAAPCs displayed relatively low OM permeabilization and tobramycin had no effect (Figure 5.4A). At a concentration higher than MICs (20 μM), MAAPC01 and MAAPC05 demonstrated enhanced permeation activity although no significant increase was observed for MAAPC02, MAAPC03, and MAAPC04 (Figure 5.5). With the exception of MAAPC04, all MAAPCs disrupted, with different degrees of susceptibility, the IM of *E. coli* ML35 at a concentration of 2 μM (Figure 5.4B). MAAPC01 and MAAPC05 exhibited the highest permeation effect, which was comparable to the positive control (melittin). In contrast, MAAPC04 did not promote IM permeabilization. We hypothesize this occurs because of its lower hydrophobic content, which generally correlates with less lytic activity. MAAPC02 displayed unexpectedly low membrane activity, which is surprising considering that its hydrophobic and polar residues are arranged on opposite sides of the peptide assuming α-helical secondary structure. It is generally accepted that a certain level of hydrophobicity is required to penetrate the membrane of prokaryotic cells, and clustering hydrophobic amino acids in AMP structures enhances antimicrobial activity.[112,113] However, it has also been argued that there is an optimal level of hydrophobicity above which further increase in hydrophobicity results in strong peptide self-assembly which decreases cell wall permeability.[112,113] In general, these effects will also depend on the geometric organization and presentation of the hydrophobicity. MAAPC01 and MAAPC05 displayed significant OM and IM permeabilization activity although these MAAPCs are less active against *E. coli* (MIC = 6.3 and 12.5 μM respectively) than the other MAAPCs (MIC = 3.1 μM) that exhibit lower permeabilization and greater bactericidal activity. The inverse relationship between the activity and membrane

permeabilization suggests that the ability of MAAPCs to permeabilize the *E. coli* membrane does not directly reflect their antibacterial activity on growing bacteria. This implies that the antibacterial activity of MAAPCs against actively growing bacteria is not solely dependent on bacterial membrane disruption (the mechanism of AMP bactericidal activity). Membrane permeability experiments on actively growing cells do not show other mechanisms of antibiotic entry into the cell (i.e., via active transport), and thus do not necessarily correlate with the total amount of MAAPC that enters a bacterium. However, this active drug influx is easily shut down on dormant cells (persisters), in which active transport is drastically diminished and membrane permeability is expected to more closely correlate with antibacterial activity.

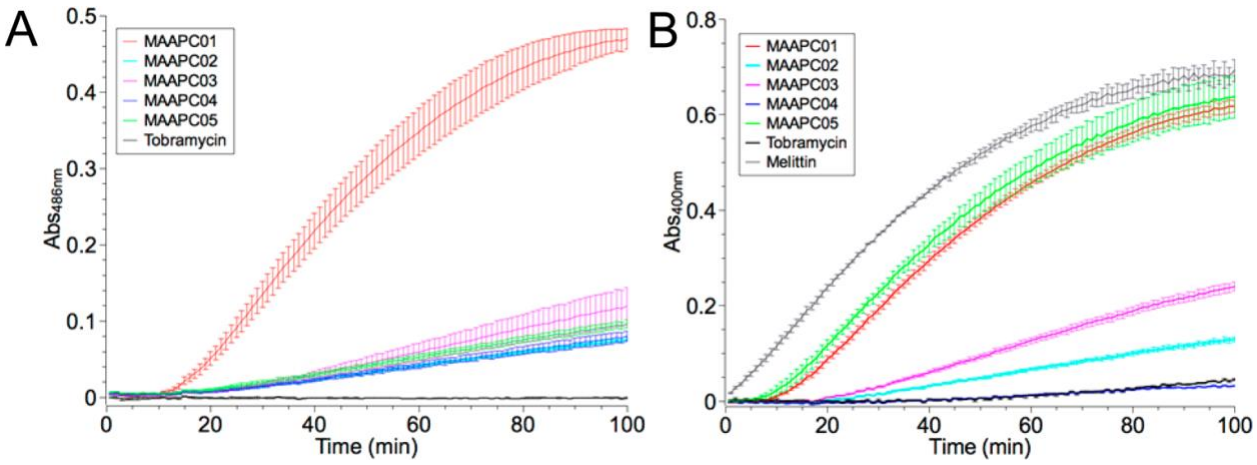

Figure 5.8: (A) E. coli D31 OM permeabilization by MAAPCs; (B) E. coli ML35 IM permeabilization by MAAPCs. The concentration for all tested compounds is 2 µM. Data are expressed as averages ± S.D., n = 3.

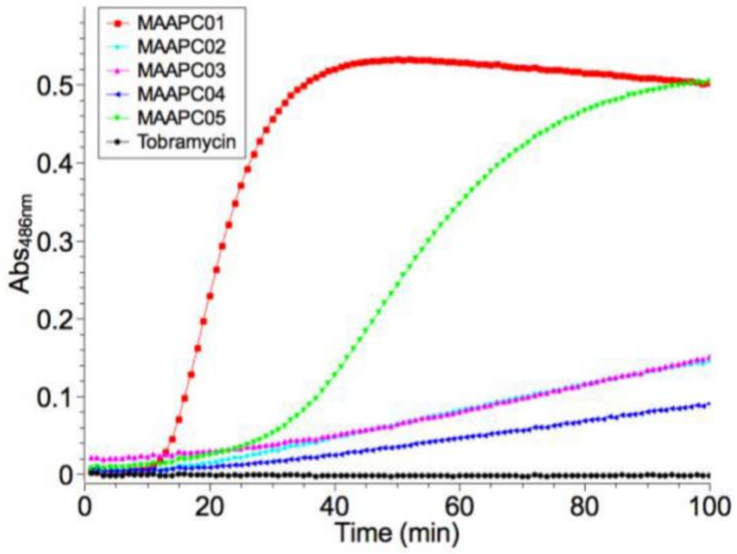

Figure 5.9: E. coli D31 OM permeabilization by MAAPCs at a concentration of 20 μM. Data are expressed as averages, n = 3.

5.2.5. Bactericidal activity against persister cells

To verify the above hypothesis, we compared the bactericidal activity of MAAPC01 and MAAPC05 to the least lytic (on bacterial membrane and hRBCs), most active, and selective conjugate (MAAPC04) against persister cells with plate killing assays. *E. coli* MG1655 and *S. aureus* S113 bacteria prepared in a persistent state were incubated for 2 hours with varying concentrations of MAAPCs or tobramycin (Figure 5.6). Consistent with previous studies,[92] tobramycin showed no activity against *E. coli* and *S. aureus* persistent bacteria over the entire range of tested concentrations, while MAAPC01 demonstrated remarkable dose-dependent bactericidal activity against both persistent cells. MAAPC05 had comparable killing potency to its *N*-terminal-conjugated analog MAAPC01 against *E. coli* persisters resulting in a 3-log reduction in colony-forming units (CFU) at a concentration of 3.1 μM lower than its MIC (12.5 μM) (Figure 5.6A). In

contrast, MAAPC04 exhibited less than a 2-log reduction in CFU at a concentration of 12.5 µM despite it being 4-fold higher than its MIC (3.1 µM) against *E. coli*. Interestingly, MAAPC05 showed reduced activity against *S. aureus* persisters in comparison to MAAPC01 (Figure 5.6B). Based on the earlier observation that MAAPC05 can permeabilize the IM of E. coli to the same extent as MAAPC01 and the fact that *S. aureus* that are Gram-positive organisms do not possess OM, we would have anticipated similar activity for MAAPC05 and MAAPC01 against *S. aureus* persister cells. Thus, it is possible that MAAPC05 has different permeability profiles depending on whether the pathogen is Gram-positive or Gram-negative. It should be noted that MAAPC04 had no bactericidal activity against *S. aureus* persisters (Figure 5.6B). It is also worth noting that the antimicrobial activity observed when the unconjugated peptide was mixed with tobramycin was similar to tobramycin alone or to the peptide alone against persisters (an example for MAAPC06 against *E. coli* persisters is shown in Figure 5.7) indicating that the synergistic effect occurs only when the peptide and tobramycin are chemically conjugated. Although MAAPC04 exhibits higher antimicrobial activity against actively growing bacteria, its lower antimicrobial activity against persisters correlates well with the membrane permeability assays. Furthermore, MAAPC01 and MAAPC05 exhibit both high membrane permeability and strong activity against persisters compared to their lower antimicrobial activity against actively growing cells. These results are consistent with our hypothesis that membrane permeability is necessary to kill antibiotic-tolerant bacteria but not the primary mechanism of action in actively growing organisms.

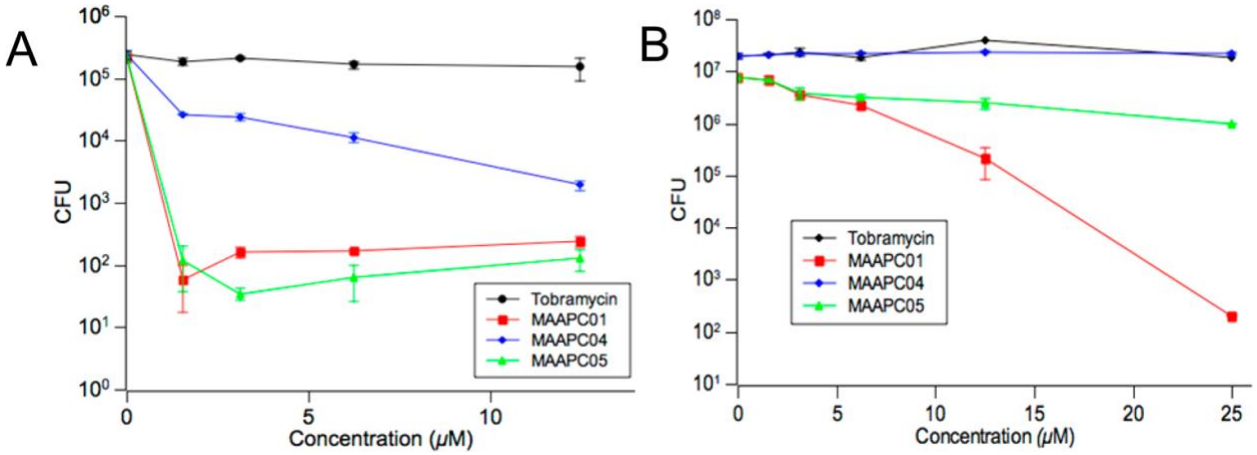

Figure 5.10: Killing activity of MAAPCs against persister cells: (A) E. coli MG1655 and (B) S. aureus SA113. E. coli MG1655 were pretreated with ciprofloxacin (1 μg/mL) while S. aureus SA113 were pretreated with ampicillin (100 μg/mL) for 3 hours to eliminate nonpersister cells.

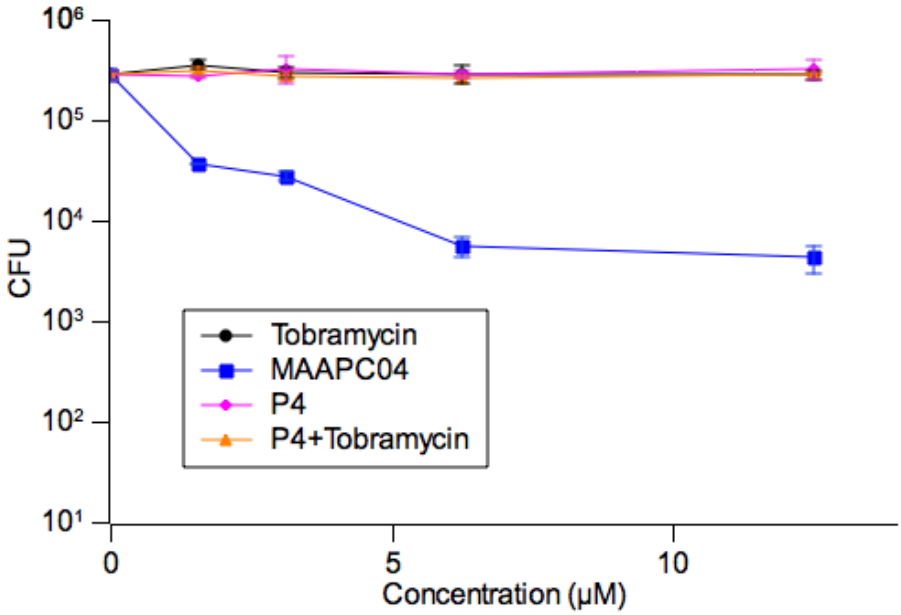

Figure 5.11: Killing activity of MAAPC04, P4 (unconjugated peptide in MAAPC04), a mixture of unconjugated P4 and tobramycin, and tobramycin alone against E. coli MG1655 persister cells. MG1655 were pre-treated with ampicillin (100μg/ml) for 3 hours to eliminate non-persister cells.

5.3. Material and method

5.3.1 Material

N,N-dimethylformamide (DMF), ethyl acetate, dichloromethane (DCM), methanol (MeOH), acetonitrile (CH3CN), magnesium sulfate (MgSO4), Lysogeny broth (LB) (Fisher Scientific). Tobramycin (TCI). Pyridine (J.T. Baker). p-Toluenesulfonyl chloride (TsCl), trifluoroacetic acid (TFA), thioanisole, triisopropylsilane (TIS) (Acros Organics). Sodium azide (NaN3) (EMD), Copper sulfate pentahydrate (CuSO4) (Reagent World). N-Fmoc-L-propargylglycine (Fmoc-Pra-OH) (AAPPTEC) (Louis- ville, KY, USA). Sodium ascorbate, *N,N*-diisopropyl-*N*-ethylamine (DIEA), triethylamine (TEA) (Alfa Aesar), 2-Chlorotrityl chloride resin (ChemImpex). Hydroxybenzotriazole), (HOBt) (ChemTech), 2-(1H-Benzotriazol- 1-yl)-1,1,3,3-tetramethyluronium hexafluorophosphate (HBTU), preloaded amino acid cartridges, melittin (AnaSpec Inc). Phenol (Amresco). Tryptic soy broth (TSB), agar, M9 minimal salts (Difco Laboratories). Nitrocefin (BioVision). Ortho-nitrophenyl-β-galactoside (ONPG), PIPES (Sigma). Human red blood cells (hRBCs) were bought from Lampire Biological Laboratories and were obtained from a single donor.

5.3.1. Synthesis of Tosyl-Boc5-tobramycin (2)

Boc5-tobramycin (1) (1 equiv) was dissolved in pyridine and cooled down with an ice bath. 4-Toluenesulfonyl chloride (TsCl) (1.5 equiv) was added to the mixture. After stirring for 2 hours at room temperature, TsCl (1.5 equiv) was added again. The solution was stirred for 12 hours at room temperature under argon. The solution was concentrated via rotary evaporation, diluted with ethyl acetate (200 mL), washed with nonsaturated brine, dried with magnesium sulfate

($MgSO_4$), and concentrated to dryness via rotary evaporation (BUCHI Rotavapor R-210). The white solid was purified by silica gel chromatography to yield 36%.

5.3.2. Synthesis of Azido-Boc5-tobramycin (3)

Tosyl-Boc5- tobramycin (1 equiv) was dissolved in DMF. NaN_3 (10 equiv) was added to the mixture. The solution was stirred at 80 °C for 12 hours under argon. The solution was diluted with ethyl acetate (200 mL), washed with DI water, dried with $MgSO_4$, and concentrated to dryness via rotary evaporation to yield 99% of a white solid.

5.3.3. Synthesis of Fmoc-Pra(BocToBocTobra)-OH (4) by Click reaction

Fmoc-Pra-OH (1 equiv) and azido-Boc5-tobramycin (1.1 equiv) were dissolved in DMF at 40 °C under argon. One mL of copper sulfate aqueous solution (0.5 equiv) and 1 mL of sodium ascorbate aqueous solution (1 equiv) were added to the mixture. The solution was stirred at 40°C for 24 hours. The solution was concentrated via rotary evaporation, diluted with ethyl acetate, washed with water, dried with $MgSO_4$, and concentrated to dryness via rotary evaporation. The white solid was purified by silica gel chromatography to yield 61%.

5.3.4. Synthesis of MAAPC05.

The (RQIKIWFQNRRWPra-(Tobra)) peptide (MAAPC05) was synthesized by Fmoc/*t*-butyl batch solid-phase synthesis on an automated peptide synthesizer (Applied Biosystems 433A), which allowed for direct conductivity monitoring of Fmoc deprotection. A 0.2 mmol scale synthesis was conducted using a preloaded 2-chlorotrityl resin. To load the first amino acid, a solution of Fmoc-

Pra(BocTobra)-OH (4) (1 equiv) and *N,N*-diisopropyl-*N*-ethylamine (DIEA) (4 equiv) in dry DCM (10 mL) was added to 2-chlorotrityl chloride resin (1 equiv) and the reaction stirred for 4 hours. The resin was transferred into a peptide vessel fitted with a polyethylene filter disk and washed with a solution of DCM/MeOH/DIEA (17:2:1; 3 × 20 mL), DCM (3 × 20 mL), DMF (2×20 mL), and dichloromethane (DCM) (2×20 mL). The grafting yield was determined by measuring the absorbance of N-(9-fluorenylmethyl) piperidine complex at 301 nm by UV–vis spectroscopy (THERMO SCIENTIFIC BIOMATE 3S) (after treatment with piperidine) and resulted 0.35 mmol/g.

5.3.5. Automatic synthesis of peptide.

Subsequent Fmoc amino acids were coupled using a "conditional double coupling" protocol on a 0.2 mmol scale. The Fmoc group was cleaved from the peptide-resin using a piperidine solution and monitored by conductivity. Subsequent amino acids (5 equiv amino acid) were activated with a mixture of (HBTU)/ (HOBt) / DIEA and attached to the *N*-terminal of the peptide-resin.

5.3.6. Cleavage of the peptide from the resin with removal of the acid-labile protecting groups

This was achieved by using 10 mL of a scavenging mixture of TFA/phenol/water/ thioanisole/TIS (10/0.75/0.5/0.5/0.25 v/w/v/v/v) for 3 hours. The resin was filtered out with a fritted filter, rinsed with 1 mL of TFA and 20 mL of DCM, the filtrate containing the unprotected peptide was concentrated to small volume, and the product was precipitated with cold diethyl ether (Fisher), isolated by filtration, and dried under vacuum overnight. The peptide was purified by preparative RP-HPLC (JASCO system) at 17 mL/ min on a Waters C18 column (250 × 22 mm, 5 mm) using a gradient of A [water (H_2O) + 0.1% TFA] and B [acetonitrile (CH_3CN) + 0.1% TFA]: 0% of B for 5 min,

0% → 70% for 7 min, 70% for 3 min, 70% → 100% for 2 min and 100% for 2 min (water and acetonitrile both from Fisher Scientific); detection at 214 nm. CH_3CN was evaporated under reduced pressure and the aqueous solution was freeze-dried to give a white solid yielding 46%.

5.3.7. MIC determination

Standard lab strains *E. coli* MG1655 and *S. aureus* SA113 are used as Gram-negative and Gram-positive strain, respectively. *E. coli* MG1655 were grown in Luria broth (LB), and SA113 were grown in Tryptic soy broth (TSB) at 37 °C. Both bacterial strains are grown under aerobic condition. MICs of MAAPCs were determined in a standard microbroth dilution assay in accordance with the guidelines of the Clinical and Laboratory Standards Institute guidelines (CLSI)[65] with suggested modifications by Hancock group.[66] An overnight culture of bacterial strains was diluted with the appropriate media and grown to mid log phase (OD600 of 0.5−0.6), then diluted 50 times before added to a 96-well microplate containing 2× serial dilutions of an MAAPC for a final count of 5×10^4 cfu/well. The plates were incubated at 37 °C for 18 hours in an ambient air incubator and read for turbidity in each well. The MIC values were determined as the lowest concentration that completely inhibited bacterial growth. Assay was performed in triplicate.

5.3.8. MBC determination

For the determination of MBCs, 5 µL of bacterial suspension from each well of the MIC plate were then transferred into 100 µL of LB or TSB in a 96-well plate and incubated for 18 hours at 37 °C.

The lowest concentration that revealed no visible bacterial growth after subculturing was taken as MBC. Assay was performed in triplicate.

5.3.9. Hemolysis

Human red blood cells (hRBCs) (1 mL) were pelleted (3500 rpm for 5 min), washed three times with PBS buffer (PBS 10 mM plus 150 mM NaCl, pH 7.4), and resuspended in PBS buffer. The cell suspension was then diluted 50 × in PBS buffer. Various concentrations of antibiotic solutions (20 µL) were added to the diluted cell suspension (180 µL) in a 96-well plate and incubated with orbital shaking at 37 °C for 1 hour. The cells from each well were then transferred into 1.5 mL tubes and pelleted by centrifugation (3500 rpm for 5 min). Then, 100 µL of supernatant from each tube were collected into a clear 96-well plate, and the absorbance of the released hemoglobin was measured with a plate reader spectrophotometer (Biotek Synergy 2) at 405 nm. Hemolysis was determined relative to the negative control (PBS) and the positive control (1% v/v Triton-X-100 (Fisher Scientific)) that lyses 100% of hRBCs). HC50 was defined as the antibiotic concentration causing 50% hemolysis. The hemolysis assay was performed in triplicate.

5.3.10. Outer membrane permeability assay on E. coli D31

E. coli D31 was used for outer membrane permeability assay. *E. coli* D31 were aerobically cultured in LB supplemented with 100 µg/mL ampicillin. An overnight culture of bacterial suspension was regrown to mid log phase (OD600 of 0.5−0.6), then washed and resuspended in 10 mM PBS buffer supplemented with 100 mM NaCl at pH 7.4. The washed cells were then diluted 5× in fresh PBS buffer containing nitrocefin (55 µg/mL), and 135 µL of the diluted cells were added to each well

of a 96-well plate. Just prior to reading, 15 µL of various concentrations of antibiotic solutions were added to the wells. The kinetics of nitrocefin cleavage were measured for 100 min at 37 °C by determining the absorbance at 486 nm using a plate reader spectrophotometer. All assays were performed in triplicate.

5.3.11. Inner Membrane Permeability Assay on E. coli ML35

E. coli ML35 was used for inner membrane permeability assay. ML35 were aerobically cultured in TSB. An overnight culture of *E. coli* ML35 was diluted and grown to mid log phase (OD600 of 0.5−0.6), then washed and resuspended in 10 mM Tris buffer supplemented with 1% v/v TSB at pH 7.4 (Tris-TSB). The washed cells were then diluted 3× in fresh Tris-TSB buffer containing 2.8 mM ONPG, and 135 µL of the diluted cells was added to each well of a 96-well plate. Just prior to reading, 15 µL of antibiotic solutions was added to the wells to a final concentration of 2 µM. Melittin was used as a positive control. The kinetics of ONPG hydrolysis were measured for 100 min at 37 °C by determining the absorbance at 400 nm using a plate reader spectrophotometer. All assays were performed in triplicate.

5.3.12. Persister Cell Assays

E. coli cells were grown in LB for 18 h at 37 °C to obtain stationary phase cultures. Nonpersister cells were eliminated by adding ciprofloxacin to a final concentration of 1 µg/mL, followed by a 3 hours incubation at 37 °C. *E. coli* cells were pelleted (5000 rpm for 5 min), washed in M9 minimal media, and resuspended in M9 minimal media to a final bacteria suspension of 5×10^6 CFU/mL. 10 µL *E. coli* suspension was added into 90 µL of M9 media containing various concentrations of

antibiotics in 96-well plates for a final cell count of 5×10^5 CFU/well. The plates were sealed and incubated with shaking at 37 °C incubator for 2 hours. After incubation, the assay mixture is serially diluted with M9 media and plated on LB agar. The agar plates were incubated overnight at 37 °C to yield visible colonies. The *E. coli* persister assays were performed in duplicate. *S. aureus* cells were grown in TSB for 18 hours at 37 °C to obtain stationary phase cultures. Nonpersister cells were eliminated by adding ampicillin to a final concentration of 100 μg/mL, followed by a 3 hours incubation at 37 °C. *S. aureus* cells were pelleted (5000 rpm for 5 min), washed with 10 mM PIPES buffer (pH 7.4), and resuspended in PIPES buffer to a final bacteria stock solution of 1×10^8 CFU/mL. 10 μL *S. aureus* suspension was added into 90 μL of PIPES buffer containing various concentrations of antibiotics in 96-well plates for a final cell count of 1×10^7 CFU/well. The plates were sealed and incubated with shaking at 37 °C incubator for 2 hours. After incubation, the assay mixture was 10× serially diluted with PIPES buffer and plated on LB agar plates. The agar plates were incubated overnight at 37 °C to yield visible colonies. The *S.aureus* persister assays were performed in duplicate.

5.4. Conclusion

We have synthesized a series of MAAPCs incorporating tobramycin with variations in the composition, sequence, and conjugation site of the peptide transporter. The MAAPCs exhibit good selectivity for bacterial cell membranes over mammalian cell membranes and do not induce any significant hemolysis of human red blood cells. MAAPCs exhibit better antibacterial activity against actively growing Gram-negative *E. coli* (MIC < 15 μM) than actively growing Gram-positive *S.aureus* (MIC < 25 μM). MAAPC01 exhibits the highest permeabilization of the outer membrane, with all other MAAPCs showing less permeation activity. Tobramycin exhibits no outer membrane activity. MAAPC01 and MAAPC05 exhibit the highest inner membrane permeability, comparable to the control melittin. MAAPC02 and 03 exhibit less membrane activity, and MAAPC04 and tobramycin show negligible inner membrane activity. Higher levels of membrane activity correlate well with antimicrobial activity against persisters, where MAAPC01 and MAAPC05 show much better activity than tobramycin alone or MAAPC04. Overall, we have demonstrated that we can design hybrid antibiotic peptide conjugates that can cross bacterial cell membranes that are impermeable to traditional antibiotics, and that their membrane activity and antibacterial activity can be finely tuned through small changes to the peptide transporter composition and sequence. These powerful new antibiotics show promise as novel therapies for resistant and difficult-to-treat bacterial infections.

Chapter 6: Future development

As mentioned in my thesis body, there are two different methods to lower the pKa of basic amino acids. The first is to conjugate electron-withdrawing groups (e.g., ester, amide) to the side chain. The other method is to increase the hydrophobicity of the Michael acceptor. In the future, it can be achieved by increasing the number of carbons in the hydrophobic chain R, as seen in Scheme 2.1.

Our synthetic toolbox is not limited to the aforementioned Michael acceptors. Many commercially available Michael acceptors could also be used, as each Michael acceptor has a different electron withdrawing group, as well as varying degrees of hydrophobicity (e.g., maleimide, vinyl sulfone, αβ−unsaturated ketones) (Figure 6.1). These electronic and structural differences can be used to generate a series of modified basic amino acids capable of activation at different pHs. Utilizing this wide range of Michael acceptors will allow us to have an increased level of tuning, in addition to the selection of lysine and arginine residues.

In the case of arginine modification, further modification of the product obtained after reaction with glyoxal is possible, due to the introduction of two hydroxyl groups in the modified arginine structure.[114]

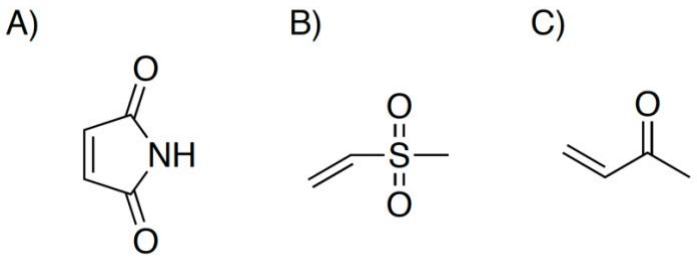

Figure 6.1: Examples of (A) maleimides, (B) vinyl sulfones, (C) αβ−unsaturated ketones.

In this project, we modified the basic amino acids of a naturally accruing AMP, Magainin 2, and a synthetic one, ZY13, to demonstrate that our toolbox is not limited to a specific category of AMPs. In fact, to narrow down the antibacterial activity of other commercially available AMPs, the same modifications can be performed on lysine and arginine in their sequence. Hence, it will be possible to modify AMPs in order to selectively target specific pathogens with different pH range of activities.

Chapter 7: Broader impact

In this project we focused on antibacterial activity of AMPs. However, AMPs are not limited to targeting bacteria species. Antimicrobial peptides are also capable of triggering cytotoxicity of human cancer cells. Positively charged AMPs can bind phosphatidylserine moieties, which have negative charge, on the outer surface of cancer cell plasma membranes. In addition, they can alter in the intracellular organelles of cancer cells, induce the release of tumor antigens and damage molecular patterns.

Therefore, AMPs could represent a potential therapeutic agent in oncology by themselves or in combination with other small molecules.[115] The idea of using AMPs as anticancer drugs does not limit the activity of AMPs as broad-spectrum antibiotic. They can still target beneficial bacteria, living in physiological pH, along with targeting cancer cells which lower the pH of the tumor microenvironment.[116] Hence, utilizing our method to engineer pH sensitive AMPs can not only have a significant impact for only targeting pathogenic bacteria but also can be used in the field of oncology to specifically target the cancer cells at lower pHs. As an example, we can talk about Magainin 2 which we modified in our project. Magainin 2 has shown anti-tumor activity in bladder tumor cells[117] and Ehlrich's murine ascites cells carcinomas.[118] In case of using intact Magainin 2 to combat cancer cells, serious side effects such as antibiotic resistance can occur to the patient. Naturally, cancer patients need to have a strong immune system and bacterial resistance can cause serious problems to these patients.

Another case of antimicrobial resistance that can be prevented by our method is antimicrobial resistance in animals. Recently, feed additives have been added to animal nutrition to improve the health and the performance of animals. These feed additives contain antibiotics allows the

occurrence of antimicrobial resistance (AMR).[119] Substitution of commercial antibiotics with engineered, pH sensitive AMPs can improve feed efficiency and the prevention/treatment of some animal diseases while avoiding antibacterial resistance.

Ultimately, the outcome of our project can be used to design a patient-specific tailored drug regimen that is most effective against the specific patient infection, tumor, ... Through this process, one can potentially determine the most effective drug combination as well as the lowest effective dosage for an individual patient. The personalized drug regimen based on the pH of the specific pathogenic condition can substitute the commercial antibiotics and have a significant impact again antibiotic resistance.

Chapter 8: Bibliography

1. Epand, R. M. *Host defense peptides and their potential as therapeutic agents*. *Host Defense Peptides and Their Potential as Therapeutic Agents* (2016). doi:10.1007/978-3-319-32949-9.
2. Stamm, L. V *et al.* Antimicrobial agents and chemotherapy. **54**, (2010).
3. Rubinstein, E. & Keynan, Y. Vancomycin-resistant enterococci. *Critical Care Clinics* **29**, 841–852 (2013).
4. Howden, B. P., Davies, J. K., Johnson, P. D. R., Stinear, T. P. & Grayson, M. L. Reduced vancomycin susceptibility in Staphylococcus aureus, including vancomycin-intermediate and heterogeneous vancomycin-intermediate strains: Resistance mechanisms, laboratory detection, and clinical implications. *Clinical Microbiology Reviews* **23**, 99–139 (2010).
5. Blaser, M. Stop the killing of beneficial bacteria. *Nature* **476**, 393–394 (2011).
6. Donskey, C. J. The role of die intestinal tract as a reservoir and source for transmission of nosocomial pathogens. *Clinical Infectious Diseases* **39**, 219–226 (2004).
7. Lorian, V. Colonization resistance. *Antimicrob Agents Chemother* **38**, 1693 (1994).
8. Owens, R. C., Donskey, C. J., Gaynes, R. P., Loo, V. G. & Muto, C. A. Antimicrobial-associated risk factors for Clostridium difficile infection. *Clinical Infectious Diseases* **46**, 19–31 (2008).
9. Brown, K., Valenta, K., Fisman, D., Simor, A. & Daneman, N. Hospital ward antibiotic prescribing and the risks of Clostridium difficile infection. *JAMA Internal Medicine* **175**, 626–633 (2015).
10. Peschel, A. & Sahl, H. G. The co-evolution of host cationic antimicrobial peptides and microbial resistance. *Nature Reviews Microbiology* **4**, 529–536 (2006).

11. Hancock, R. E. W. & Sahl, H. G. Antimicrobial and host-defense peptides as new anti-infective therapeutic strategies. *Nature Biotechnology* **24**, 1551–1557 (2006).

12. Shai, Y. Mechanism of the binding, insertion and destabilization of phospholipid bilayer membranes by α-helical antimicrobial and cell non-selective membrane-lytic peptides. *Biochimica et Biophysica Acta - Biomembranes* **1462**, 55–70 (1999).

13. Jenssen, H., Hamill, P. & Hancock, R. E. W. Peptide antimicrobial agents. *Clinical Microbiology Reviews* **19**, 491–511 (2006).

14. Viswanathan, V. K. & Hecht, G. Innate immunity and the gut. *Current Opinion in Gastroenterology* **16**, 546–551 (2000).

15. Michael Zasloff. Antimicrobial peptides of multicellularorganisms. *Nature* **415**, 389–395 (2002).

16. Brogden, K. A. Antimicrobial peptides: Pore formers or metabolic inhibitors in bacteria? *Nature Reviews Microbiology* **3**, 238–250 (2005).

17. Jin, L. *et al.* A Designed Tryptophan- and Lysine/Arginine-Rich Antimicrobial Peptide with Therapeutic Potential for Clinical Antibiotic-Resistant Candida albicans Vaginitis. *Journal of Medicinal Chemistry* **59**, 1791–1799 (2016).

18. Schmidt, N. W. & Wong, G. C. L. Antimicrobial peptides and induced membrane curvature: Geometry, coordination chemistry, and molecular engineering. *Current Opinion in Solid State and Materials Science* **17**, 151–163 (2013).

19. Viswanathan, V. K. & Hecht, G. Innate immunity and the gut. *Current Opinion in Gastroenterology* **16**, 546–551 (2000).

20. Hancock, R. E. W. & Lehrer, R. Cationic peptides: A new source of antibiotics. *Trends in Biotechnology* **16**, 82–88 (1998).

21. Nakajima, Y. Mode of Action and Resistance Mechanisms of Antimicrobial Macrolides. *Macrolide Antibiotics: Chemistry, Biology, and Practice: Second Edition* **55**, 453–499 (2003).

22. Huang, H. W. Action of antimicrobial peptides: Two-state model. *Biochemistry* **39**, 8347–8352 (2000).

23. Matsuzaki, K. *et al.* Relationship of membrane curvature to the formation of pores by magainin 2. *Biochemistry* **37**, 11856–11863 (1998).

24. Matsuzaki, K. Why and how are peptide-lipid interactions utilized for self-defense? Magainins and tachyplesins as archetypes. *Biochimica et Biophysica Acta - Biomembranes* **1462**, 1–10 (1999).

25. Kaminski, H. M. & Feix, J. B. Effects of D-Lysine substitutions on the activity and selectivity of antimicrobial peptide CM15. *Polymers (Basel)* **3**, 2088–2106 (2011).

26. Selsted, M. E. & Ouellette, A. J. Mammalian defensins in the antimicrobial immune response. *Nature Immunology* **6**, 551–557 (2005).

27. Ganz, T. Defensins: Antimicrobial peptides of innate immunity. *Nature Reviews Immunology* **3**, 710–720 (2003).

28. Lehrer, R. I. Primate defensins. *Nature Reviews Microbiology* **2**, 727–738 (2004).

29. Zanetti, M. Cathelicidins, multifunctional peptides of the innate immunity. *Journal of Leukocyte Biology* **75**, 39–48 (2004).

30. Falagas, M. E. & Kasiakou, S. K. Colistin: The revival of polymyxins for the management of multidrug-resistant gram-negative bacterial infections. *Clinical Infectious Diseases* **40**, 1333–1341 (2005).

31. Schmidt, N. W. *et al.* Criterion for amino acid composition of defensins and antimicrobial peptides based on geometry of membrane destabilization. *J Am Chem Soc* **133**, 6720–6727 (2011).

32. Yang, L. *et al.* Mechanism of a prototypical synthetic membrane-active antimicrobial: Efficient hole-punching via interaction with negative intrinsic curvature lipids. *Proc Natl Acad Sci U S A* **105**, 20595–20600 (2008).

33. Yang, L. *et al.* Synthetic antimicrobial oligomers induce a composition-dependent topological transition in membranes. *J Am Chem Soc* **129**, 12141–12147 (2007).

34. Tsaggari, N., Sarigiannis, Y. & Vlasiou, M. Bioinspired Interactions of Zn (II) and Cu (II) with the Antimicrobial Peptide Holothuroidin : Discovering the Action Mechanism †. **5**, 15102–15103 (2018).

35. Hamai, C., Yang, T., Kataoka, S., Cremer, P. S. & Musser, S. M. Effect of average phospholipid curvature on supported bilayer formation on glass by vesicle fusion. *Biophysical Journal* **90**, 1241–1248 (2006).

36. Ouellette, A. J. Paneth cell α-defensins in enteric innate immunity. *Cellular and Molecular Life Sciences* **68**, 2215–2229 (2011).

37. Ayabe, T. *et al.* Modulation of mouse paneth cell α-defensin secretion by mIKCa1, a Ca2+-activated, intermediate conductance potassium channel. *Journal of Biological Chemistry* **277**, 3793–3800 (2002).

38. Selsted, M. E., Miller, S. I., Henschen, A. H. & Ouellette, A. J. Enteric defensins: Antibiotic peptide components of intestinal host defense. *Journal of Cell Biology* **118**, 929–936 (1992).

39. So, P. T. C., Gruner, S. M. & Erramilli, S. Pressure-induced topological phase transitions in membranes. *Physical Review Letters* **70**, 3455–3458 (1993).

40. Shearman, G. C., Ces, O., Templer, R. H. & Seddon, J. M. Inverse lyotropic phases of lipids and membrane curvature. *Journal of Physics Condensed Matter* **18**, (2006).

41. Schmidt, N., Mishra, A., Lai, G. H. & Wong, G. C. L. Arginine-rich cell-penetrating peptides. *FEBS Letters* **584**, 1806–1813 (2010).

42. Manning, G. S. Limiting laws and counterion condensation in polyelectrolyte solutions. 7. Electrophoretic mobility and conductance. *Journal of Physical Chemistry* **85**, 1506–1515 (1981).

43. Zimm, B. H. & Bret, M. Le. Counter-ion condensation and system dimensionality. *Journal of Biomolecular Structure and Dynamics* **1**, 461–471 (1983).

44. Trias, J. & Nikaido, H. Protein D2 channel of the Pseudomonas aeruginosa outer membrane has a binding site for basic amino acids and peptides. *Journal of Biological Chemistry* **265**, 15680–15684 (1990).

45. Mishra, A., Gordon, V. D., Yang, L., Coridan, R. & Wong, G. C. L. HIV TAT forms pores in membranes by inducing saddle-splay curvature: Potential role of bidentate hydrogen bonding. *Angewandte Chemie - International Edition* **47**, 2986–2989 (2008).

46. Mishra, A. *et al.* Translocation of HIV TAT peptide and analogues induced by multiplexed membrane and cytoskeletal interactions. *Proc Natl Acad Sci U S A* **108**, 16883–16888 (2011).

47. Kyte, J. & Doolittle, R. F. A simple method for displaying the hydropathic character of a protein. *Journal of Molecular Biology* **157**, 105–132 (1982).

48. Eisenberg, D., Weiss, R. M., Terwilliger, T. C. & Wilcox, W. Hydrophobic moments and protein structure. *Faraday Symposia of the Chemical Society* **17**, 109–120 (1982).

49. Hessa, T. *et al.* Recognition of transmembrane helices by the endoplasmic reticulum translocon. *Nature* **433**, 377–381 (2005).

50. Wang, Z. & Wang, G. APD: The antimicrobial peptide database. *Nucleic Acids Research* **32**, 590–592 (2004).

51. Rädler, J. O., Koltover, I., Salditt, T. & Safinya, C. R. Structure of DNA-cationic liposome complexes: DNA intercalation in multilamellar membranes in distinct interhelical packing regimes. *Science (1979)* **275**, 810–814 (1997).

52. Koltover, I., Salditt, T., Rädler, J. O. & Safinya, C. R. An inverted hexagonal phase of cationic liposome-DNA complexes related to DNA release and delivery. *Science (1979)* **281**, 78–81 (1998).

53. Gillies, E. R., Goodwin, A. P. & Fréchet, J. M. J. Acetals as pH-sensitive linkages for drug delivery. *Bioconjugate Chemistry* **15**, 1254–1263 (2004).

54. Lynn, D. M. & Langer, R. Degradable Poly (-amino esters): Synthesis , Characterization , and Self-Assembly with Plasmid DNA. 10761–10768 (2000).

55. Uchida, K. & Stadtman, E. R. Modification of histidine residues in proteins by reaction with 4- hydroxynonenal. *Proc Natl Acad Sci U S A* **89**, 4544–4548 (1992).

56. Jin, Y. *et al.* Tracking bacterial infection of macrophages using a novel red-emission pH sensor. *Analytical and Bioanalytical Chemistry* **398**, 1375–1384 (2010).

57. *TEPZZ 9¥7_ 6A_T*.

58. Grundler, V. & Gademann, K. Direct arginine modification in native peptides and application to chemical probe development. *ACS Medicinal Chemistry Letters* **5**, 1290–1295 (2014).

59. Glomb, M. A. & Lang, G. Isolation and characterization of glyoxal - Arginine modifications. *Journal of Agricultural and Food Chemistry* **49**, 1493–1501 (2001).

60. Bruice, T. C. & Fife2, T. H. *Hydroxyl Group Catalysis. III.1 The Nature of Neighboring Hydroxyl Group Assistance in the Alkaline Hydrolysis of the Ester Bond*. https://pubs.acs.org/sharingguidelines (1962).

61. Kurtoglu, Y. E., Mishra, M. K., Kannan, S. & Kannan, R. M. Drug release characteristics of PAMAM dendrimer-drug conjugates with different linkers. *International Journal of Pharmaceutics* **384**, 189–194 (2010).

62. Zasloff, M. *Magainins, a class of antimicrobial peptides from Xenopus skin: Isolation, characterization of two active forms, and partial cDNA sequence of a precursor (vertebrate peptide antibiotics)*. vol. 84 https://www.pnas.org (1987).

63. Jin, L. *et al.* A Designed Tryptophan- and Lysine/Arginine-Rich Antimicrobial Peptide with Therapeutic Potential for Clinical Antibiotic-Resistant Candida albicans Vaginitis. *Journal of Medicinal Chemistry* **59**, 1791–1799 (2016).

64. He, J. *et al.* Novel synthetic antimicrobial peptides against Streptococcus mutans. *Antimicrobial Agents and Chemotherapy* **51**, 1351–1358 (2007).

65. *M07-A10 Methods for Dilution Antimicrobial Susceptibility Tests for Bacteria That Grow Aerobically; Approved Standard-Tenth Edition*. www.clsi.org. (2015).

66. Wiegand, I., Hilpert, K. & Hancock, R. E. W. Agar and broth dilution methods to determine the minimal inhibitory concentration (MIC) of antimicrobial substances. *Nature Protocols* **3**, 163–175 (2008).

67. THE FIT2D HOME PAGE. https://www.esrf.fr/computing/scientific/FIT2D/.

68. Schwarz, U. S. & Gompper, G. Stability of Inverse Bicontinuous Cubic Phases in Lipid-Water Mixtures. (2000).

69. Shearman, G. C., Ces, O., Templer, R. H. & Seddon, J. M. Inverse lyotropic phases of lipids and membrane curvature. *Journal of Physics: Condensed Matter* **18**, S1105 (2006).

70. Magnet, S. & Blanchard, J. S. Molecular insights into aminoglycoside action and resistance. *Chemical Reviews* **105**, 477–497 (2005).

71. Poehlsgaard, J. & Douthwaite, S. The bacterial ribosome as a target for antibiotics. *Nature Reviews Microbiology* **3**, 870–881 (2005).

72. Fourmy, D., Recht, M. I., Blanchard, S. C. & Puglisi, J. D. Structure of the A Site of Escherichia coli 16S Ribosomal RNA Complexed with an Aminoglycoside Antibiotic Published by : American Association for the Advancement of Science Stable URL : http://www.jstor.org/stable/2892058. *Advancement Of Science* **274**, 1367–1371 (2009).

73. Avent, M. L., Rogers, B. A., Cheng, A. C. & Paterson, D. L. Current use of aminoglycosides: Indications, pharmacokinetics and monitoring for toxicity. *Internal Medicine Journal* **41**, 441–449 (2011).

74. Magnet, S. & Blanchard, J. S. Molecular insights into aminoglycoside action and resistance. *Chemical Reviews* **105**, 477–497 (2005).

75. Chow, J. W. SPECIAL SECTION : ANTIMICROBIAL RESISTANCE Aminoglycoside Resistance in Enterococci. *Clinical Infectious Diseases* **31**, 586–589 (2000).

76. Mingeot-Leclercq, M. P., Glupczynski, Y. & Tulkens, P. M. Aminoglycosides: Activity and resistance. *Antimicrobial Agents and Chemotherapy* **43**, 727–737 (1999).

77. Daigle, D. M., McKay, G. A. & Wright, G. D. Inhibition of aminoglycoside antibiotic resistance enzymes by protein kinase inhibitors. *Journal of Biological Chemistry* **272**, 24755–24758 (1997).

78. Lilly, T. *et al.* Inhibitor of Aminoglycoside-2"-O- Adenylyltransferase. **22**, 824–831 (1982).

79. Murase, K. *et al.* EF-Tu Binding Peptides Identified, Dissected, and Affinity Optimized by Phage Display GDP conformation of EF-Tu. Because EF-Tu is abundant in the cell, other functions have been suggested, particu-larly during periods of cellular stress when protein syn-g. *Chemistry & Biology* **10**, 161–168 (2003).

80. Elchert, B. *et al.* Application of the Synthetic Aminosugars for Glycodiversification: Synthesis and Antimicrobial Studies of Pyranmycin. *J Org Chem* **69**, 1513–1523 (2004).

81. Hanessian, S., Tremblay, M. & Swayze, E. Tobramycin analogues with C-5 aminoalkyl ether chains intended to mimic rings III and IV of paromomycin. *Tetrahedron* **59**, 983–993 (2003).

82. Fridman, M., Belakhov, V., Yaron, S. & Baasov, T. A new class of branched aminoglycosides: Pseudo-pentasaccharide derivatives of neomycin B. *Organic Letters* **5**, 3575–3578 (2003).

83. Bastida, A. *et al.* Exploring the use of conformationally locked aminoglycosides as a new strategy to overcome bacterial resistance. *J Am Chem Soc* **128**, 100–116 (2006).

84. Zhanel, G. G. *et al.* Comparison of the next-generation aminoglycoside plazomicin to gentamicin, tobramycin and amikacin. *Expert Review of Anti-Infective Therapy* **10**, 459–473 (2012).

85. Aggen, J. B. *et al.* Synthesis and spectrum of the neoglycoside ACHN-490. *Antimicrobial Agents and Chemotherapy* **54**, 4636–4642 (2010).

86. Sun, J., Deng, Z. & Yan, A. Bacterial multidrug efflux pumps: Mechanisms, physiology and pharmacological exploitations. *Biochemical and Biophysical Research Communications* **453**, 254–267 (2014).

87. Delcour, A. H. Outer membrane permeability and antibiotic resistance. *Biochimica et Biophysica Acta - Proteins and Proteomics* **1794**, 808–816 (2009).

88. Nikaido, H. Bacterial resistance to antibiotics as a function of outer membrane permeability. *Journal of Antimicrobial Chemotherapy* **22**, 17–22 (1988).

89. Taber, H. W., Mueller, J. P., Miller, P. F. & Arrow, A. S. Bacterial uptake of aminoglycoside antibiotics. *Microbiological Reviews* **51**, 439–457 (1987).

90. Davis, B. D. Mechanism of bactericidal action of aminoglycosides. *Microbiological Reviews* **51**, 341–350 (1987).

91. Cohen, N. R., Lobritz, M. A. & Collins, J. J. Microbial persistence and the road to drug resistance. *Cell Host and Microbe* **13**, 632–642 (2013).

92. Schmidt, N. W. *et al.* Engineering persister-specific antibiotics with synergistic antimicrobial functions. *ACS Nano* **8**, 8786–8793 (2014).

93. Justyna, W. 乳鼠心肌提取 {HHS} {Public} {Access}. *Physiol Behav* **176**, 139–148 (2017).

94. Sahl, H.-G. *et al.* Mammalian defensins: structures and mechanism of antibiotic activity. *Journal of Leukocyte Biology* **77**, 466–475 (2005).

95. Schmidt, N. W., Mishra, A., Wang, J., Degrado, W. F. & Wong, G. C. L. Influenza virus A M2 protein generates negative gaussian membrane curvature necessary for budding and scission. *J Am Chem Soc* **135**, 13710–13719 (2013).

96. Schmidt, N. W. *et al.* Pentobra: A potent antibiotic with multiple layers of selective antimicrobial mechanisms against Propionibacterium acnes. **135**, 1581–1589 (2015).

97. Knutson, J. S. 基因的改变NIH Public Access. *Bone* **23**, 1–7 (2014).

98. Schmidt, N., Mishra, A., Lai, G. H. & Wong, G. C. L. Arginine-rich cell-penetrating peptides. *FEBS Letters* **584**, 1806–1813 (2010).

99. Schmidt, N. W. *et al.* Molecular basis for nanoscopic membrane curvature generation from quantum mechanical models and synthetic transporter sequences. *J Am Chem Soc* **134**, 19207–19216 (2012).

100. Schmidt, N. W. *et al.* Criterion for amino acid composition of defensins and antimicrobial peptides based on geometry of membrane destabilization. *J Am Chem Soc* **133**, 6720–6727 (2011).

101. Deshayes, S. *et al.* Designing Hybrid Antibiotic Peptide Conjugates to Cross Bacterial Membranes. *Bioconjugate Chemistry* **28**, 793–804 (2017).

102. Asensio, J. L. *et al.* A simple structural-based approach to prevent aminoglycoside inactivation by bacterial defense proteins. Conformational restriction provides effective protection against neomycin-B nucleotidylation by ANT4. *J Am Chem Soc* **127**, 8278–8279 (2005).

103. Hanessian, S., Massé, R. & Capmeau, M. L. Aminoglycoside Antibiotics: Synthesis of 5''-Amino-5''-Deoxyneomycin and 5''-Amino-5''-Deoxyparomomycin. *Journal of Antibiotics* **30**, 893–896 (1977).

104. Döring, G., Flume, P., Heijerman, H. & Elborn, J. S. Treatment of lung infection in patients with cystic fibrosis: Current and future strategies. *Journal of Cystic Fibrosis* **11**, 461–479 (2012).

105. Mishra, A. *et al.* Translocation of HIV TAT peptide and analogues induced by multiplexed membrane and cytoskeletal interactions. *PNAS* **108**, 16883–16888 (2011).

106. Schmidt, N. W. & Wong, G. C. L. Antimicrobial peptides and induced membrane curvature: Geometry, coordination chemistry, and molecular engineering. *Current Opinion in Solid State and Materials Science* vol. 17 151–163 (2013).

107. Giangaspero, A., Sandri, L. & Tossi, A. *Amphipathic a helical antimicrobial peptides A systematic study of the effects of structural and physical properties on biological activity*. http://www.bbcm.univ.

108. Gonzalez Iii, U. S. & Spencer, J. P. *Aminoglycosides: A Practical Review*. *Am Fam Physician* vol. 58 https://www.aafp.org/afp/1998/1115/p1811.html (1998).

109. Jureti6, D. *et al. Magainin 2 amide and analogues Antimicrobial activity, membrane depolarization and susceptibility to proteolysis*. vol. 249 (1989).

110. Wei, S. Y. *et al.* Solution structure of a novel tryptophan-rich peptide with bidirectional antimicrobial activity. *Journal of Bacteriology* **188**, 328–334 (2006).

111. Chen, Y. *et al. Rational Design of α-Helical Antimicrobial Peptides with Enhanced Activities and Specificity/Therapeutic Index **.

112. Jiang, Z., Vasil, A. I., Vasil, M. L. & Hodges, R. S. "Specificity determinants" improve therapeutic indices of two antimicrobial peptides piscidin 1 and dermaseptin S4 against the gram-negative pathogens Acinetobacter baumannii and Pseudomonas aeruginosa. *Pharmaceuticals* **7**, 366–391 (2014).

113. Kuroda, K., Caputo, G. A. & Degrado, W. F. The Role of Hydrophobicity in the Antimicrobial and Hemolytic Activities of Polymethacrylate Derivatives. (2009) doi:10.1002/chem.200800xxx.

114. Watson, A. J. A. & Williams, J. M. J. The Give and Take of Alcohol Activation. *Science (1979)* **329**, 635–636 (2010).

115. Wodlej, C. *et al.* Interaction of two antitumor peptides with membrane lipids - Influence of phosphatidylserine and cholesterol on specificity for melanoma cells. *PLoS ONE* **14**, (2019).

116. Zhang, X., Lin, Y. & Gillies, R. J. Tumor pH and its measurement. *Journal of Nuclear Medicine* vol. 51 1167–1170 (2010).

117. Lehmann, J. *et al.* Antitumor Activity of the Antimicrobial Peptide Magainin II against Bladder Cancer Cell Lines. *European Urology* **50**, 141–147 (2006).

118. Baker, M. A., Maloy, W. L., Zasloff, M. & Jacob, L. S. *Anticancer Efficacy of Magainin2 and Analogue Peptides*. http://aacrjournals.org/cancerres/article-pdf/53/13/3052/2450843/cr0530133052.pdf.

119. Silveira, R. F., Roque-Borda, C. A. & Vicente, E. F. Antimicrobial peptides as a feed additive alternative to animal production, food safety and public health implications: An overview. *Animal Nutrition* vol. 7 896–904 (2021).